Neural Mechanisms of Signal Convergence in the Primate Primary Visual Pathway

By

Kacie Dougherty

Dissertation

Submitted to the Faculty of

the Graduate School of Vanderbilt University

in partial fulfillment of the requirements

for the degree of

DOCTOR OF PHILOSOPHY

in

Psychology

December 15, 2018

Nashville, Tennessee

Approved:

Randolph Blake, Ph.D.

Bruce Cumming, M.D., Ph.D.

Alexander Maier, Ph.D.

Jeffery Schall, Ph.D.

To my parents, Madison, Michele Cox, and Alex Maier.

Thank you for your constant support and for inspiring me to work hard and be kind.

ACKNOWLEDGMENTS

I would like to thank my dissertation committee—Dr. Randolph Blake, Dr. Bruce Cumming, Dr. Alexander Maier, and Dr. Jeffrey Schall—for providing very helpful advice and feedback that contributed to the studies presented in this dissertation.

The **Introduction** to this dissertation relies heavily on a review paper by Michael Schmid, and Alexander Maier, and me in press at *Journal of Comparative Neurology*: https://doi.org/10.1002/cne.24417.

The study presented in **Chapter 1** was carried out by Brock M. Carlson, Jacob A. Westerberg, Paul Martin, Alexander Maier, and me. I thank M. Schall, Dr. W. Zinke, Dr. M. Schmid, Dr. V.A. Casagrande, Dr. F. Briggs, M. Feurtado, B. Williams, R. Williams, M. Maddox, L. McIntosh, and J. Parker for technical advice and assistance. The work in Chapter One was supported by a research grant from the National Eye Institute (1R01EY027402-01). K.D. and J.A.W. were supported by a National Eye Institute Training Grant (5T32 EY007135-23) when this work was done.

The study presented in **Chapter 2** is currently under review at *Current Biology*. A previous version was uploaded to bioRxiv, https://doi.org/10.1101/320218. In addition to myself, authors for Chapter Two include Michele A. Cox (co-first author), Jacob A. Westerberg, and Alexander Maier. I thank M. Schall, Dr. W. Zinke, S. Amemori, Dr. T. Apple, M. Feurtado, K. George-Durrett, Dr. A. Graybiel, N. Halper, P. Henry, M. Johnson, Dr. C. Jones, M. Maddox, L.

McIntosh, Dr. A. Newton, J. Parker, C. Thompson, K. Torab, C. Subraveti, B. Williams, and R. Williams for technical advice and assistance. I also thank Dr. B. Cumming, Dr. P. Martin, B.M. Carlson and N. Valov for comments on an earlier version of the writing included in this chapter. The work in Chapter Two was supported by a research grant from the National Eye Institute (1R01EY027402-01). I was supported by a National Eye Institute Training Grant (5T32 EY007135-23) when this work was done.

The study presented in **Chapter 3** was published in *Cerebral Cortex* in 2017: https://doi.org/10.1093/cercor/bhv304. Co-authors on this manuscript include Michele A. Cox, Taihei Ninomiya, David A. Leopold, and Alexander Maier. The work in Chapter Three was supported by the Intramural Research Program of the NIMH and grants by the Whitehall Foundation, the Knights Templar Ey Foundation and the Alfred P. Sloan Foundation to AM. I would like to thank Dr. J. Schall and Dr. A. Bollimunta for comments on an earlier draft of the study presented in Chapter Three. I would also like to thank N. Nichols, S. Saha, K. Smith, D. Yu, & J. Yu for technical assistance, and Dr. P. Balaram for assistance with the anatomical figure.

TABLE OF CONTENTS

Page

LIST OF TABLES

Page

LIST OF FIGURES

Page

Introduction

The ease with which we see is remarkable, especially if we consider that light falls on not one but two retinas and is transformed into a singular coherent view. Much of this transformation rests on the coordinated activity of neurons in the primary visual pathway, including the lateral geniculate nucleus of the dorsal thalamus (LGN) and the primary visual cortex (V1) (**Figure 0.1**). The neural circuits of the LGN, V1, and the circuitry between them have been studied extensively using both anatomical and physiological techniques. Despite the wealth of studies on this circuitry, we still cannot definitively answer a fundamental question about binocular vision: Where in this primary visual pathway do the signals from the two eyes meet, or converge on single neurons? The answer to this question has the potential to lead to therapies for many binocular vision disorders, which constitute some of the most common eye diseases in the world.

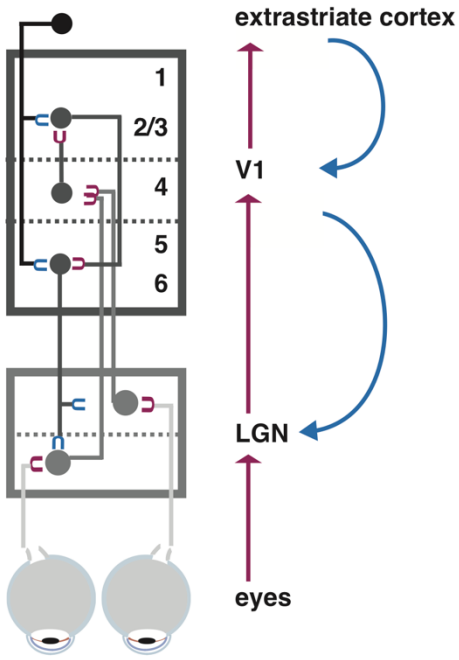

Figure 0.1 Excitatory connections feedforward (maroon) and feedback (blue) connections between the eyes, LGN, and V1.

There are two primary goals of this dissertation: First, I seek to identify the neural site where the signals from the two eyes first interact in the primary visual pathway of primates. I studied this question in behaviorally-trained, non-human primates using fMRI guided

neurophysiological recordings with multi- and single-contact electrode arrays. Specifically, I measured visual responses of single neurons in the LGN and V1 to stimuli presented to one or both eyes through a mirror stereoscope to narrow in on the neural site where binocular signals first interact. In the LGN, I take special consideration of the three primary parallel streams of visual processing—the parvocellular, magnocellular, and koniocellular neurons—separately. In V1, I probed visual neural responses across the cortical depth and analyzed how signals from each eye converge within this microcircuit.

The question of where the signals from the two eyes meet is centered on a feedforward process, where separate inputs flowing from the retina to the rest of the brain converge upon the same neurons. However, these feedforward inputs to the brain do not meet a blank slate. Instead, sensory activation is integrated with ongoing brain activity (**Figure 0.1**). As a second aim of my dissertation, I seek to delineate the convergence of feedforward inputs with ongoing activity in V1. These aims describe two separate types of signal convergence in the early visual system. Below, I detail the motivation, background, premise and rationale for each of these goals.

0.1 Binocular integration

Even though each eye's perspective differs from the other, our visual perception of the world resembles a singular view. To create this unified perspective, our brains need to combine the separate outputs of the two eyes into a unified binocular signal. In other words, outputs from one eye must interact with outputs from the other eye.

Knowing *where* the outputs from the two eyes converge is critical for our understanding of binocular vision and promises the discovery of new therapeutic targets for binocular visual disorders, such as strabismus and amblyopia.

The primary visual pathway of primates accommodates two structures where the outputs of the two eyes might first meet and interact (**Figure 0.2**) (for review see (Casagrande and Boyd, 1996, Howard, 2002, Parker and Cumming, 2001, Cumming and DeAngelis, 2001): Retinal ganglion cells from each eye project in two isolated streams to the dorsal lateral geniculate nucleus of the thalamus (LGN). The LGN projects to the primary visual cortex, which constitutes a bottleneck for visual input to all other cortical areas (Felleman and Van Essen, 1991, Markov et al., 2013, Lennie and Movshon, 2005, Schmid et al., 2013, Schmiedt et al., 2014). The primary visual cortex is the first structure in the primary visual pathway where almost all neurons are excited by stimulation of either eye (Hubel and Freeman, 1977, Smith et al., 1997). This feature

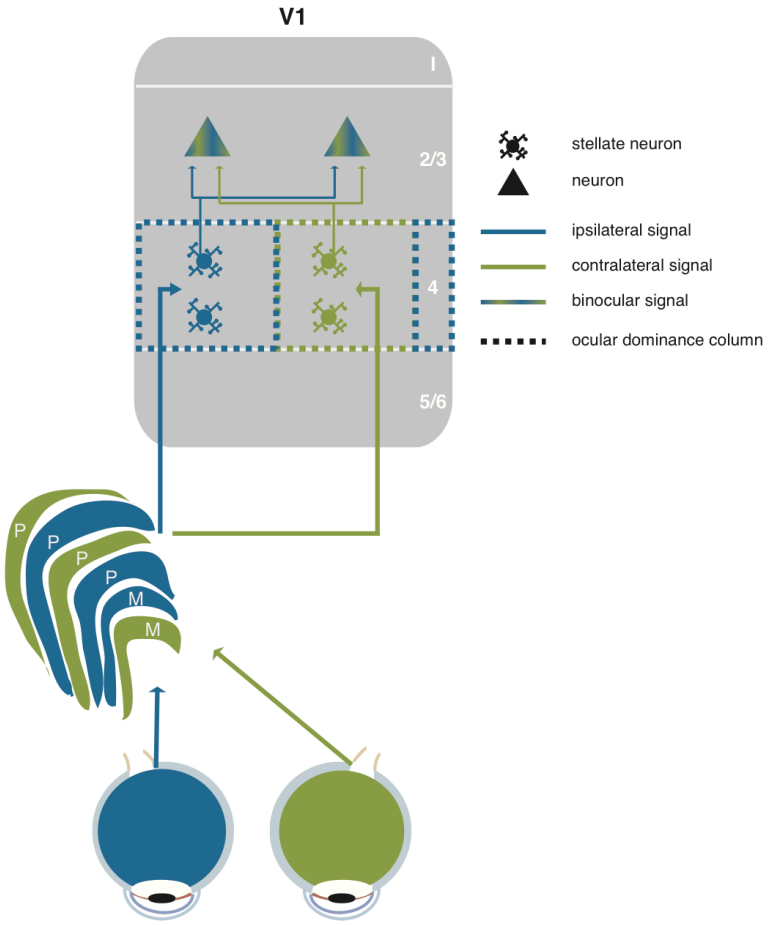

Figure 0.2 Paths of each eye's output in the primate primary visual pathway.
Simplified schematic of primary visual pathway of macaque monkeys. Retinal neurons project visual sensory information to the LGN, which is divided into several, eye-specific layers (blue and green). LGN neurons primarily project to layer 4 (arrows) as well as other sublayers of the primary visual cortex. The prevailing model of binocular combination places the site of binocular convergence in layer 2/3.

suggests that the signals from the two eyes are merged together into a binocular response in this structure (Hubel and Wiesel, 1969). Unlike the primary visual cortex, almost all LGN neurons are excited by stimulation of one eye only. This means that only stimulation from one eye, but not the other, will result in a significant increase or decrease of in the number of action potentials, or spikes, in LGN neurons. Nevertheless, the LGN is a candidate structure for the two eyes' outputs to meet and interact in that the spike rate of a neuron that responds to its driving eye is modulated, enhanced or suppressed, when the other eye is stimulated as well. This *binocular modulation* might serve computations that require the two eyes' outputs to interact before they merge together.

Indeed, we know that the visual system adjusts the relative strength of each eye's outputs before merging them to a single binocular signal. This fact is evidenced by the observation that our visual perception hardly changes when we close one eye, even though this action virtually halves the input to the visual system. To account for the difference in visual activation between these two viewing conditions, the brain needs to adjust the relative strength (gain) of the signals from each eye in a way that depends on activation of the other eye. This computational step likely takes place prior to binocular merging because the relative strength of the outputs from each eye would be lost in a merged binocular signal. Several neurophysiological and psychophysical studies on this subject converged on the idea that the gain of the outputs of the eyes are adjusted while the two signals are still separate (Baker et al., 2007, Ding and Sperling, 2006, Meese et al., 2006, Moradi and Heeger, 2009, Truchard et al., 2000).

The underlying process is most likely carried out by neurons that are excited by one eye only (monocular neurons). Specifically, when monocular neurons are excited by a visual stimulus in their driving, "dominant eye", this visual response can be either enhanced or inhibited when the other, "non-dominant eye" is also stimulated. These two types of binocular modulation have been termed binocular facilitation and binocular suppression, respectively.

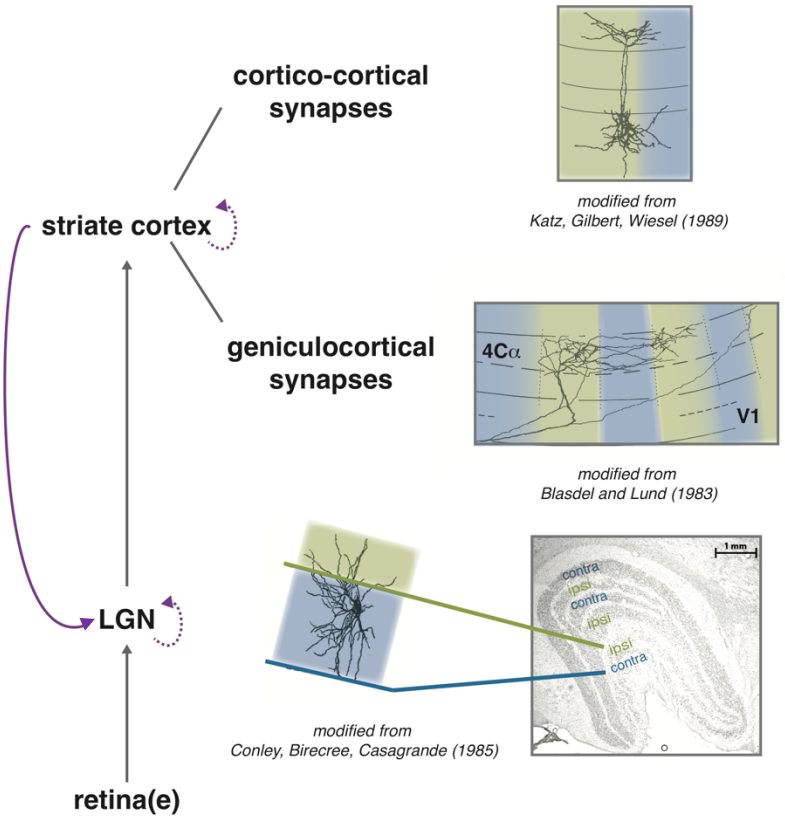

Figure 0.3 Possible sites of binocular modulation in the primary visual pathway.
1) The outputs of the two eyes arrive in segregated eye-specific (green/blue) layers in the LGN, but some anatomical connections can bridge between them (top). 2) The projections of LGN neurons to primary visual cortex are also largely segregated by eye along the tangential dimension, terminating in eye-specific ocular dominance columns (green/blue). However, some of these LGN projections appear to form synapses outside their respective ocular dominance columns. 3) Projections from layer 4 neurons to other neurons within primary visual cortex are not bound to the boundaries of the ocular dominance columns. 4) Connections within the LGN or visual cortex as well as corticogeniculate feedback could provide a structural substrate for binocular modulation. Adapted from Blasdel and Lund, 1983.

These two types of binocular modulation come about in three different ways along the primary visual pathway: 1) Binocular modulation emerges in LGN. (2) Binocular modulation occurs in V1, but LGN neurons still exhibit secondary binocular modulation from cortical feedback to this structure. (3) Binocular modulation occurs through a combination of 1 and 2 (**Figure 0.3**).

Below, we will discuss these alternatives and summarize our current understanding of binocular modulation in the primary visual pathway.

0.2 Binocular modulation of LGN spiking responses

Over the past half century, neurophysiological studies across many eminent laboratories have probed whether LGN neurons exhibit binocular modulation. The bulk of this work was based on extracellular recordings in anesthetized cats and monkeys. These model species were chosen because their eyes are positioned on the head in a way that is similar to humans, resulting in similarly sized binocular visual fields (Heesy, 2004). Many other mammalian species have more lateralized position of the eyes and consequently deviate in their anatomy of binocular combination (Howarth et al., 2014, Kondo et al., 1993, Grieve, 2005, Longordo et al., 2013, Niell and Stryker, 2008, Scholl et al., 2013, Jeffery et al., 1981).

Studies in cat LGN

Only a small number (2% - 11%) of cat LGN neurons can be driven to increase or reduce their spontaneous spiking through either eye (Bishop et al., 1962, Erulkar and Fillenz, 1960, Kinston et al., 1969) (**Table 0.1**).

Table 0.1 Estimated proportions of monocular, binocular, and binocularly modulated neurons in cat and monkey LGN based on several studies.
(Bishop et al., 1962, Erulkar and Fillenz, 1960, Kinston et al., 1969, Marrocco and McClurkin, 1979, Rodieck and Dreher, 1979, Cheong et al., 2013, Zeater et al., 2015).

	CAT LGN	MONKEY LGN
exclusively monocular neurons	20%	70-90%
binocularly facilitated neurons	10%	5%
binocularly suppressed neurons	70%	10-30%
binocular neurons	2-10%	3%

However, visual responses of most cat LGN neurons are significantly altered when a second visual stimulus is simultaneously presented to the non-dominant eye, i.e. their spike rate differs between binocular and monocular stimulation (**Figure 0.4**) (Guido et al., 1989, Sengpiel et al., 1995, Xue et al., 1987). The retinal region of the non-dominant eye that, when stimulated, elicits this binocular modulation is called the non-dominant eye receptive field, and it is generally larger than dominant-eye receptive fields (Sanderson et al., 1971). More than three fourths of cat LGN cells (~82%) feature such a non-dominant eye receptive field, and 88% of these neurons are inhibited by stimulation of the non-dominant eye (Sanderson et al., 1971). Unlike dominant-eye receptive fields in the LGN, which typically exhibit center-surround organization, in that stimulation of the center results in the opposite effect as stimulation of the surrounding region, non-dominant eye receptive fields show a homogenous organization (Sanderson et al., 1971) but see (Schmielau and Singer, 1977). Binocular modulation of cat LGN responses is greatest when the stimulus in the non-dominant eye matches the spatial frequency of the stimulus in the dominant eye (Tong et al., 1992, Sengpiel et al., 1995), though binocular modulation can be evoked across a wide range of spatial frequencies (Moore et al., 1992, Sengpiel et al., 1995).

While most studies used stimuli of relatively low spatial frequencies (< 0.8 cycles per degree), binocular modulation has been observed for stimuli as high as five or more cycles per degree, suggesting that binocular modulation in cat LGN acts at high spatial acuity (Guido et al., 1989) (the peak contrast sensitivity for cats lies between 1 and 5 cycles per degree (Blake et al., 1974, Pasternak and Merigan, 1981). The spiking responses of most cat LGN neurons increase with increasing stimuli contrast. The resulting contrast response functions can be measured for stimuli presented to one eye alone (monocular stimulation) or for identical stimuli presented at the same position of both eyes' retina (dioptic stimulation) (Tong et al., 1992). Assuming binocular suppression, which dominates cat LGN, binocular modulation under these conditions could take one of three different forms: 1) Dioptic stimulation results in decreased responses relative to monocular stimulation at all contrast levels, i.e., stimulating the non-dominant eye has the same suppressive effect for any stimulus contrast; 2) dioptic stimulation results in decreased responses relative to monocular stimulation for high contrasts only, i.e., binocular suppression is limited to high contrasts; 3) dioptic stimulation results in a shift of the slope of the contrast response function relative to that for monocular stimulation, i.e., the dynamic range of contrast responses is enhanced. The majority of cat LGN cells exhibit the first type of binocular modulation (Tong et al., 1992). Therefore, binocular modulation in cat LGN appears to primarily reduce the neurons' response gain.

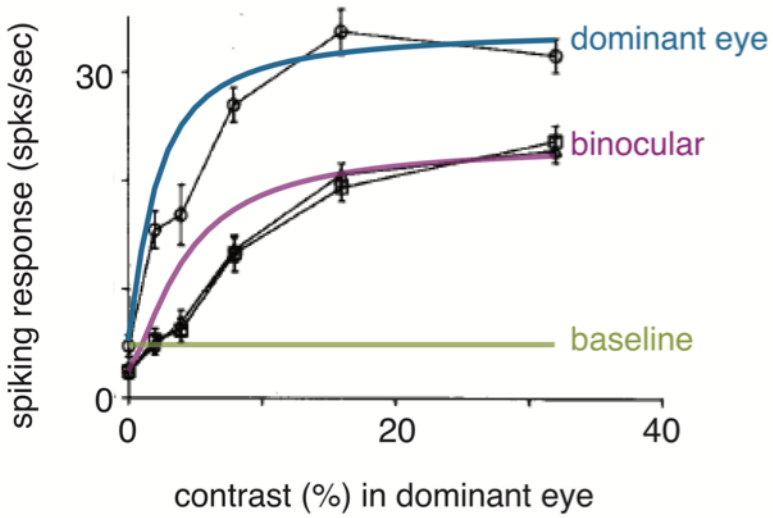

Figure 0.4 Binocular modulation of monocular neurons.
Data from a previously published example cat LGN neuron. Ordinate represents the magnitude of the neuron's spiking response to visual stimulation and abscissa plots the contrast of the visual stimulus (shown to the neuron's dominant eye). Model fits using a Naka-Rushton equation (Naka and Rushton, 1966) for binocular (purple line) and monocular (green line) responses are superimposed on the actual data (black traces). The solid blue line represents the estimated baseline firing rate of the neuron based on the activity plotted for the monocular condition at 0% contrast. Note the overall drop in response gain for the binocular stimulation condition, indicating that even though the LGN neuron can only be activated by one eye (the dominant eye), this neuron is nonetheless sensitive to stimulation of the opposite (non-dominant) eye, resulting in an overall reduced visual response when both eyes are stimulated. No difference was found between a dioptic condition (triangles) and a dichoptic condition (squares) in which the spatial frequency in the two eyes were different. Adapted Tong et al., 1992, Conley et al., 1985, Fitzpatrick et al., 1985, Katz et al., 1989.

Studies in monkey LGN

Similar to the cat, only a small minority (< 3%) of neurons in monkey LGN can be driven through both eyes (Cheong et al., 2013, Zeater et al., 2015, Dacey, 1994). Monkey LGN also contains neurons that modulate their spiking under binocular viewing (Marrocco and McClurkin, 1979) (**Table 0.1**). And, similar to the cat, between 70% and 100% of this modulation takes the form of binocular suppression. One notable difference between the two species is that the fraction of LGN cells for which binocular modulation has been reported is drastically smaller in

monkeys (<10-30%) compared to cats (Marrocco and McClurkin, 1979, Rodieck and Dreher, 1979) (see **Table 0.1**). This difference in proportions of binocularly modulated LGN neurons might be due to differences in LGN anatomy between carnivores and primates, which I will discuss below. Another possibility is that the magnitude of binocular modulation depends on the type of visual stimulation. For example, investigations in cat LGN relied primarily on slowly moving grating stimuli to measure contrast responses, whereas almost all studies on binocular modulation in macaque monkey LGN used bars or light flashes that covered the entire visual field to evoke neural responses (Marrocco and McClurkin, 1979, Rodieck and Dreher, 1979) but see (Schroeder et al., 1990).

0.3 Primate specializations

The primate LGN is organized in parvocellular (P), magnocellular (M), and koniocellular (K) layers (Brunso-Bechtold and Casagrande, 1982, Norton et al., 1988, Xu et al., 2001). P cells, which make up the majority of LGN neurons, form the primary four dorsal layers of the LGN (Dreher et al., 1976). M cells, which constitute less than 20% of LGN neurons, are located in the two ventral-most primary layers (Hendry and Reid, 2000). K neurons, which constitute less than 10% of LGN neurons, are almost exclusively located within the intercalated zones that span between the primary LGN layers (Casagrande et al., 2007, Hendry and Reid, 2000). M and P neurons can be reliably distinguished using neurophysiological criteria, which includes systematic differences in the transiency of their responses, selectivity to spatial and temporal frequency, color (cone) opponency, contrast response functions and recording locations within the LGN (Brunso-Bechtold and Casagrande, 1982, Norton et al., 1988, Xu et al., 2001). K neurons tend to differ in their spectral response from M and P neurons, and can be

cytochemically distinguished via optogenetic targeting by their expression of CamKIIα, a kinase which is absent in all other LGN neurons (Hendry and Yoshioka, 1994, Klein et al., 2016).

The distinction between P, M and K neurons is particularly important for binocular vision because the physiology and anatomical connectivity of these cells differs distinctively, which might affect binocular modulation in these pathways. Several psychophysical studies have found that motion information, believed to be carried by the M pathway, is integrated across the eyes differently than other visual properties (Andrews and Blakemore, 2002, Carlson and He, 2000, Sun et al., 2002). This hypothesis is corroborated by neurophysiological data (Tailby et al., 2010), but how this finding relates to the responses of specific LGN subpopulations is unclear. Some researchers suggest that binocular modulation occurs with equal frequency in P and M layers (Marrocco and McClurkin, 1979, Schroeder et al., 1990), while others report that binocular modulation is exclusive to the M layers (Rodieck and Dreher, 1979). Interestingly, anatomical studies in *New World* monkeys show that M neurons tend to be oriented orthogonally to the laminar boundaries and stay less confined to their home layer than P cells (Conley et al., 1985). This idiosyncratic morphology might constitute a unique mechanism to provide M cells with inputs from both eyes. No single neuron data to date speak to whether K neurons exhibit binocular modulation. Intriguingly, a fraction (~10-30%) of K neurons respond to both eyes (Cheong et al., 2013, Zeater et al., 2015). K neurons uniquely receive input from the superior colliculus (Stepniewska et al., 1999), which might exclusively provide them with binocular input. The superior colliculus receives inputs from both eyes as well as inputs from V1, and approximately 80% of neurons respond to stimuli in either eye in primates (Marrocco and Li, 1977), with ~30% responding equally strong to input from either eye (Marrocco and Li, 1977).

0.4 Potential role of intrageniculate cells in binocular modulation.

Neurons in the primary layers of the LGN receive direct synaptic inputs from one eye only (Guillery, 1970, Hayhow, 1958, Hickey and Gullery, 1974, Kaas et al., 1972, Laties and Sprague, 1966, Stone and Hansen, 1966). Therefore, neural processes must extend across laminar boundaries for binocular modulation to emerge in the LGN. In the cat, several types of geniculate cells could fulfill this criterion (Sanderson et al., 1971). First, large multipolar class I cells, located in interlaminar zones, receive binocular input from the optic tract, and also feature dendrites that extend beyond the cells' home layer (Hayhow, 1958, Laties and Sprague, 1966). Second, geniculocortical class II cells feature dendrites that extend into other layers (Guillery, 1966). Third, one type of LGN interneuron (subtype b) features axons that extend into other layers of the LGN (Tombol, 1969). Lastly, another type of cell that is present in all major laminae has dendrites that cross into other layers and contacts other dendrites there (Famiglietti, 1970). Binocular modulation could arise in cat LGN through the activity of any of these four cell types, or a combination thereof.

In primates, evidence of similar anatomical connections among LGN layers is sparser. However, some primate LGN neurons, particularly those close to primary laminar borders, have dendrites that extend across the border of origin into interlaminar zones (K layers) and sometimes even into the adjacent layer that is innervated by the other eye (Campos-Ortega et al., 1968, Saini and Garey, 1981). In addition, neurons within the interlaminar zones feature dendrites that span into both neighboring laminae, providing a potential substrate for interactions between monocular neurons across laminar borders (Guillery and Colonnier, 1970).

0.5 Binocular modulation at the input stage to visual cortex

An alternative to the hypothesis that the outputs from the two eyes first meet and interact in the LGN is that this convergence first occurs in primary visual cortex. LGN relay cells from M and P laminae primarily project onto granular layer 4 (layer 4C in primates) stellate cells in primary visual cortex (**Figure 0.3**). Layer 4C cells have been described as predominantly monocular (Hubel and Wiesel, 1968). Lesioning a geniculate layer corresponding to one eye results in patchy degeneration of cortical tissue in macaque V1 layer 4C, suggesting spatial segregation of each eye's input (Hubel and Wiesel, 1972). Indeed, proline (dye) injections in one eye reveal alternating bands (columns) of ocular dominance in the granular layer, which further demonstrates that eye-specific LGN inputs to macaque V1 layer 4C are spatially distinct (Hubel and Wiesel, 1972, Blasdel and Lund, 1983). However, the spatial segregation of eye-specific inputs in V1 seems far less strict than in the LGN as some LGN afferents terminate in V1 ocular dominance bands corresponding to the other eye (Blasdel and Lund, 1983). Therefore, the signals from the two eyes might interact at the level of geniculocortical synapses in layer 4C, the input stage to visual cortex. Another possibility is that binocular modulation in primary visual cortex is mediated via interneurons in layer 4C. For example, inhibitory basket cells in layer 3 of cat visual cortex span ocular dominance columns (Buzás et al., 2001). Basket cells also reside in the granular layer, although it is unknown whether these neurons span ocular dominance columns (Martin et al., 1983). In any case, most neurons outside of layer 4C of primary visual cortex are driven through either eye, which suggests that the signals from the two eyes are merged when visual processing reaches these layers (Hubel and Wiesel, 1962)

Single neuron studies in cat visual cortex

A large body of literature on binocular modulation in cat visual cortex has shown that binocular stimulation generally results in a reduction of activity compared to monocular stimulation, especially if the orientation of the stimuli in each eye are orthogonal (Sengpiel and Blakemore, 1994, Sengpiel et al., 1995, Sengpiel et al., 1998).

Several neurophysiological studies have probed the specific origins of binocular modulation in cat area A17 and A18, which are homologous to primate visual cortex. For example, Ohzawa and Freeman relied on the fact that, unlike LGN neurons (Xue et al., 1987), responses of visual cortical neurons vary with binocular disparity (i.e., a slight positional shift of the same image between the two eyes). In this study, both the relative phase (disparity) and contrast of the stimuli shown to each eye were varied (Freeman and Ohzawa, 1990). Interestingly, the neurons' disparity tuning remained constant, even for large interocular contrast differences, e.g., 2.5% contrast in one eye and 50% contrast in the other eye. This result suggests that binocular modulation occurs before area 17 neurons produce action potentials since their spiking output has already been adjusted to the contrast of the stimulus shown to the other eye.

Truchard, Ohzawa, & Freeman (2000) found that increasing the contrast of a grating in one eye results in a large reduction in monocular contrast gain, and that this reduction is largely independent of the contrast gain of the other eye (Truchard et al., 2000). In other words, their data suggest that, under binocular viewing, most contrast gain control occurs at the monocular level.

On the other hand, transfer of visual adaptation from one eye to the other (interocular transfer) has been pointed out as evidence that some interocular gain control occurs at the binocular level. Specifically, following several hundred milliseconds to several seconds of

exposure to stimuli presented to one eye, responses to stimulation of the opposite eye are reduced for both binocular neurons (Hammond and Mouat, 1988, Maffei et al., 1986) and monocular neurons alike (Howarth et al., 2014). This finding suggests that monocular neurons are not only modulated by their counterparts that encode the other eye, but also by neurons that receive inputs from both eyes and thus encode a binocular signal.

Single neuron studies in macaque V1

There have been numerous studies on the effects of binocular stimulation in monkey primary visual cortex, although the vast majority of them used stimuli that did not match between the eyes (for review see (Cumming and DeAngelis, 2001, Freeman, 2017, Henriksen et al., 2016, Macknik and Martinez-Conde, 2008, Parker et al., 2016, Logothetis, 1998, Leopold, 2005). Similar to the cat, most neurons in V1 are driven through either eye (Hubel and Wiesel, 1968), and the predominant effect of binocular stimulation is binocular suppression (Endo et al., 2000, Kumagami et al., 2000).

One of these studies in monkey V1 specifically addressed if signals from the two eyes interact *within* this area. In this experiment, a grating was presented at one contrast level to one eye, and a target of varying contrast was presented to the other eye to determine the contrast levels needed to elicit a certain criterion neuronal response. When a lower contrast grating is shown to one eye, a higher contrast grating needs to be shown to the other eye to elicit the criterion response (Smith et al., 1997). This finding mirrors the results from the cat outlined above (Truchard et al., 2000): Given that dichoptic gratings of varying contrast can elicit the same neuronal response, binocular modulation seems to occur prior to the spiking of V1 neurons. According to these findings, the site of first binocular modulation lies either within the LGN or

at the input level to V1, such as in layer 4C. **In this dissertation, I will explore both of these possibilities in two separate studies, as detailed below**.

0.6 Interlaminar dynamics in primary visual cortex

To summarize what I have discussed so far, the formation of a binocular response is likely to first occur in V1. This process can be explained in a feedforward fashion by assuming convergence of monocular synaptic inputs onto certain V1 neurons. However, it is important to note that, in addition to feedforward processing, V1 also receives modulatory (feedback) cortico-cortical and subcortical-cortical inputs.

Interestingly, these processing streams are highly segregated among the laminae: As mentioned in paragraph **0.5**, in macaque primary visual cortex, reticulo-geniculate afferents terminate in granular layer 4C (Blasdel and Lund, 1983), and this feedforward, caudal-to-rostral path progresses with neurons originating in supragranular layers terminating in layer 4 of target regions (Rockland and Pandya, 1979). Cortico-cortical axons sending axons in the opposing, rostral-to-caudal direction terminate in supragranular and infragranular layers, notably sparing middle layer 4C (Rockland and Pandya, 1979, Gilbert, 1983), while subcortical pulvinar projections mainly terminate in superficial layers of V1 (Rezak and Benevento, 1979, Felleman and Van Essen, 1991). These two streams of neural activation are thought to serve different physiological functions (Markov et al., 2013). Yet, it is largely unknown how modulatory (feedback) activity converges with incoming, feedforward inputs within the functioning V1 microcircuit.

Experimenters can exploit their anatomical segregation within the cortical microcircuit to disentangle feedforward activity from feedback processes (Bannister, 2005, Felleman and Van

Essen, 1991, Douglas and Martin, 2004, Douglas, 1989, Lübke and Feldmeyer, 2007). Other work has suggested that feedback and feedforward streams may also be distinct in their temporal (spectral) characteristics. Namely, high frequency neural activity (> 30 Hz) has been shown to be predominantly of local origin, while low frequency (< 20 Hz) activity has been shown to span multiple brain areas (Buffalo et al., 2011, Donner and Siegel, 2011), which is consistent with feedback activity. An important extension of this finding is that systematic correlations between high frequency and low frequency activity in the brain may reflect an interaction between local processes and activity extrinsic to that site (Jensen and Colgin, 2007, Engel et al., 2001, Canolty and Knight, 2010, Donner and Siegel, 2011, Wang et al., 2012). Such a systematic relationship between frequency components, known as cross-frequency coupling, occurs if high frequency power co-varies with the phase of a low frequency signal of a neural population response. Such phase-to-amplitude coupling has been demonstrated in several cortical areas (Bruns and Eckhorn, 2004, Canolty et al., 2006, Lakatos et al.), including macaque visual cortex (Spaak et al., 2012, van Kerkoerle et al., 2014). A complete, well-defined mechanism for phase-to-amplitude coupling remains to be determined. Nonetheless, it has been hypothesized that large amplitude, low frequency activity may affect the resting potential of local neurons, thereby altering the probability of incoming synaptic signals translating into spiking output (Fröhlich and McCormick, 2010).

What is the relevance of cross-frequency coupling for visual processing? Psychophysical studies have demonstrated that visual sensitivity vacillates somewhat rhythmically. These findings suggest that sensory performance depends on when stimuli are presented with respect to cycles of rhythmic excitability (VanRullen and Koch, 2003). Similarly, the performance benefits of attentional selection have been found to exhibit similar rhythmic (~10Hz) fluctuations

(VanRullen et al., 2007, Landau and Fries, 2012). One possible mechanism for these psychophysical findings is that slow fluctuations in visual performance are related to co-varying rhythmic gating of neural activity in sensory cortex. This type of neural coupling should be evidenced by a systematic relationship between low frequency fluctuations within the extracellular medium (local field potential, or LFP) and spiking activity. **In this dissertation, I will investigate whether low frequency LFP fluctuations couple with spiking activity during visual processing and determine how this process manifests across the layers of the V1 microcircuit.**

0.7 Summary

In this dissertation, I aim to 1) narrow in on the location of where the signals from the two eyes first interact in the primary visual pathway in primates and 2) investigate an important aspect of microcircuit dynamics during visual processing. Towards the goal, I conducted two studies (described in Chapter One and Chapter Two) in which I tested whether LGN and V1 neurons are sensitive to both eyes. I considered a neuron to be sensitive to both eyes if it responded following stimulation of either eye (*binocularly driven neurons*), or if its spiking response to a binocular visual stimulus deviated from its response to a visual stimulus presented the preferred (dominant) eye alone (*binocularly modulated neurons*). In the first study, I recorded the spiking activity of single LGN neurons in parvocellular, magnocellular, and koniocellular layers while we presented drifting sine-wave gratings at varying contrast levels to one or both eyes of awake, behaving macaques. In the second study, I recorded neurons across the layers of V1 using a similar paradigm. The outcome of these experiments combined suggests that virtually all primate V1 neurons, and some LGN neurons are sensitive to both eyes, suggesting that the signals from the

two eyes meet sooner than previously appreciated. Based on these findings, I propose a revised model of binocular convergence.

Towards the second goal, I investigated the relationship of neural activity within and between layers of the V1 microcircuit before and during visual activation. Specifically, I considered a low-frequency dominated neural activity in the deep layers of V1, and its relationship to the spiking activity across all layers. This experiment demonstrated a previously unknown systematic relationship between low frequency activity in the lower layers of V1 and spiking activity throughout the cortical column during visual processing, suggesting that modulatory feedback to V1 regulates incoming visual inputs.

Overall, this work advances our understanding of where the signals from the two eyes begin to interact, and highlights the functional impact of ongoing dynamics in neural activity during visual processing in the microcircuit of primary visual cortex.

1. Binocular modulation of LGN neurons

1.1 Summary

In this chapter, I begin by addressing aim one of this dissertation: to narrow in on where the signals from the two eyes first interact in the primary visual pathway in primates. The main recipient of the outputs of the two eyes is the LGN, as detailed in the **0.1 Introduction**. For this reason, I first targeted this structure in an awake macaque. Using linear multicontact electrode arrays or single-contact electrodes, I recorded spiking responses of single units to visual stimuli presented to one or both eyes at varying contrast levels. I determined whether binocular modulation occurred among LGN units by testing for a difference in spiking response under binocular and monocular stimulation across the contrast range. Overall, there was little binocular modulation in the LGN. Across all LGN neurons, significant modulation of spiking responses at the temporal frequency of the stimulus (F1 response) occurred only when a high contrast stimulus was in the dominant eye. This F1 modulation at high contrast was significant for the population response of both M and K neurons, but not for P neurons. While the majority of LGN neurons in our sample did not modulate under binocular stimulation, 14-26% of individual units showed a significant difference between the F1 response for monocular (0.0) and binocular (0.8-1.0) conditions with zero (0.0), low (0.11-0.13), and high contrast (0.8-1.0) levels in the dominant eye. These values are largely congruent with previous work in the anesthetized preparation (Marrocco and McClurkin, 1979, Rodieck and Dreher, 1979). In other words, the majority of LGN units do not process the outputs of both eyes, but a subgroup are sensitive to both eyes, suggesting that a limited amount of binocular processing occurs in this structure.

1.2 Introduction

Binocular vision affords human and other primates several advantages, including stereovision, hyperacuity, and improved visual detection (Blake and Fox, 1973, Blake et al., 1981, Blake and Wilson, 2011). Despite great advances in uncovering the neural bases of binocular vision, there are still some fundamental questions left unanswered. One of these questions is where the signals from the two eyes begin to combine. Understanding how the outputs of the two eyes combine in the visual pathway is of particular importance because this knowledge promises to advance strategies to improve vision in individuals with binocular vision disorders. An important step towards achieving this understanding is determining where within the primary visual pathway the signals from the two eyes meet.

In primates, retinal ganglion cells from each eye project separately to the lateral geniculate nucleus of the dorsal thalamus (LGN). The LGN is commonly considered a "monocular" structure because almost all LGN neurons are excited by stimulation of one eye only (but see (Cheong et al., 2013, Zeater et al., 2015). Congruent with this physiological observation, neurons within each LGN layer receive direct axonal input from one eye exclusively (Kaas et al., 1972).

Despite the LGN's characterization as monocular, researchers have recognized its potential involvement in binocular integration. This hypothesis stems from additional features of its anatomical organization. For example, each of the four most dorsal primary layers, or P layers, neighbors at least one layer that receives input from the eye that does not project to that layer. Similarly, the two most-ventral primary layers, or M layers, sit adjacent to one another. Adjacent layers are retinotopically aligned, such that nearby connections between layers that receive inputs from different eyes could be relevant to binocular integration.

The anatomical features described above could implicate the LGN in binocular integration. How could this depiction be reconciled with decades of vision research converging on the idea that almost all primate LGN neurons respond to one eye and not the other? One possibility is that interactions between the signals from the two eyes occur through modulation of responses. For example, imagine a given LGN neuron is excited when a stimulus is presented to the left eye but not when a stimulus is shown to the right eye. Binocular modulation occurs when the firing rate of this neuron decreases (or increases) both eyes are stimulated rather than the left eye alone. In other words, LGN neurons could be either truly monocular in the sense that they are only sensitive to one eye, or they could be binocularly facilitated or suppressed due to binocular modulation.

Previous work in anesthetized cats suggested that more than two thirds of LGN neurons undergo (mostly suppressive) binocular modulation. The origin of this binocular modulation remains unclear, with several studies aimed at determining whether the modulation was of cortical or geniculate origin producing equivocal results. Notably, the LGN of cats differs from that of macaques in that cat LGN seems to contain a greater degree of connectivity between the eye-specific layers (Sanderson et al., 1971, Hayhow, 1958, Laties and Sprague, 1966, Guillery, 1966, Tombol, 1969, Famiglietti, 1970). Indeed, two studies testing for binocular modulation in primate LGN found that two thirds of LGN neurons show no binocular modulation at all (Rodieck and Dreher, 1979, Marrocco and McClurkin, 1979). One of these studies suggested that the few primate LGN neurons that do modulate under binocular viewing were specific to the M layers (Rodieck and Dreher, 1979). However, this finding was not corroborated in the other study (Marrocco and McClurkin, 1979). Later studies also raised concern about the effects of anesthesia on LGN function, and its binocular function in particular (Schroeder et al., 1988,

Garraghty et al., 1982). More recent work has demonstrated that some neurons in the K layers, situated between the M and P layers, actually respond to both eyes (Cheong et al., 2013, Zeater et al., 2015). To our knowledge, no one has tested whether K neurons modulate under binocular viewing. Thus, the specificity of binocular modulation in the three main laminar compartments of primate LGN remains unclear.

Here, we test for binocular modulation among the P, M, and K LGN neurons in an awake behaving macaque monkey. To do so, we presented drifting sine wave gratings at different contrast levels to one or both eyes while we recorded spiking activity from well-isolated and functionally characterized LGN single neurons from P, M, and K layers, respectively. Specifically, we showed gratings at zero (0.0), low (0.11-0.13), or high contrast (0.8-1.0) in the dominant eye and compared responses at each of these levels when no stimulus (0.0) or a high contrast grating was present in the non-dominant eye (0.8-1.0). Following data collection, we compared these LGN responses under monocular stimulation to responses to binocular stimulation as a function of stimulus contrast. We concluded that neuron(s) were sensitive to one eye only if we found no statistically significant difference between monocular and binocular stimulation. Conversely, if we found a significant difference between monocular and binocular stimulation, we concluded that neuron(s) were sensitive to both eyes. Across the LGN sample (n = 51), we observed a significant difference in the F1 response between binocular and monocular stimulation for high contrast stimulation only. However, individual units (14-26%) showed a significant difference between monocular and high contrast stimulation at all three dominant eye contrast levels. Overall, binocular modulation was modest, matching earlier reports in the anesthetized animal. Our results further corroborate earlier reports that binocular modulation is

more prevalent among M than P neurons, and we extend this finding to show that some K neurons are binocularly modulated as well.

1.3 Results

On each recording day, we inserted either a linear multicontact electrode array or single-contact tungsten electrode through a guide tube and lowered the electrode until the array was positioned in the LGN. After isolating one or more single units, we manually mapped the receptive field (RF) location for the neuron(s) under study by presenting drifting sine wave gratings or bars while the animal fixated on a fixation cross. We moved the drifting grating or bar on the left and right sides of the monitor to find the dominant eye and verify that responses were monocular. All stimuli were presented through a mirror stereoscope, aligned so that the animal could fuse what was presented to the left and right eyes, respectively.

After mapping the RF, we presented drifting sine-wave gratings at different contrast levels to the dominant eye of the neuron, the non-dominant (silent) eye, or both eyes over the RF location and recorded extracellular voltages. In addition, we collected responses to white and black luminance patches, as well cone-isolating stimuli. Offline, we extracted spiking activity from recorded extracellular voltage data (see **1.5 Methods**). In 26 recording sessions from one macaque, we isolated 51 single units. We identified unit each as a P, M, or K cell based on their responses to the cone-isolating stimuli, recording depth, their contrast response functions and their response transiency. This analysis yielded 32 P units, 14 M units, and 5 K units.

Binocular modulation among P, M, and K neurons

We were primarily interested in whether primate LGN neurons modulate under binocular stimulation. For all units, we varied the contrast shown to the dominant eye between 3 contrast levels: zero (0.0), low (0.08-0.13), and high contrast (0.8-1.0), and showed either no stimulus (0.0) or a high contrast stimulus (0.8-1.0) in the non-dominant eye. First, we looked at the mean responses to these stimulus conditions as a function of time for each the P, M, and K neurons (**Figure 1.1**).

Congruent with previous work (but see (Cheong et al., 2013, Zeater et al., 2015), we found that no LGN neurons responded to their non-dominant (silent) eye. Also congruent with previous research, responses across the contrast range led to linear responses for P neurons but not for M or K neurons. There was no striking difference between the average monocular and binocular response for any of the contrast levels. However, the average M response at high contrast showed a tendency for greater responses under binocular stimulation (*binocular facilitation*) relative to monocular stimulation, while the average K responses showed a tendency for lower responses under binocular stimulation relative to monocular stimulation (*binocular suppression*) (**Figure 1.1**).

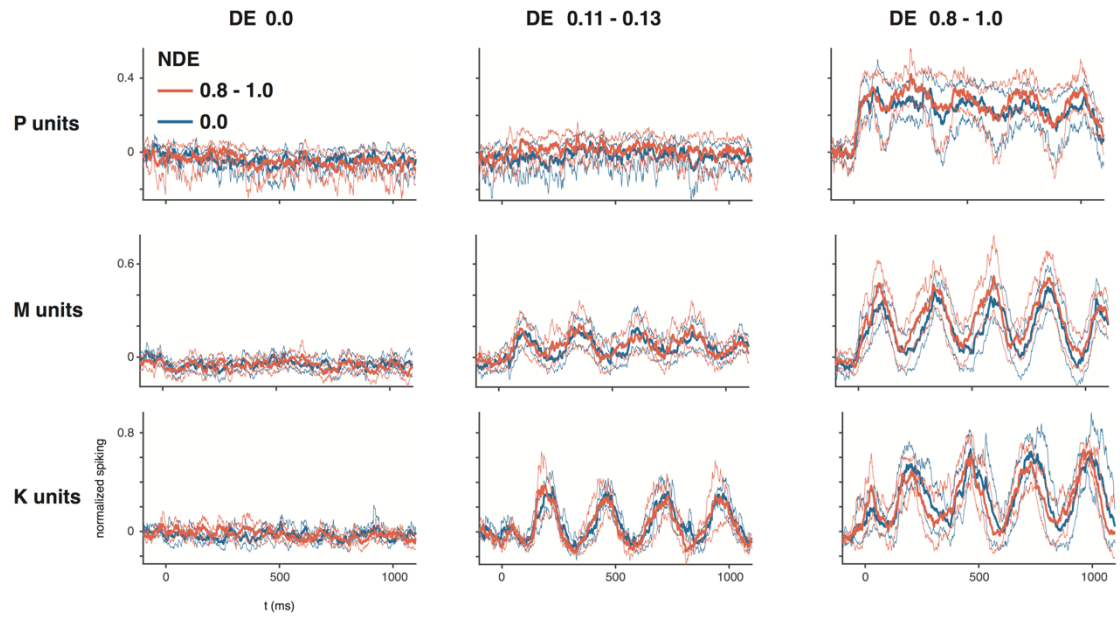

Figure 1.1 Mean responses of P, M, and K neurons to binocular and monocular stimulation.
Mean responses to either no stimulus (blue) or a high contrast grating (orange) presented to the non-dominant eye under increasing contrast levels in the dominant eye (columns) for P, M, and K groups (rows). Thin blue and orange lines mark 25% and 75% confidence limits on the means. N reported in **Table 1.1.**

We next considered the mean spiking response (F0) as well as the power of the response at the temporal frequency of the drifting grating (F1) across the entire stimulation period (0-1000 ms). For each unit, we normalized the response to each condition by subtracting the minimum monocular response (of the 3 monocular conditions—zero, low, and high), and dividing by the difference between the maximum and minimum monocular responses. We then averaged these normalized contrast responses across P, M, and K units (**Figure 1.2**). For F0 responses, we observed a tendency for binocular facilitation at high contrast for P and M neurons, and binocular suppression at low and high contrast for K units. For F1 responses, we observed a tendency for binocular facilitation for M units (but not P) at high contrast and binocular

suppression for K units at high contrast. However, there was considerable variability for these mean comparisons.

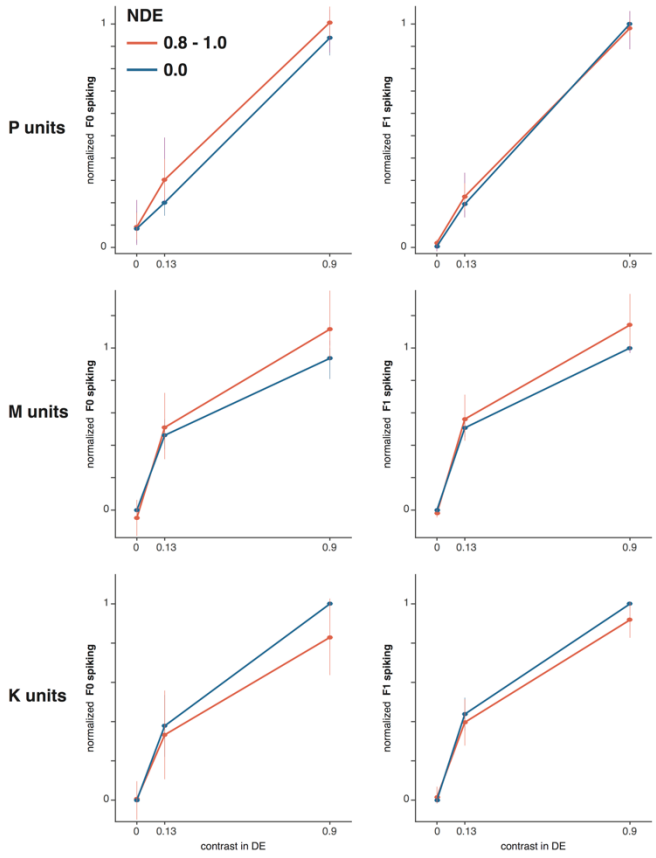

Figure 1.2 Mean contrast responses under monocular and binocular stimulation for P, M, and K units.
Mean normalized contrast response functions for either no stimulus (blue) or a high contrast grating (orange) presented to the non-dominant eye. Each unit was normalized to the maximum and minimum of the monocular (dominant eye) responses. Error bars represent 25% and 75% confidence limits on the means. N reported in Table **1.1.**

To approach these response comparisons between monocular and binocular stimulation more quantitatively, we used ROC analysis (see **1.5 Methods**) to test for significant differences between monocular and binocular stimulation for F0 and F1 responses. We observed significant modulation of F0 responses for P neurons only (**Table 1.1**, $\alpha = 0.05$). For F1 responses, we

observed significant modulation across all neurons and K neurons ($\alpha = 0.05$) as well as M neurons ($\alpha = 0.1$) at high contrast. P neurons also showed significant F1 modulation at zero contrast (see **Proportion of P, M, and K units modulate under binocular viewing**).

Table 1.1 Significance testing of P, M, and K neurons across contrast levels.
ROC analysis based on normalized contrast responses. Each unit normalized to the minimum and maximum of the monocular dominant eye responses. Each ROC analysis compared the response at the specified dominant eye contrast (columns) with either zero or high contrast in the non-dominant eye. Groups significant at $\alpha = 0.05$ in bold and italics, at $\alpha = 0.1$ in bold.

DE contrast		*0.0*		*0.11-0.15*		*0.8-1.0*	
		N total	*AUC*	N total	*AUC*	N total	*AUC*
F0	all	51	0.52	46	0.46	51	0.48
	P	32	0.59	29	0.59	32	***0.62***
	M	14	0.50	13	0.62	14	0.50
	K	5	0.44	4	0.59	5	0.66
F1	all	51	0.51	46	0.51	51	***0.59***
	P	32	***0.62***	29	0.57	32	0.56
	M	14	0.61	13	0.57	14	**0.61**
	K	5	0.50	4	0.53	5	***0.80***

Proportion of P, M, and K units modulating under binocular viewing

We decided to look at units on an individual basis to uncover the proportion of P, M, and K neurons that show significant binocular modulation. For each unit we ran an ROC analysis using F0 and F1 responses to compare monocular and binocular conditions at each contrast level (**Table 1.2**). Overall, there were fewer neurons that showed a significant difference for F0 responses than for F1 responses. For F1 responses, a quarter of neurons showed a significant effect at zero and low contrast in the dominant eye and 14% showed an effect at high contrast.

Table 1.2 Proportion of P, M, and K neurons showing significant binocular modulation. ROC analysis based on normalized contrast responses. Each unit normalized to the minimum and maximum of the monocular dominant eye responses. Each ROC analysis compared the response at the specified dominant eye contrast (columns) with either a zero or high contrast in the non-dominant eye. Groups with proportions 0.20 or greater are shown in bold.

DE contrast		0.0			0.11-0.15			0.8-1.0		
		N total	sig	proportion	N total	sig	proportion	N total	sig	proportion
F0	all	51	8	0.16	46	3	0.07	51	4	0.08
	P	32	3	0.09	29	1	0.03	32	3	0.09
	M	14	4	**0.29**	13	1	0.08	14	0	0.0
	K	5	1	**0.20**	4	1	**0.25**	5	1	**0.20**
F1	all	51	13	**0.26**	46	12	**0.26**	51	7	0.14
	P	32	8	**0.25**	29	6	**0.21**	32	4	0.13
	M	14	3	**0.21**	13	4	**0.31**	14	3	**0.21**
	K	5	2	**0.40**	4	2	**0.50**	5	0	0.0

We were particularly interested in the direction of binocular modulation, facilitation or suppression, for units showing a significant effect. For P, M, and K neurons, we counted the number of units showing a significant modulation that showed binocular facilitation and binocular suppression. Overall, we observed only binocular suppression for units showing significant F0 modulation (**Figure 1.3a**). For F1 responses, while several units in each LGN subgroup showed binocular suppression, there were others showing facilitation (**Figure 1.3b**). Eight P neurons showed significant modulation at zero contrast. A greater F1 response with no stimulus in the dominant eye would suggest that these neurons are either binocular (or respond to either eye), that there was a problem with the physical display, or that the statistical test yielded a false positive. A lower response, on the other hand, would suggest that the non-dominant eye suppresses the neuron's baseline firing rate (called *non-dominant suppression* in (Schroeder et al., 1990). Two of these neurons showed non-dominant eye suppression indeed, while the remaining six neurons showed facilitation ($\alpha = 0.10$, only two neurons at $\alpha = 0.05$). While the reasons that the six neurons respond to their non-dominant eye warrant further investigation, we

note that the mean power at the temporal frequency of the grating stimulus (4 Hz) does not suggest a strong visual response under binocular stimulation for each of these neurons (**Figure 1.4**).

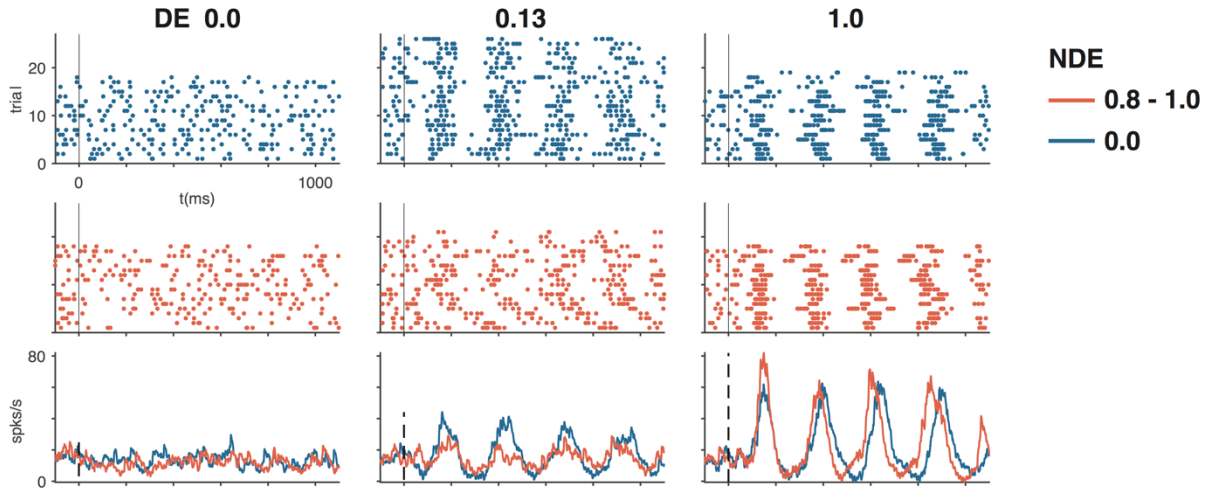

Figure 1.3 Example LGN unit showing significant binocular modulation.
Responses of example M unit to monocular and binocular stimulation at three different dominant eye (DE) contrast levels (columns). Rasters show spiking responses for each trial. Last row shows mean spike density functions for each condition. This unit showed a significant difference between monocular and binocular stimulation at low and high contrast levels ($\alpha = 0.1$).

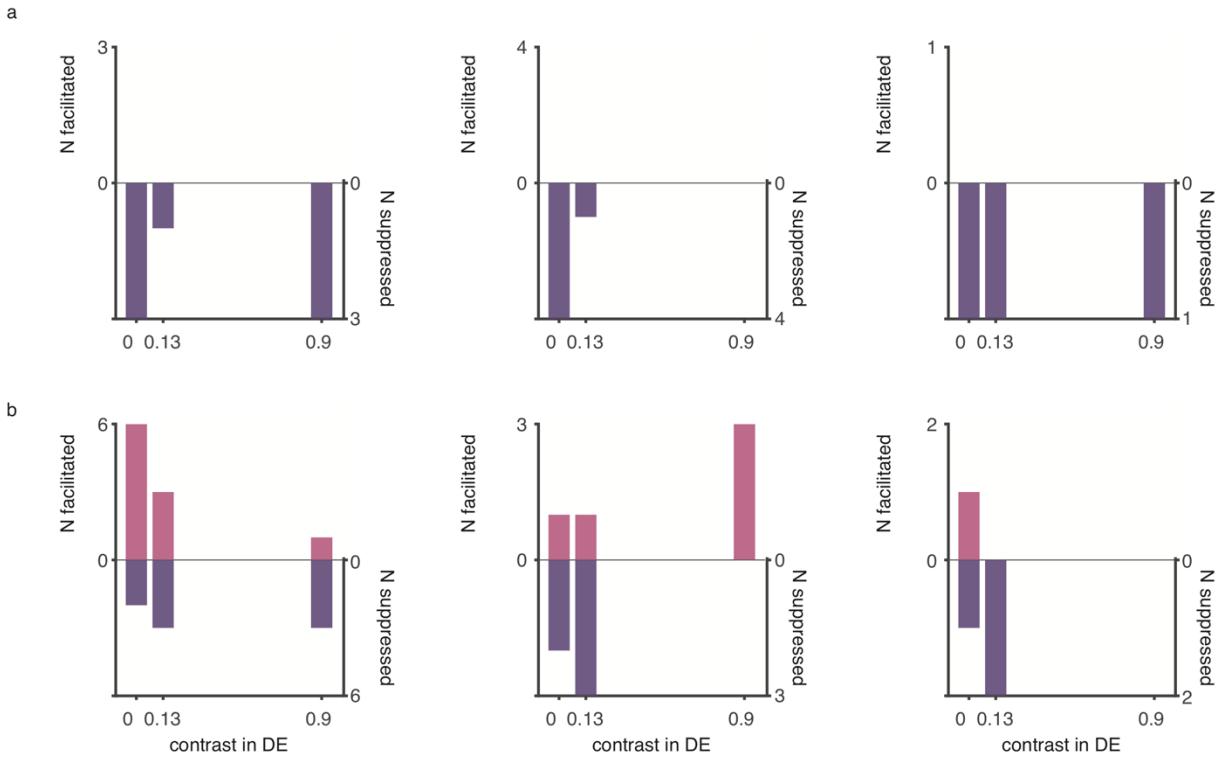

Figure 1.4 Number of units with significant binocular modulation showing binocular facilitation or binocular suppression for P, M, and K groups (from left to right).
Significance based on ROC analysis with $\alpha = 0.1$. (a) Values based on F0 responses. (b) Values based on F1 responses.

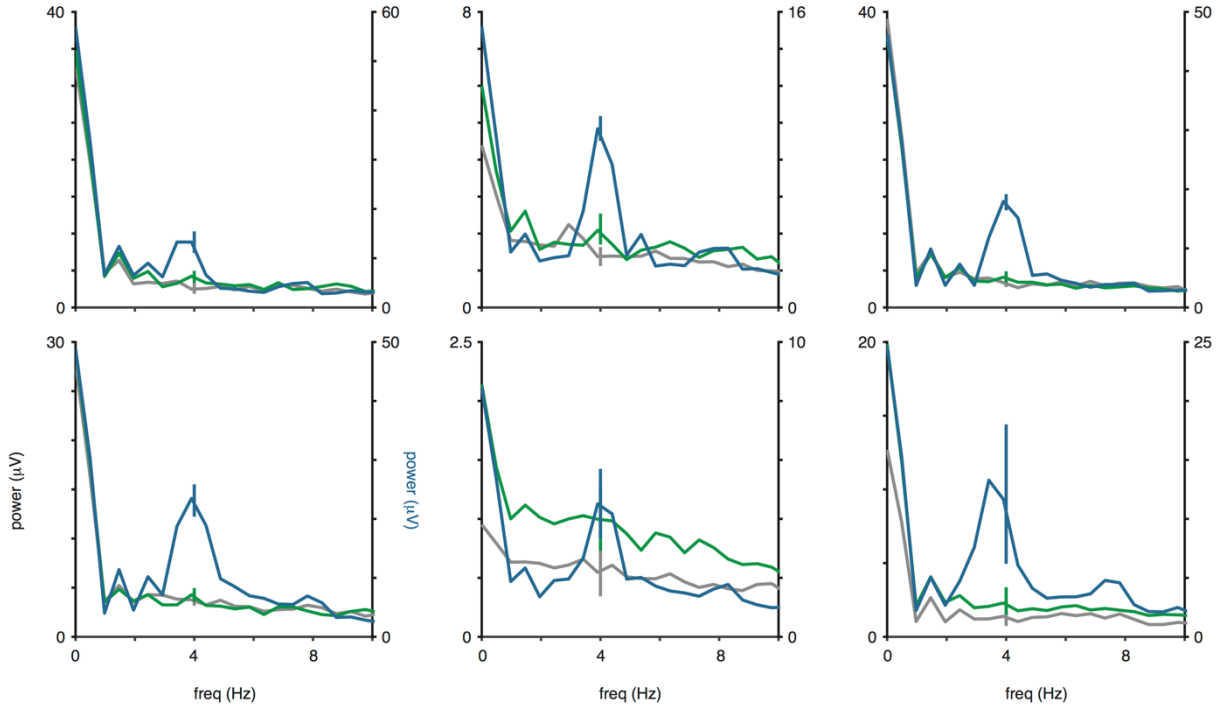

Figure 1.5 Power spectral density for six P units showing significant binocular modulation at zero contrast in the non-dominant eye.
Mean power of the spiking responses for no stimulus (gray) and non-dominant eye stimulation (green) conditions at high contrast (left y-axis), and for dominant eye high contrast stimulation (right y-axis) for each of the six significant P units that showed greater responses for the binocular condition at zero contrast. Error bars represent 95% confidence intervals on the means.

1.4 Discussion

We aimed to determine whether LGN neurons are sensitive to both eyes. Across P, M, and K neurons, there were no striking differences in the magnitude of the responses between monocular and binocular (high contrast stimulus in the non-dominant eye) conditions at any stimulus contrast level. However, there were small differences in the mean normalized contrast responses for each group (**Figure 1.2**). Based on those mean differences (**Table 1.1**), we set out to determine the fraction of neurons that were sensitive to both eyes (**Table 1.2**).

About 30% of M neurons and 20% of P neurons showed significant modulation of the F1 response at low contrast. The modulation at low contrast is interesting in light of models of binocular combination in which the two eyes have an antagonistic relationship at monocular stages (Ding and Sperling, 2006). Most of the units with a significant effect at medium contrast showed binocular suppression. Binocular suppression is what would be predicted if the two eyes' signals inhibit one another. Specifically, if the non-dominant eye is stimulated at high contrast and the dominant eye of the neuron at low contrast, the strength of the inhibition from the non-dominant eye might more easily suppress the response of the neuron at lower contrast.

No M units and only two P units with significant modulation showed binocular suppression at high contrast. In some ways, this is surprising if we are to expect that at some point in processing binocular stimuli, the visual system accounts for the fact that both eyes are stimulated, resulting in normalization (by suppression) of the signals for each eye. It is possible that most binocular contrast normalization occurs at the next step in the visual hierarchy, in V1. If the signals from the two eyes have an antagonistic relationship at the level of the LGN, it makes sense if there were less suppression when the dominant eye is driven by a high contrast stimulus than at lower contrast levels. In other words, activation by a high contrast stimulus might make a neuron less susceptible to any suppressive effect from the non-dominant eye.

Cheong et al. (2013) and Zeater et al. (2015) showed that ~30% of K neurons in the marmoset are binocular. As K layers are less readily accessible in macaques, we recorded only 5 K units. One of these units showed a significantly greater response with a stimulus in the non-dominant eye relative to no stimulus. However, given the small sample size, more work is needed to determine if some K neurons in the macaque are binocular as well.

Overall, the amount of binocular modulation in the LGN was not overwhelming. However, stimulation of the non-dominant eye affected (F1) responses of about 25% of all neurons (**Table 1.1**). In other words, it may be unwise to consider that LGN neurons are strictly sensitive to one eye, and some binocular interactions seems to occur in this structure indeed. Because this modulation is small and affects only a subset of the neural population, it will take larger sample sizes to better determine at which contrast levels binocular interactions in this structure occur. Importantly, the source of this binocular modulation remains open question. Specifically, whether the binocular modulation in the LGN occurs from extensive feedback projections from cortex, or from interlaminar connections in the LGN (Campos-Ortega et al., 1968) is unclear.

1.5 Methods

Surgical procedures

The monkey was implanted with a custom-designed plastic head holder and a plastic recording chamber (Crist Instruments) in two separate surgeries under sterile conditions. The animal was administered isoflurane anesthesia (1.5-2.0%). Then, the animal was positioned in a stereotax while vital signs, including blood pressure, heart rate, SpO_2, CO_2, respiratory rate and body temperature were continuously monitored throughout the whole procedure. During surgery, the head holder or the recording chamber was attached to the skull using transcranial ceramic screws (Thomas Recording) and self-curing dental acrylic (Lang Dental Manufacturing). A craniotomy was performed above the LGN (0.7 anterior-posterior; 1.2 medial-lateral) concurrent with the positioning of the recording chamber. Following the procedure, the animal was given analgesics and antibiotics, and closely observed by researchers, facility veterinarians and animal care staff for at least three days.

Data acquisition and pre-processing

During each recording session, either a standard single-contact tungsten microelectrode (FHC) or a linear multielectrode array (U-Probe, Plexon Inc., Vector Array, NeuroNexus) with either 24 or 32 contacts of 0.1 mm inter-contact spacing was inserted into the brain through a guide tube. Extracellular voltage fluctuations (0.5 Hz – 30 kHz) were recorded inside an electromagnetic radio frequency-shielded booth. These signals were amplified, filtered and digitized using a 128-channel Cerebus® Neural Signal Processing System (NSP; Blackrock Microsystems). A broadband (0.3 Hz – 7.5 kHz) signal sampled at 30 kHz and a low frequency-dominated signal (0.3 Hz – 500 Hz) sampled at 1 kHz was saved for offline analysis. The NSP also recorded the output of a photodiode signal (OSI Optoelectronics) placed on the monitor to track stimulus-related events at 30 kHz. The NSP further digitized the output of the optical eye tracking system (EyeLink II) at 1 kHz, as well as digital event markers sent from the behavioral control system (MonkeyLogic, (Asaad et al., 2013). Both the photodiode signal and event markers were used to align the neural data with visual and behavioral events.

We extracted single neurons with KiloSort, an open-source unsupervised machine-learning algorithm for spike-sorting (Pachitariu et al., 2016), using the default parameters for sorting and cluster merging, except for the spike threshold which we set to 2.5 standard deviations. We extracted 1 ms of data around each KiloSort'ed spike time from the original broadband signal for each simultaneously recorded electrode contact. We then averaged across impulses to create a spatiotemporal map of the spike waveform (time x electrode contacts). The region of the spatiotemporal waveform map that exceeded +/- 30% of maximum modulus had to span fewer than 3 electrode contacts (0.3 mm) and 0.9 ms to be included in the study. Neurons

that met these criteria were localized to the electrode contact where they evoked the largest amplitude.

Spike rates were downsampled to 1 kHz. For each neuron, spike times were converted to a time-varying signal (spike density function) using 0 to represent time points without a spike and 1 for time points where a spike was detected. This time-varying signal was then convolved using a Poisson distribution resembling a postsynaptic potential (Sayer et al., 1990), with the spike rate (R) computed at time (t):

$$R(t) = \left[1 - \exp\left(-\frac{t}{\tau_g}\right)\right] * \left[\exp\left(-\frac{t}{\tau_d}\right)\right]$$

where τ_g and τ_d are the time constants for growth and decay, respectively. Values of 1 and 20 for τ_g and τ_d respectively were used based on a previous study (Thompson et al., 1996).
the signal was multiplied by the sampling frequency to convert units to spikes per second.

Eye position was measured continuously using a commercially eye tracker (see details below).

Visual display

Stimuli were presented on a linearized CRT monitor with a refresh rate of either 60 Hz (resolution 1280 × 1024) or 85 Hz (resolution 1024 × 768) (mode: 85 Hz). These visual stimuli were generated using custom-written code for MonkeyLogic (Asaad et al., 2013) in MATLAB (R2012-2014, The MathWorks) on a PC (Dell, Windows 7 or Windows 10) with a NVIDIA graphics card. Animals viewed all stimuli through a custom-built mirror stereoscope that employed infrared-light passing cold mirrors (Edmund Optics). The animal, mirrors and monitor were positioned so that the animal's right eye viewed stimuli presented on the right side of the monitor and the animal's left eye viewed stimuli on the left side of the monitor. To prevent light

scatter from one side of the monitor to the opposing eye, a black, non-reflective septum was placed between the monitor and the back side of the mirrors, effectively dividing the left and right sides of the apparatus.

Infrared-light sensitive cameras, placed directly behind the cold mirrors on the stereoscope, were used to track gaze position with commercially available eye tracking software (Eye Link II). Gaze position was converted to an analog signal and inputted to MonkeyLogic/MATLAB (NIDAQ PCI-6229) at 1 kHz. At the beginning of each recording session, the stereoscope was calibrated to facilitate binocular fusion of the left and right sides of the monitor using a behavioral task that relied on acquiring the same gaze position for corresponding locations on each side of the monitor (Maier et al., 2007, Maier et al., 2008). To further aid fusion, an oval aperture or set of intersecting circles in each corner was displayed at the edge of each half-screen.

RF mapping

When we encountered a neuron that we believed to be in the LGN based on electrode position, depth, visual response to light, we mapped its receptive field using a receptive field app (RFspotter, CocoaSpikes) running on an iPad (Apple) and mixed the output of the iPad through a VGA cable (*spark d-fuser, *SPARK LIVE LTD) with a fixation displayed with MonkeyLogic. We used a Cartesian grating and/or a bar of white light to manually map the receptive field. First, we determined that the neuron responded to stimulation of one eye only by moving a stimulus to the left or right side of the display. Then, we homed in on the location of the receptive field in the dominant eye of the neuron.

Visual stimulation

We trained each animal trained to fixate on a small (0.2 degrees of visual angle, dva) cross presented at the center of each eye's visual field. Animals held fixation for several (< 5) seconds while we presented stimuli. If the animals successfully held fixation within a 1 dva radius around the fixation cross for the entire stimulus sequence, liquid juice reward was delivered. If the animals broke fixation or blinked, the trial was aborted and a short timeout (1-5 s) was given before the start of the next trial.

MRI

Animals were anesthetized using the same procedure as outlined under *Animal Care and Surgical Procedures*. Anesthetized animals were placed inside a Philips Achieva 7T MRI scanner at the Vanderbilt University Institute of Imaging Science and remained anesthetized throughout the duration of the scan. Vital signs were monitored continuously. T1-weighted 3D MPRAGE scans were acquired with a 32-channel head coil equipped for SENSE imaging. Images were acquired using a 0.5 mm isotropic voxel resolution with the following parameters: repetition time (TR) 5 s, echo time (TE) 2.5 ms, flip angle 7°.

Data analysis

We only used KiloSort'ed units that showed a significant response to the dominant eye at the temporal frequency of the drifting grating ($\alpha = 0.05$). The mean firing rate of the neuron (F0) across the whole stimulation period had to be at least 5 spikes per second or greater. For every condition used in the analysis, there had to be at least 10 trials for that condition.

To compute normalized spiking, we transformed the mean responses for each neuron to z-scores. Specifically, we first subtracted their baseline firing rate. Then, we divided this value by the difference between the maximum firing rate to stimulation of the dominant eye and the baseline firing rate. Similarly, we normalized contrast response data across conditions for each neuron by subtracting the minimum monocular response from the mean response at each contrast level. Then, we divided each resulting value by the difference between the maximum monocular response and minimum monocular response.

We used receiver-operating characteristics (ROC) analysis (Green and Swets, 1966) to determine whether there was a significant difference between stimulation conditions at the group and single-neuron level. Specifically, we ran an ROC analysis with twelve thresholds using data across units (group level) or trials (single units). All data based on the entire stimulation period (0-1000 ms). Statistical significance was determined by comparing the area under the curve to a bootstrapped distribution of area under the curve values computed on 10,000 repetitions of shuffled data.

2. Binocular modulation of monocular V1 neurons

2.1 Summary

In the last chapter, I investigated whether LGN neurons, that respond to one eye only, modulate under binocular stimulation. Overall, the number of single LGN units that showed some modulation, while worthy of reporting, was somewhat underwhelming, especially considering that the source of that modulation (local or cortical) is yet to be determined. If we are interested in determining where the signals from two eyes first interact, I think we must look elsewhere. For that reason, in this chapter, I investigate binocular interactions in the primary visual cortex, the main target of the LGN. The work of many researchers has established that the primary visual cortex is home to many binocular neurons (driven by stimulation of either eye) as well as monocular neurons (driven by stimulation only one eye).

Monocular neurons are most prevalent in the main input layers of V1 while binocular neurons dominate the layers above and below. This observation has given rise to the idea that the two eyes' signals remain separate until they converge outside V1's input layers. In this chapter, I focus specifically on monocular neurons and neurons in layer 4 (L4) as they are likely some of the first neurons in V1 to receive input from the LGN following visual stimulation.

Here, we show that despite responding to only one eye, monocular neurons in all layers, including the input layers, of V1 discriminate between stimulation of their driving eye alone and stimulation of both eyes. Some monocular V1 neurons responses are significantly greater when both eyes are stimulated, however, most V1 monocular neurons respond less to binocular stimulation. To home in on the source of binocular modulation in L4, we compared the latency of binocular modulation of neurons in all layers. In L4, facilitation occurred at the onset of the

visual response, and could be explained by converging thalamocortical inputs. Spiking suppression first occurred in the upper layers of V1, suggesting that the bulk of V1 binocular modulation involves cortical inhibition. These findings, combined, suggest that binocular signals arise at an earlier processing stage than previously appreciated as even so-called monocular neurons in V1's input layers encode what is shown to both eyes.

2.2 Introduction

One of the most prominent features differentiating humans and other primates from their closest ancestors is that their eyes face to the front. One consequence of front-facing eyes is that their respective views largely overlap. Due to this overlap, primate brains need to combine the two eyes' views into a singular view (Parker and Cumming, 2001). For this binocular combination to occur, the signals from the eyes need to meet at some point along the primary visual pathway. While prior research has narrowed down possible locations underlying this convergence, we do not know the exact meeting point of the two eyes' signals.

Primate retinae do not receive feedback from the visual structures to which they project (Reperant et al., 1989). This absence of feedback suggests that the output of each eye is entirely separate from that of the other. Following visual transduction in the retina, the monocular signals from retinal ganglion cells mainly project to the lateral geniculate nucleus of the thalamus (LGN) (Casagrande and Boyd, 1996). For almost all primate LGN neurons, visually stimulating one eye leads to a response (dominant eye) while stimulating the other does not (non-dominant or silent eye). In other words, stimulation of each eye separately evokes responses in two mutually exclusive groups of LGN neurons. This segregation of eye-specific responses within the LGN

suggests that the formation of a binocular signal occurs at a subsequent stage of visual processing.

As the next step in the primary visual pathway, LGN neurons primarily project to the primary visual cortex (V1) (Casagrande and Boyd, 1996). Neighboring LGN neurons that respond to stimulation of the same eye tend to innervate the same neurons in V1 layer 4 (in primates termed layer 4C, or L4) (Hubel and Wiesel, 1972). In line with this connectivity, many L4 neurons do not respond when a stimulus is shown to one of the eyes (Hubel and Wiesel, 1968, Blasdel and Fitzpatrick, 1984). L4 neurons converge onto neurons in the layers above (Douglas, 1989), and most V1 neurons outside of L4 respond to stimuli shown to both eyes (Hubel and Wiesel, 1968). These findings have led to the popular interpretation that the signals from each eye remain largely segregated in L4 of V1.

The prevailing model of binocular convergence builds on all of these findings by proposing that V1 neurons in superficial layers (L2/3) of V1 receive inputs from both L4 neurons that respond to one eye as well as from L4 neurons that respond to the other eye (Hubel and Wiesel, 1972). This model explains why most L2/3 neurons respond to either eye (to varying degrees). L2/3 neurons project to neurons in the lower layers (L5/6) of V1, which also respond to stimulation of either eye (Casagrande and Boyd, 1996).

Notably, the model outlined above assigns no significant role to the fact that L4 neurons also receive inputs from other V1 neurons in addition to the inputs from the LGN (Ahmed et al., 1994, Binzegger et al., 2004). Yet, these intracortical connections raise the interesting possibility that even monocular L4 neurons can encode a de-segregated binocular signal. This situation could arise if the firing rates of monocular neurons change reliably when both eyes are stimulated simultaneously. In other words, even though stimuli shown to their non-dominant eye

alone do not evoke responses, monocular neurons might systematically modulate responses when stimuli are shown to both eyes simultaneously. Indeed, previous studies showed that some monocular V1 neurons are tuned for interocular disparity, and thus sensitive to both eyes (Ohzawa and Freeman, 1986, Prince et al., 2002, Read and Cumming, 2004). However, whether such neurons can also be found in L4 is unclear because prior experiments lacked appropriate laminar resolution.

Here we use laminar neurophysiology to determine whether the signals from the two eyes remain fully segregated in L4 of V1. To do so, we examined the extent to which neurons across all layers of V1 are sensitive to one or both eyes. Specifically, we employed linear multielectrode arrays to record V1 laminar neural responses in macaques that viewed stimuli with one eye, the other eye or both eyes simultaneously. We found that binocular neurons, which significantly responded to either eye (paired t-test, $\alpha = 0.05$), comprised 78% of V1 neurons across all layers. In line with earlier work, we located the bulk of monocular neurons, which responded to only one eye (paired t-test, $\alpha = 0.05$), to L4. Strikingly, we found that, although activated by only one eye, L4 monocular neurons responded significantly differently when both eyes were stimulated simultaneously. These findings suggest that, despite their name, monocular neurons in the primary input layers of V1 actually encode both eyes' views. Thus, binocular signals arise at an earlier processing stage than commonly thought.

2.3 Results

In each session, we penetrated the *dura mater* over V1 with a linear multielectrode array and positioned the array so that its contacts spanned the depth of cortex (**Figure 2.1a**) (Maier et al., 2010, Dougherty et al., 2017, Cox et al., 2017). While we recorded extracellular voltages, we displayed visual stimuli through a mirror stereoscope to stimulate the eyes independently (**Figure 2.2a**, **upper panel**). After mapping the population receptive field (RF) location for the neurons under study (**Figure 2.1b**, see **2.5 Methods**), we presented static sine-wave gratings over the RF location to the dominant eye of the neuron, the non-dominant eye, or both eyes (**Figure 2.2a**, **lower panel**; **Figure 2.2b**). Following data collection, we extracted spiking activity from the extracellular voltage measurements (see **2.5 Methods**).

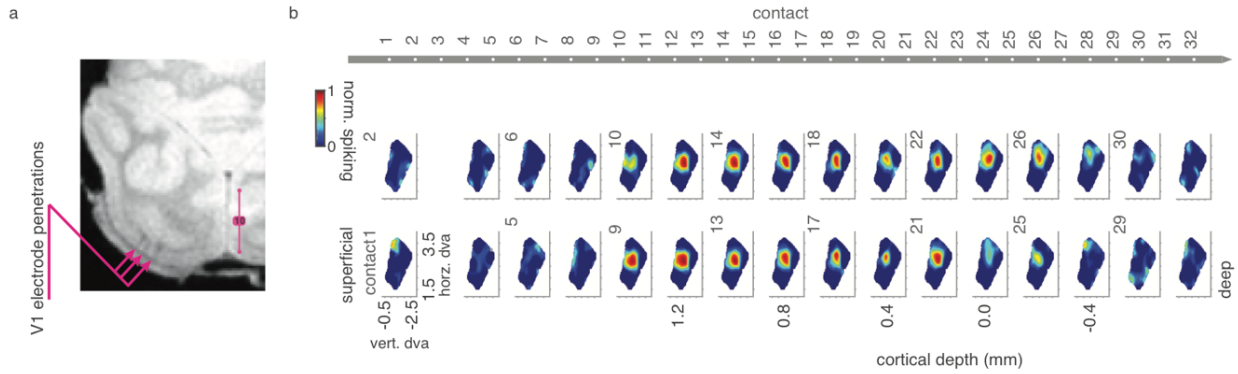

Figure 2.1 V1 Laminar alignment.
(a) Magnetic resonance image (axial slice). Arrows point to the susceptibility artifact caused by cerebrospinal fluid in the area where electrodes were located.
(b) Example response field matrices extracted from multiunit activity from 32 electrode contacts during a single electrode penetration of V1. Each map is Gabor-filtered, and z-score transformed.

Responses of V1 monocular neurons modulate during binocular stimulation

We collected visual responses for 290 neurons throughout all V1 layers across both animals (261 from E48, 29 from I34). Congruent with previous work (Hubel and Wiesel, 1968, Blasdel and Fitzpatrick, 1984), stimulation of either eye led to a statistically significant response (paired t-

test, $\alpha = 0.05$) for the majority of V1 neurons (n = 226). Monocular neurons that significantly responded to only one eye (paired t-test, $\alpha = 0.05$) made up just 22% of the population (n = 64).

For a subset of neurons in our sample (n = 138), we also collected responses to congruent (dioptic) stimulation of both eyes simultaneously. We reasoned that if monocular neurons were truly sensitive to only one eye, their responses should not differ between stimulating their dominant eye (monocular stimulation) or stimulating both eyes at the same time (binocular stimulation). Instead, we found that monocular neurons showed a significant difference between binocular and monocular stimulation. Specifically, monocular neurons exhibited a smaller median response to binocular stimulation than to dominant-eye stimulation (n = 33, two-tailed Wilcoxon signed-rank test, p = 0.029; **Figure 2.2c**, **Table 2.1**). When we redefined monocular neurons using an even stricter criterion that excluded any neuron which showed a (nonsignificant) change from baseline for silent eye stimulation, we observed the same effect (n = 8, two-tailed Wilcoxon signed-rank test, p = 0.0078; **Figure 2.3a**). We verified that fixational eye movements did not affect this result (n = 33, two-tailed Wilcoxon signed-rank test, p = 0.0076; **Figure 2.3b**). These results combined suggest that monocular V1 neurons can encode a binocular signal.

The prevailing model of binocular processing suggests that signals from each eye remain separate in L4 of V1 before merging to a binocular signal in the layers above (Hubel and Wiesel, 1972). If the binocularly modulating monocular neurons that we recorded were all located outside L4, our results would fit the model. If, on the other hand, monocular neurons in L4 showed sensitivity to both eyes, the model would require revision. Given this distinction, we were curious to locate the binocularly modulating neurons within the laminar microcircuit.

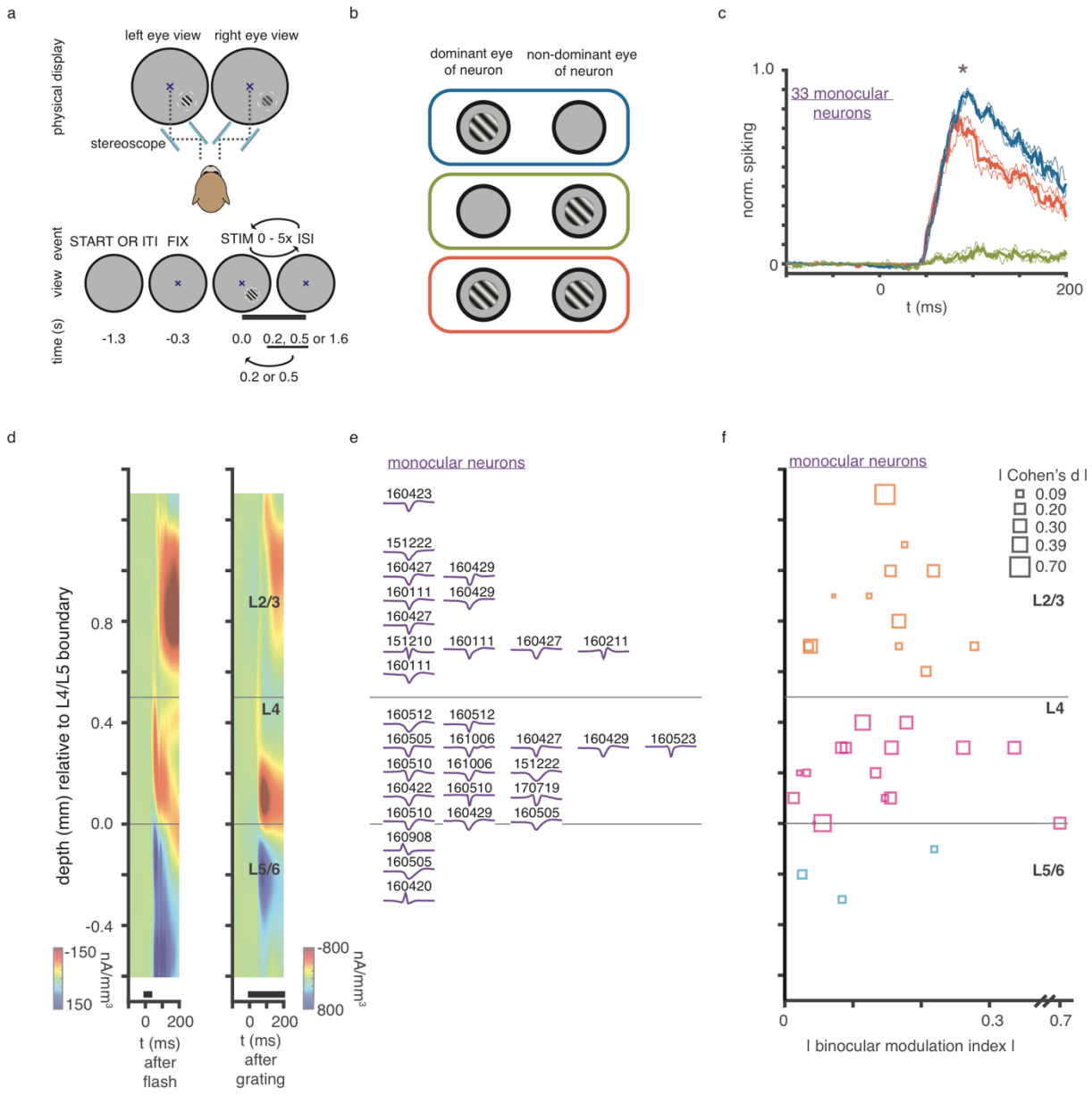

Figure 2.2 Responses of V1 Monocular Neurons Modulate During Binocular Stimulation.

(a) Upper panel: Top-down view of experimental setup. Visual stimuli were presented to fixating macaque monkeys at the mapped receptive field location (white dashed circles) through a mirror stereoscope that consisted of two pairs of mirrors (blue lines). The mirrors were angled in a way that each eye of the animal saw the left and right halves of the monitor, respectively (dashed black lines). Lower panel: Schematic representation of the time series of stimulus presentation. Animals were rewarded for fixating on a central screen location while grating stimuli were presented in one or both eyes (see **2.5 Methods** for details).
(b) On every stimulus presentation, a sine-wave grating was presented over the RF location to either the dominant eye of the neuron (blue), non-dominant eye (green), or both eyes (orange).

Eye dominance was determined by statistically comparing the responses to stimulation of the left eye and right for each neuron (see **2.5 Methods**).
(c) Median normalized spiking responses of monocular V1 neurons to the dominant eye (blue), both eyes (orange), and the non-dominant eye (green). Binocular stimulation significantly altered the monocular neurons' responses compared to stimulation of their dominant eye (two-tailed Wilcoxon signed-rank, $p = 0.029$, $N = 33$). Responses to the non-dominant eye alone were non-significant at $\alpha = 0.05$. Thin lines represent the 25% and 75% confidence limits on the median (chosen to account for the fact that the data was not normally distributed).
(d) Left panel: Mean CSD (baseline-corrected, smoothed and interpolated) response to a full-field white flash ($N = 33$ penetrations, both animals). Right panel: Same as left panel for the response to a sine-wave grating presented at the RF location ($N = 45$ penetrations, both animals). Current sinks, which are linked to excitatory synaptic activity, are indicated in red. Current sources, which are caused by passive return currents, are shown in blue. 0 mm marks the L4-L5 border, as estimated by the bottom of the initial current sink that is evoked by the geniculo-cortical volley of activation (see **2.5 Methods**). Gray horizontal lines mark the estimated boundaries of L4.
(e) Average spike waveforms for the monocular neurons shown in (c) at their relative position of cortical depth. Numbers indicate date of collection. Two neurons included in (c) are not shown because we lacked appropriate laminar resolution (see **2.5 Methods**).
(f) Magnitude of binocular modulation across cortical depth for neurons shown in (e). Marker size indicates rectified Cohen's d for each monocular neuron.

Table 2.1 Fraction of neurons with significant binocular response modulation at high contrasts, ROC analysis with sliding 10 ms windows, $\alpha = 0.05$.

	15 consecutive, significant windows	***10 consecutive, significant windows***	***20 consecutive, significant windows***
binocular neurons	80/105	84/105	76/105
monocular neurons	22/33	23/33	20/33
suppressed monocular neurons	18/23	19/23	18/23
facilitated monocular neurons	4/10	4/10	2/10
liberal group of monocular neurons	33/50	34/50	31/50
liberal group of suppressed monocular neurons	23/31	24/31	23/31
liberal group of facilitated monocular neurons	10/20	10/20	8/20

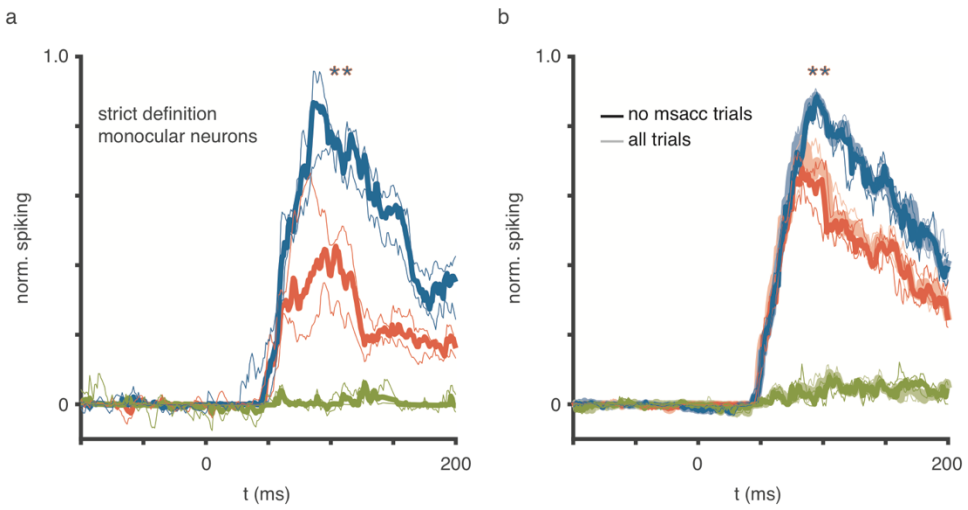

Figure 2.3 Binocular modulation upholds with a stricter criterion for defining monocular neurons, occurs in L4 and is unrelated to microsaccades.
(a) Median responses of monocular neurons that were deemed completely unresponsive to the non-dominant eye using a stricter criterion (N = 8). Binocular modulation is significant (two-tailed Wilcoxon signed-rank, p = 0.0078). All conventions as in **Figure 2.2**.
(b) Median responses of monocular neurons (same as **Figure 2.2c**, N = 33) to binocular (orange), dominant eye (blue), and non-dominant eye (green) stimulation. Lighter colors represent responses using all trials. Darker colors indicate subset of trials without microsaccades. All other conventions as in **Figure 2.2**. Binocular modulation remains significant with all microsaccade-containing trials excluded (two-tailed Wilcoxon signed-rank, p = 0.0076).

Even monocular neurons in V1's primary input layer modulate under binocular viewing

We used current source density analysis (CSD; see **2.5 Methods**) to estimate the location of each neuron relative to the L4-L5 boundary (marked as 0.0 in **Figure 2.2d**). Congruent with previous work (Hubel and Wiesel, 1968, Hubel and Wiesel, 1972), we found that L4 contained the majority of monocular neurons (within 0.0 to 0.5 mm above the L4-L5 boundary), with smaller fractions of monocular neurons in the layers above and below (**Figure 2.2e**). Importantly, the waveforms of monocular neurons did not resemble the tri-phasic waveforms associated with axonal spikes (Lemon and Prochazka, 1984), suggesting that we did not mistake LGN afferents for V1 neurons (**Figure 2.2e**). Furthermore, the characteristics of monocular neurons in our sample resembled those of previous reports in two important aspects: First, most binocular

neurons (87%) that we recorded showed significant orientation tuning, whereas almost half of monocular neurons (42.4%) did not (**Figure 2.4b**) (Hubel and Wiesel, 1968, Hubel and Wiesel, 1977, Blasdel and Fitzpatrick, 1984). Second, monocular neurons had significantly higher baseline firing rates than binocular neurons (two-sample t-test, $t_{288} = 4.83$, $p = 2.22 \times 10^{-6}$) (**Figure 2.4c**), congruent with previous work (Snodderly and Gur, 1995)but see (Blasdel and Fitzpatrick, 1984).

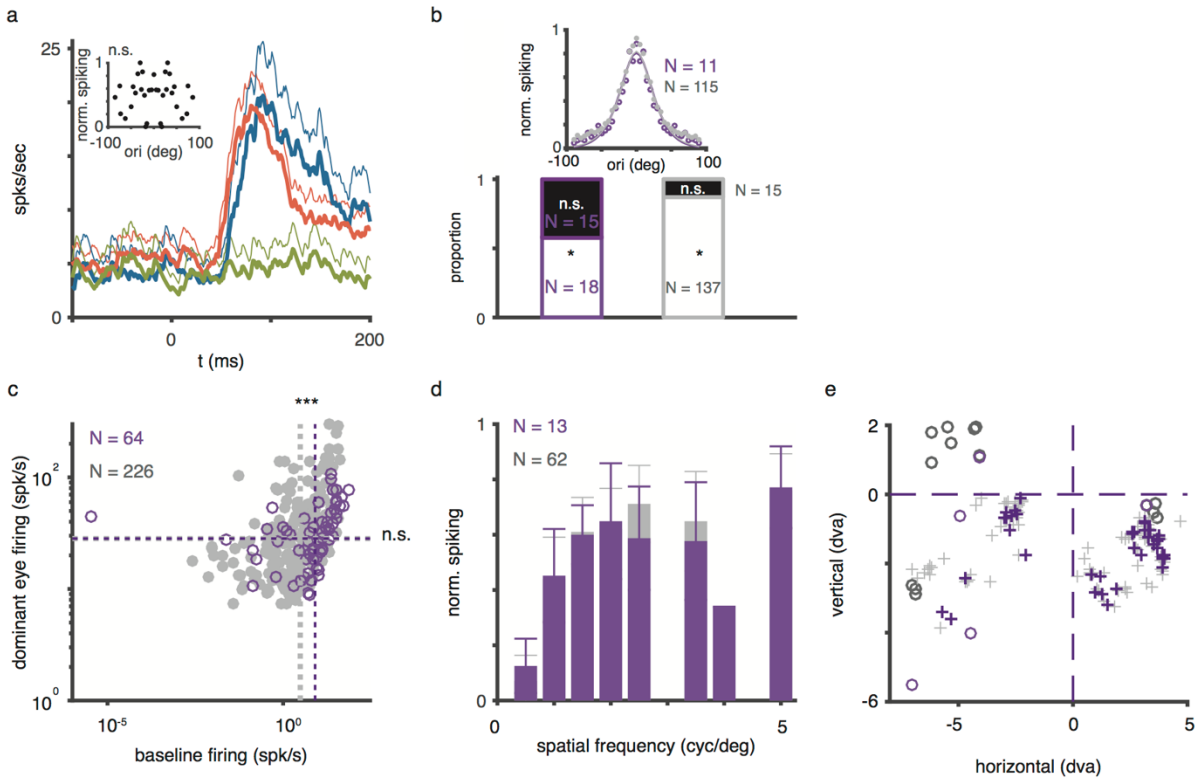

Figure 2.4 Orientation tuning, spatial frequency tuning, firing rate characteristics, and RF locations of monocular and binocular V1 neurons.

(a) L4 non-orientation tuned monocular neuron showing significant binocular modulation. Median responses to binocular (orange), dominant eye (blue), and non-dominant eye (green) stimulation (thick lines). Significance assessed via ROC analysis ($\alpha = 0.05$). Thin lines represent 95% confidence bound. Inset: Normalized responses to high contrast gratings shown at varying orientations. There was no significant effect of orientation (ANOVA, $p > 0.05$).

(b) Top: Mean orientation tuning functions for monocular (purple) and binocular units (gray), using Gaussian fit. Units without a significant effect for orientation (ANOVA, $p < 0.05$) and a Gaussian fit with r^2 less than 0.5 were excluded from analysis. Bottom: Fraction of significant orientation-tuning among monocular neurons (left) and binocular neurons (right).
(c) Baseline firing rate versus dominant eye response for monocular and binocular neurons, respectively. Color coding as in (b). The baseline firing rate of monocular neurons was significantly higher than that of binocular neurons (two-sample t-test, $t_{288} = 4.83$, $p = 2.22 \times 10^{-6}$).
(d) Monocular and binocular neurons showed the same spatial frequency tuning (multiple two sample t-tests, all $p > 0.05$). Errors bars represent SEM.
(e) Receptive field center locations for monkeys I34 (circles) and monkey E48 (crosses). Color coding as in (b).

To determine if monocular neurons in L4, specifically, modulated under binocular stimulation, we quantified the binocular modulation shown in **Figure 2.2c** for each monocular neuron. Specifically, we took the difference in firing rate between monocular (dominant eye) stimulation and binocular stimulation and divided by the sum of these two values. This analysis revealed that both eyes affected the activity of most L4 monocular neurons (**Figure 2.2f**, see also **Table 2.1**). Statistical hypothesis testing showed that 11 of the 17 monocular neurons inside L4 (64.7%) exhibited a significant response difference between monocular (dominant eye) stimulation and binocular stimulation (ROC analysis, $\alpha = 0.05$; **Figure 2.5a**, **2.5 Methods**). Outside of L4, 11 of the monocular neurons (68.8%) exhibited significant binocular modulation as well.

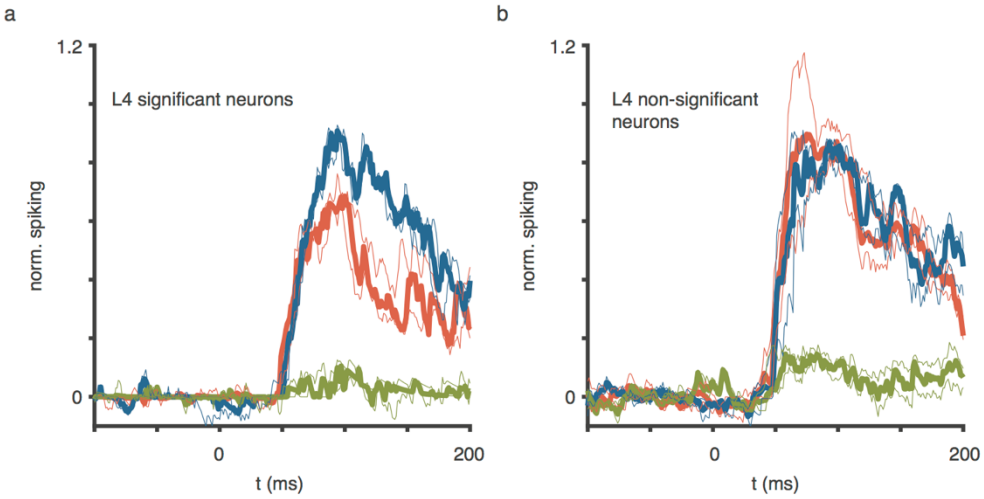

Figure 2.5 Responses of L4 neurons with significant binocular modulation effect.
(a) Median responses of L4 monocular neurons (n = 11) that show a significant difference between binocular and dominant eye stimulation based on ROC analysis ($\alpha = 0.05$). All other conventions as in **Figure 2.2**.
(b) Same as (a) for L4 monocular neurons (N = 6) that did not show a significant difference between binocular and dominant eye stimulation.

We were interested in investigating the relationship between orientation tuning and binocular modulation because prior work suggested that some L4 neurons receiving direct thalamic inputs show less selective orientation tuning than other V1 neurons (Hubel and Wiesel, 1968). Due to the experimental time limitations that come with working with awake animals, we were only able to reliably determine the orientation tuning for five L4 monocular neurons. Four of these neurons showed a significant effect for orientation (ANOVA, $p < 0.05$). Three neurons of those four neurons also showed a significant effect of binocular modulation (ROC analysis, $\alpha = 0.05$). Importantly, the un-tuned, monocular L4 neuron also showed significant binocular modulation (**Figure 2.4a**). Thus, stimulation of both eyes affects even un-tuned, monocular L4 neurons.

Binocular modulation of V1 monocular neurons is both suppressive and facilitatory

Visual inspection of **Figure 2.2c** suggests that across the population binocular stimulation suppresses responses of V1 monocular neurons compared to dominant eye stimulation alone. We wondered how many (if any) individual monocular neurons show either no binocular suppression, or enhanced (facilitated) responses during binocular stimulation. To answer this question, we rank-ordered all monocular neurons from most-facilitated to most-suppressed (**Figure 2.6a**). This analysis revealed two distinct groups of binocularly modulating neurons: The first group decreased firing rates during binocular stimulation (binocularly suppressed neurons) and comprised over two-thirds of monocular neurons. The remaining third of neurons increased firing rates during binocular stimulation (binocularly facilitated neurons).

The mean response across the binocularly suppressed neurons revealed significant modulation (one-tailed Wilcoxon signed-rank test, $p = 1.44 \times 10^{-5}$; **Figure 2.6b).** Individual testing of binocularly suppressed neurons revealed that more than 80% **(**19/23) of these monocular neurons significantly reduced their activity upon binocular stimulation ($p < 0.05$, ROC analysis, see also **Table 2.1**). The mean response across the binocularly facilitated neurons showed significant enhancement under binocular stimulation (one-tailed Wilcoxon signed-rank, $p = 9.77 \times 10^{-4}$; **Figure 2.6c**). Testing on an individual neuron basis revealed that about half (4/10) of these neurons enhanced their spiking significantly when both eyes were stimulated rather than their dominant eye alone (ROC analysis, **Table 2.1**).

We also repeated this comparison for a more liberally-defined group of monocular neurons (one-tailed paired t-test, $p > 0.01$). Using this liberal criterion yielded a larger sample size ($n = 51$) at the expense of including neurons that show a minimal response to the non-dominant eye. Nonetheless, this liberally-defined group yielded comparable results to those

shown in **Figure 2.6b** and **2.6c** (**Figure 2.7a**, one-tailed Wilcoxon signed-rank, $p = 6.17 \times 10^{-7}$, N = 31; **2.7b,** one-tailed Wilcoxon signed-rank, $p = 4.78 \times 10^{-5}$, N = 20).

Psychophysical studies have shown that binocular combination differs at varying contrast levels (Legge and Rubin, 1981, Ding and Sperling, 2006). We therefore wondered if stimulus contrast affects the binocular modulation of monocular neurons for either of these two groups of neurons. To test for the impact of stimulus contrast, we recorded the responses of a subsample of monocular neurons to binocular stimuli presented at several contrast levels (see **Table 2.2** for contrast levels and N). Specifically, we either did not display a stimulus (monocular conditions) or showed a high contrast grating (binocular conditions) to the non-dominant eye. We then paired these conditions with stimuli of varying contrast in the dominant eye.

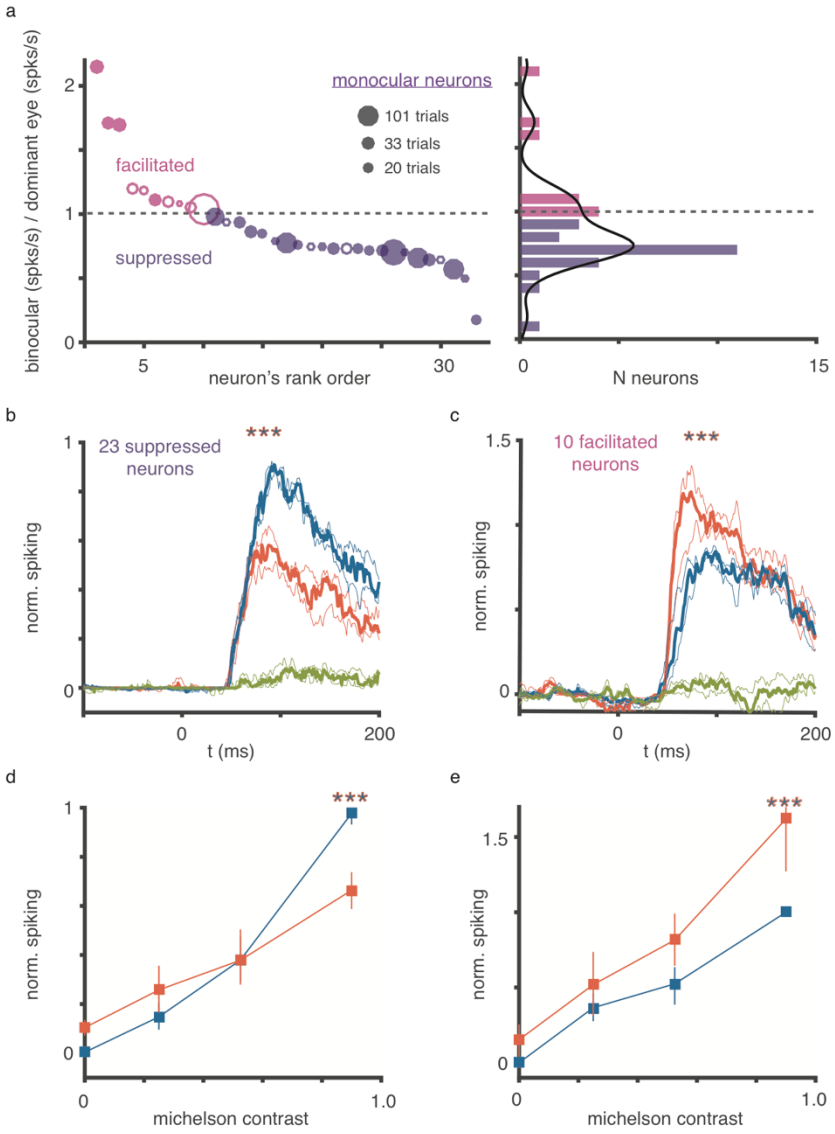

Figure 2.6 Binocular Modulation is both Suppressive and Facilitatory.
(a) Left panel: Rank ordering of monocular neurons from most facilitated to most suppressed, using the ratio of their binocular response to their dominant eye response. Solid circles indicate neurons with significant binocular modulation based on ROC analysis ($\alpha = 0.05$ for 15 or more consecutive 10 ms sliding windows). Facilitated neurons that respond more when both eyes are stimulated are shown in pink. Suppressed neurons that reduce their response during binocular stimulation are shown in purple. Dashed horizontal line demarcates equal responses during monocular and binocular stimulation. Circle size indicates trial number. Right panel: Histogram of the data shown to the left, with a kernel density estimate superimposed in black.
(b) Median normalized responses of *suppressed* monocular neurons that reduced firing rates during binocular stimulation. Their population response to binocular stimulation differed significantly from monocular stimulation (one-tailed Wilcoxon signed-rank, $p = 1.44 \times 10^{-5}$, $n = 23$). All conventions as in **Figure 1c**. Response to the non-dominant eye was non-significant at $\alpha = 0.05$.

(c) Same as (b) for *facilitated* monocular neurons that increased spiking during binocular stimulation. Their population response under binocular stimulation was significantly greater than the for stimulating their dominant eye alone (one-tailed Wilcoxon signed-rank, $p = 9.77 \times 10^{-4}$, $n = 10$).
(d) Mean normalized contrast responses for suppressed monocular neurons during exclusive dominant eye stimulation (blue, non-dominant eye at 0.0 contrast) and binocular stimulation (orange, non-dominant eye at 0.8 or greater contrast). All contrast values and sample sizes are detailed in **Table 2.2**. Error bars represent 90% confidence limits. When the contrast of the stimulus in the dominant eye equal was 0.8 or greater, neurons were significantly suppressed (one-tailed Wilcoxon signed-rank test, $p = 2.15 \times 10^{-5}$, Bonferroni corrected for multiple comparisons). Differences at all other contrast levels were not significant.
(e) Same as (d) for facilitated monocular neurons. When the contrast of the stimulus in the dominant eye equal was 0.8 or greater, binocular stimulation resulted in significantly greater spiking responses than when stimulating the dominant eye alone (one-tailed Wilcoxon signed-rank test, $p = 9.77 \times 10^{-4}$, Bonferroni corrected for multiple comparisons).

For both binocularly suppressed and facilitated monocular neurons, only high contrast stimulation of the dominant eye resulted in significant binocular modulation (**Figure 2.6d**; one-tailed Wilcoxon signed-rank test, $p = 2.15 \times 10^{-5}$, Bonferroni corrected for multiple comparisons; **Figure 2.6e**; one-tailed Wilcoxon signed-rank test, $p = 9.77 \times 10^{-4}$, Bonferroni corrected for multiple comparisons). These results suggest that monocular V1 neurons modulate their firing rates at relatively high visual contrast levels only, congruent with the psychophysical observation that binocular combination differs fundamentally between high and low contrast levels.

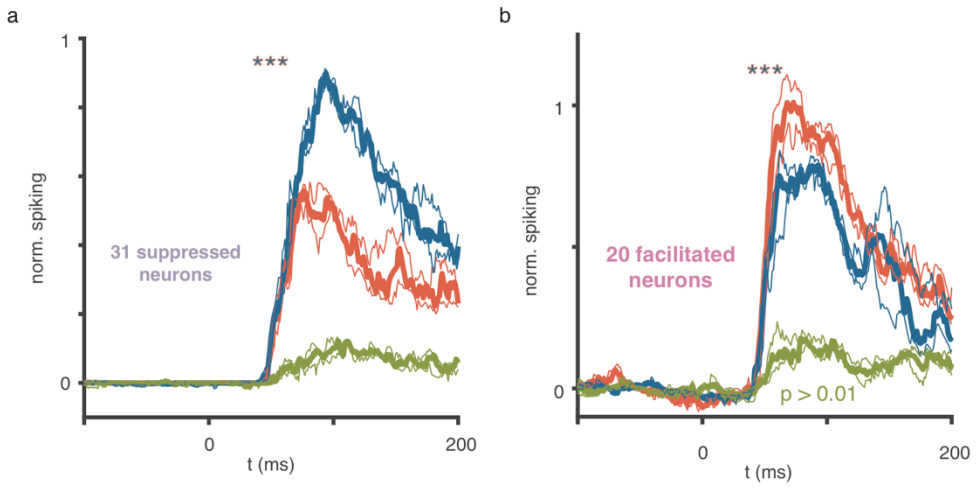

Figure 2.7 Responses of liberally-defined monocular neurons.
(a) Median responses to dominant eye (blue), non-dominant eye (green), and binocular (orange) stimulation for liberally-defined monocular neurons that had a non-significant response to the non-dominant eye at $\alpha = 0.01$ (binocular versus dominant eye response, one-tailed Wilcoxon signed-rank, $p = 6.17 \times 10^{-7}$, $N = 31$).
(b) Same as (a) for more liberally-defined, facilitated monocular neurons (one-tailed Wilcoxon signed-rank, $p = 4.78 \times 10^{-5}$, $N = 20$).

Table 0.2 Number of neurons used for computing the contrast response functions shown in Figure 2.6.

	dominant eye Michelson contrast	0.0	0.2 – 0.3	0.45 – 0.5	0.8 – 1.0
suppressed group	monocular conditions	n/a	16	16	23
	binocular conditions	23	15	16	23
facilitated group	monocular conditions	n/a	5	6	10
	binocular conditions	10	4	4	10

Temporal dynamics of binocular suppression implies intracortical processing

What could cause the binocular modulation of L4 neurons described above? One possibility is that some L4 neurons receive convergent inputs from LGN afferents carrying signals from both eyes (Blasdel and Lund, 1983). If this mechanism were involved, the difference between the overall visual response onset and the binocular modulation (effect) onset of L4 neurons should be small. Alternatively, monocular neurons may receive indirect inputs from the other eye either via lateral connections within L4, or via interlaminar connections that connect L4 cells to neurons in other layers. Both these mechanisms involve more synapses and thus more processing time.

Given the rationale outlined above, we decided to compare visual response onsets and binocular modulation onsets of monocular neurons in L2/3, L4, and L5/6 (**2.5 Methods**; see **Figure 2.8a,b** for the effect of binocular stimulation on binocular neurons). Congruent with the canonical microcircuit model [10], we found that L4 neurons tended to respond to visual stimulation before L2/3 neurons, followed by L5/6 neurons (L4, 42.1 ms; L2/3, 45.2 ms; L5/6, 46.4 ms; **Figure 2.9a**). As expected, binocular modulation significantly trailed the visual response by several milliseconds (median response onset: 50 ms, median binocular modulation onset: 62 ms; one-tailed Wilcoxon rank sum, $p = 2.01 \times 10^{-17}$). Interestingly, binocular modulation tended to occur first among L2/3 neurons, followed by L4 neurons and L5/6 neurons (L2/3, 47.6 ms; L4, 50.1 ms; L5/6, 54.7 ms; **Figure 2.9b**). This observation suggests that the bulk of binocular modulation of L4 neurons occurs following binocular processing outside V1's primary input layers.

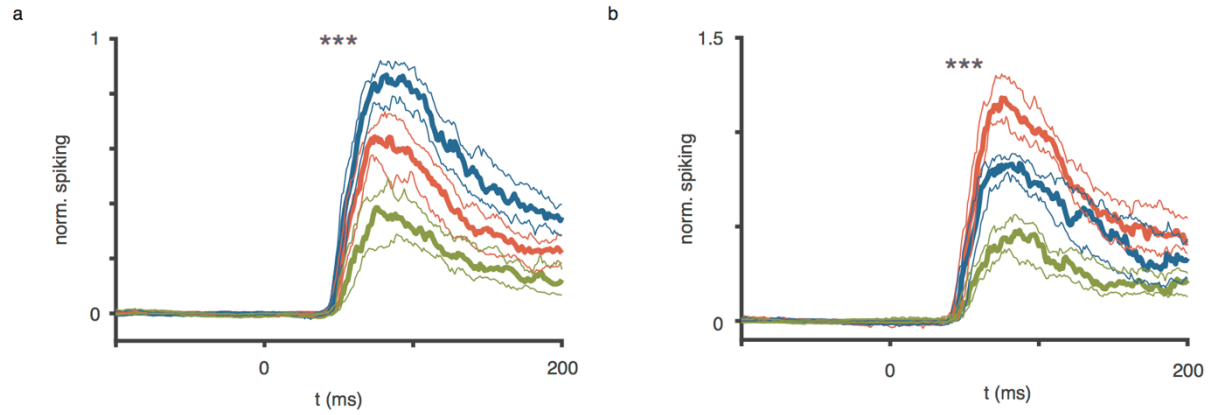

Figure 2.8 Binocular modulation of binocular neurons and liberally-defined monocular neurons.
(a) Population average for binocular neurons with significantly reduced responses during binocular stimulation compared to stimulation of their preferred eye alone (one-tailed Wilcoxon signed-rank, $p = 8.53 \times 10^{-10}$, $N = 50$). Thin lines represent 95% confidence bounds.
(b) Same as (a) for binocular neurons that significantly increased their responses during binocular stimulation over monocular stimulation of their preferred eye (one-tailed Wilcoxon signed-rank, $p = 5.69 \times 10^{-11}$, $N = 55$).

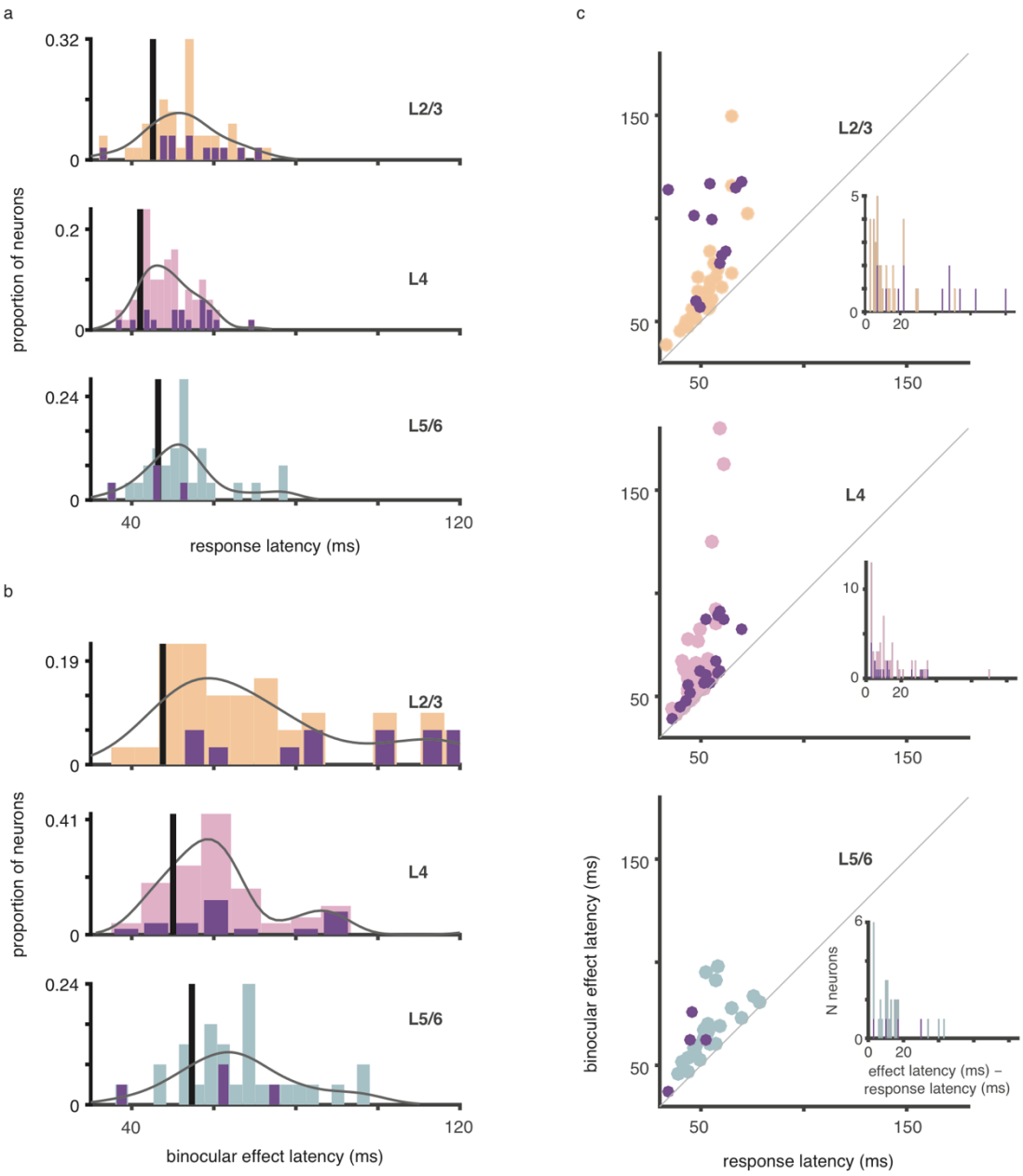

Figure 2.9 Binocular Modulation Tends to First Occur Outside of the Primary Input Layers.

(a) Response onset distributions for L2/3, L4, and L5/6 neurons. Colored histograms encompass all neurons within each laminar compartment. Overlaid purple bars highlight the monocular neurons. Gray lines are kernel density fits. Black vertical lines indicate 75%-to-maximum of fitted distributions.

(b) Binocular modulation onset distributions for L2/3, L4, and L5/6 neurons. Conventions as in (a).

(c) Visual response onset versus binocular modulation onset for L2/3, L4, and L5/6 neurons. Purple markers indicate monocular neurons. Gray line represents unity line.

L4 Binocular facilitation occurs earlier than binocular suppression

The above analyses suggest that under binocular stimulation most L4 neurons modulate via lateral connections within L4, or connections between L4 and L2/3 or L5/6. However, inspecting the data on a neuron-by-neuron basis revealed that some L4 neurons, including some monocular neurons, showed a more rapid onset of binocular modulation that virtually coincides with sensory activation (**Figure 2.9c**). One possible mechanism for this early L4 binocular modulation is that LGN afferents carrying signals from each eye converge onto L4 neurons. It is conceivable that the functional impact of some LGN afferents associated with the non-dominant eye might not be strong enough to drive a spiking response on their own, but may nonetheless be effective enough to modulate responses to the dominant eye. As LGN inputs to L4 are excitatory (da Costa and Martin, 2011), the result should be a rapid onset of facilitatory binocular modulation. Indeed, we found that most of the facilitated monocular neurons were located in granular L4 (7/10). Furthermore, binocularly facilitated L4 neurons tended to modulate earlier than binocularly suppressed L4 neurons (**Figure 2.10**). In other words, facilitatory binocular modulation by and large precedes suppressive binocular modulation in L4 (one-tailed Wilcoxon rank sum, $p = 0.16$).

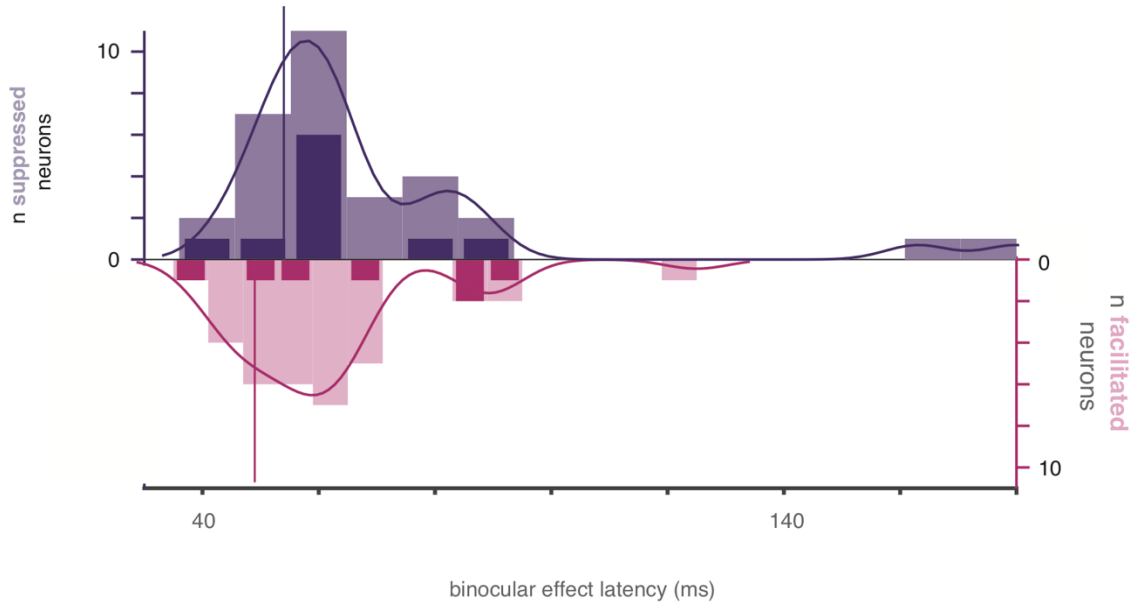

Figure 2.10 L4 binocular facilitation precedes binocular suppression.
Histogram of binocular modulation onset for suppressed L4 neurons (top, n = 32) and facilitated L4 neurons (bottom, n = 34). The darker purple and darker pink bars represent suppressed monocular neurons (n = 10) and facilitated monocular neurons (n = 7), respectively. Solid lines represent kernel density. Vertical lines represent the 0.25 quantile for the L4 facilitated neurons (purple, 49 ms) and L4 suppressed neurons (54 ms), respectively.

A neuron's degree of ocular preference predicts its degree of binocular modulation

We next wondered how the above findings relate to the well-documented V1 phenomenon of ocular dominance (Hubel and Wiesel, 1968, Hubel and Wiesel, 1977), which describes neuronal preferences for one eye over the other eye. To answer this question, we estimated ocular dominance by computing an ocularity index for all single neurons and multiunits (see **2.5 Methods**; see (Hubel and Wiesel, 1968, Hubel and Wiesel, 1977, Schiller et al., 1976) for the variance of ocular dominance across cortical depth). An ocularity index value of -1 corresponds to neurons exclusively driven through the ipsilateral eye, a value of 1 corresponds to neurons driven exclusively through the contralateral eye, and a value of 0 corresponds to neurons driven equally through either eye.

Our sample spanned the entire index range of ocular dominance (**Figure 2.11a**). Across the neuronal population, the spread of ocular dominance resembled a normal distribution (Chi-square goodness of fit, $\chi^2 = 9.64$, d.f. = 7, p = 0.21; **Figure 2.11b**). We repeated this analysis for multiunits (see **2.5 Methods**), as these data provide a larger sample. Multiunit responses reflect the activity of neurons up to 350 μm away from the electrode contact (Mineault et al., 2013), which can bridge across ocular dominance columns (Horton and Hocking, 1996). Given this coarser spatial sampling, we expected multiunits to exhibit a stronger bias towards binocular responses. Indeed, multiunits had lower mean rectified ocularity indices than single neurons (one-tailed two-sample t-test, $p = 1.98 \times 10^{-25}$, $t_{1285} = 10.58$). Like the single neuron population, multiunit ocular dominance was normally distributed (Chi-square goodness of fit, $\chi^2 = 3.95$, d.f. = 7, p = 0.79; **Figure 2.11c**), suggesting that the mode of ocular dominance in V1 is an equal response to either eye.

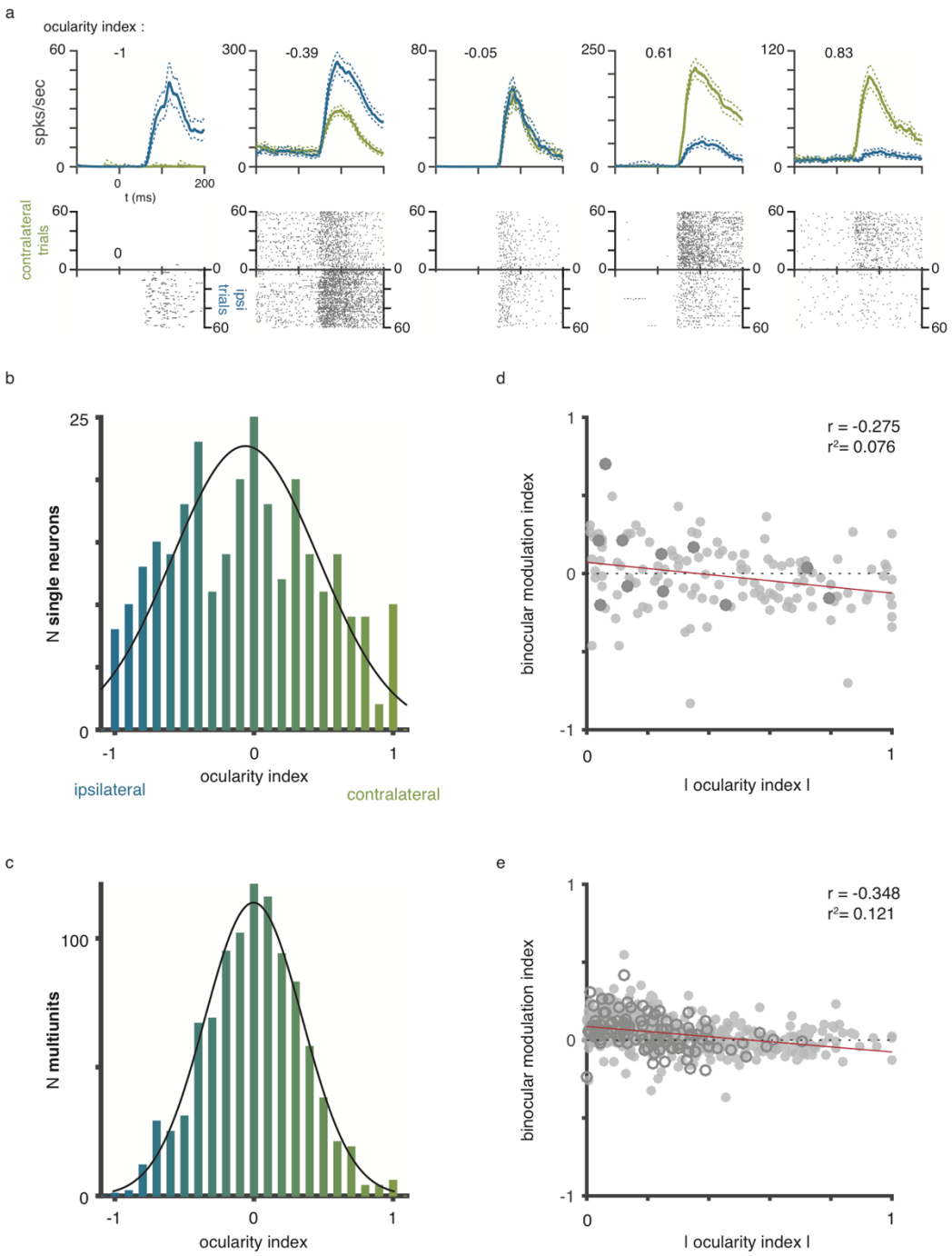

Figure 2.11 Ocular Dominance Correlates with Binocular Modulation.
(a) Responses for five example neurons of varying ocular dominance. Top row: Mean spike density functions (thick lines) with 95% confidence intervals (thin lines). Responses to the contralateral eye are shown in green. Responses to the ipsilateral eye are shown in blue. Corresponding raster plots (60 randomly selected trials for each condition) are shown below. The resulting ocularity index (see **2.5 Methods**) for each neuron is shown in the top left corner.

(b) Histogram overlaid with fitted Gaussian (black line) for the ocularity indices of all recorded single neurons (n = 290, Chi-square goodness of fit, $\chi^2 = 9.64$, d.f. = 7, p = 0.21, H_0 = underlying distribution is normal).
(c) Same as (b) for all multiunits recorded in our sample (n = 997). Fit is Gaussian (Chi-square goodness of fit, $\chi^2 = 3.95$, d.f. = 7, p = 0.79, H_0 = underlying distribution is normal).
(d) Binocular modulation as a function of ocularity across all of the neurons that we measured under binocular stimulation (n = 138). Higher ocularity indices indicate greater preference for one eye over the other. Lower binocular modulation indices indicate more response suppression during binocular stimulation. The solid red line represents a linear regression using least-squares (p = 0.0011, r = -0.275, $r^2 = 0.0756$). The dashed line indicates the expected relationship if there were no systematic response differences between a monocular neuron's ocular bias and its binocular modulation. Darker markers represent neurons from monkey I34.
(e) Rectified ocularity index versus binocular modulation index across all multiunits with binocular data (n = 602). The solid red line represents a linear regression using least-squares (p = 1.29×10^{-18}, r = -0.348, $r^2 = 0.121$). All conventions as in (d).

Given this wide range of ocular dominance among our sample of V1 neurons, we wondered whether ocular dominance and binocular modulation were systematically related. To test for this relationship, we calculated a binocular modulation index, as described for **Figure 2.2f**, that quantifies both the strength and direction of binocular modulation (see **2.5 Methods**). We then assessed whether a neuron's ocular dominance had any explanatory power for the neuron's binocular modulation.

Interestingly, and largely congruent with the findings described above, we found a significant correlation between the binocular modulation index and the rectified ocularity index (p = 0.0011, r = -0.275, $r^2 = 0.0756$; **Figure 2.11d**). This significant correlation suggests that the more a neuron prefers one eye over the other, the more binocular stimulation suppresses that neuron. We observed the same significant correlation for our larger sample of multiunits (p = 1.29×10^{-18}, r = -0.348, $r^2 = 0.121$; **Figure 2.11e**), across all V1 layers (L2/3, p = 6.20×10^{-10}, r = -0.418, $r^2 = 0.174$; L4, p = 1.19×10^{-10}, r = -0.438, $r^2 = 0.192$; L5/6, p = 0.005, r = -0.197, $r^2 = 0.039$; **Figure 2.12**).

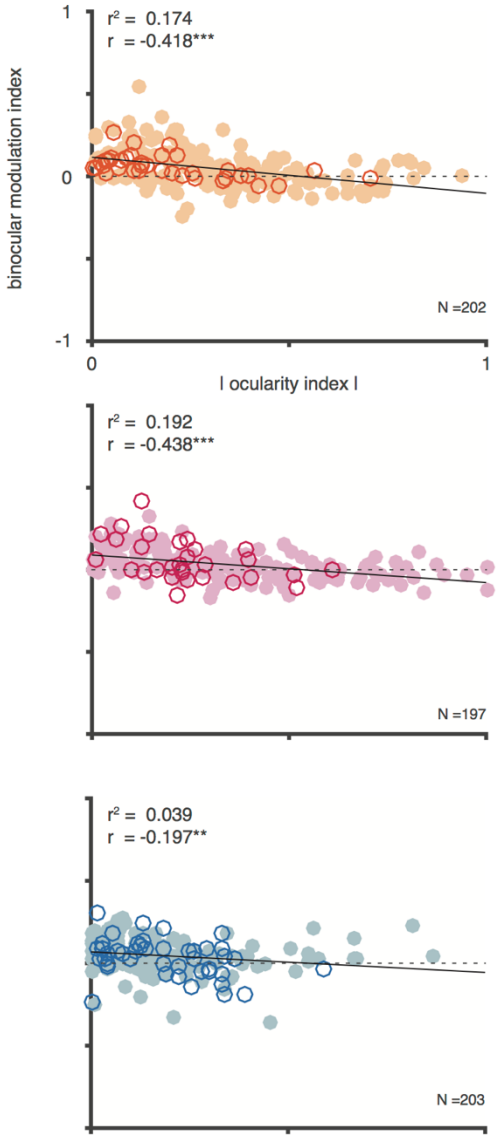

Figure 2.12 Rectified ocularity index versus binocular modulation index for multiunits in L2/3, L4, and L5/6.
Hollow circles represent multiunits from monkey I34. Higher ocularity indices indicate greater preference for one eye over another. Lower binocular modulation indices indicate greater degree of suppression during binocular stimulation. The solid black line represents a linear regression using least-squares for each the supragranular ($p = 6.20 \times 10^{-10}$), granular ($p = 1.9 \times 10^{-10}$), and infragranular compartments ($p = 0.005$). The dashed line indicates the expected relationship if there were no systematic response differences between a monocular neuron's preference for one eye and its binocular modulation.

2.4 Discussion

This study demonstrates that almost all primate V1 neurons, including those in layer 4C, encode sensory signals from both eyes. We found that there are both facilitatory as well as suppressive effects of binocular stimulation among monocular neurons. The temporal profile of binocular modulation suggests that at least some form of binocular facilitation in L4 could arise from additive synaptic activation of neurons that directly receive inputs from both eyes. In contrast, binocular suppression seems to depend on one or more steps of intracortical processing. These findings suggest that established models of binocular processing that segregate monocular signals in L4 (**Figure 2.13a**) (Hubel and Wiesel, 1972) need revision (**Figure 2.13b**). Moreover, we found that the more a V1 neuron responds to one eye compared to the other, the more binocular stimulation suppresses its responses. This result is significant because several theoretical models on binocular vision rest on the idea that activation of a monocular neuron's non-dominant eye can reduce its response (Ding and Sperling, 2006, Blake, 1989, Read et al., 2002, Said and Heeger, 2013), yet until now empirical support has been lacking.

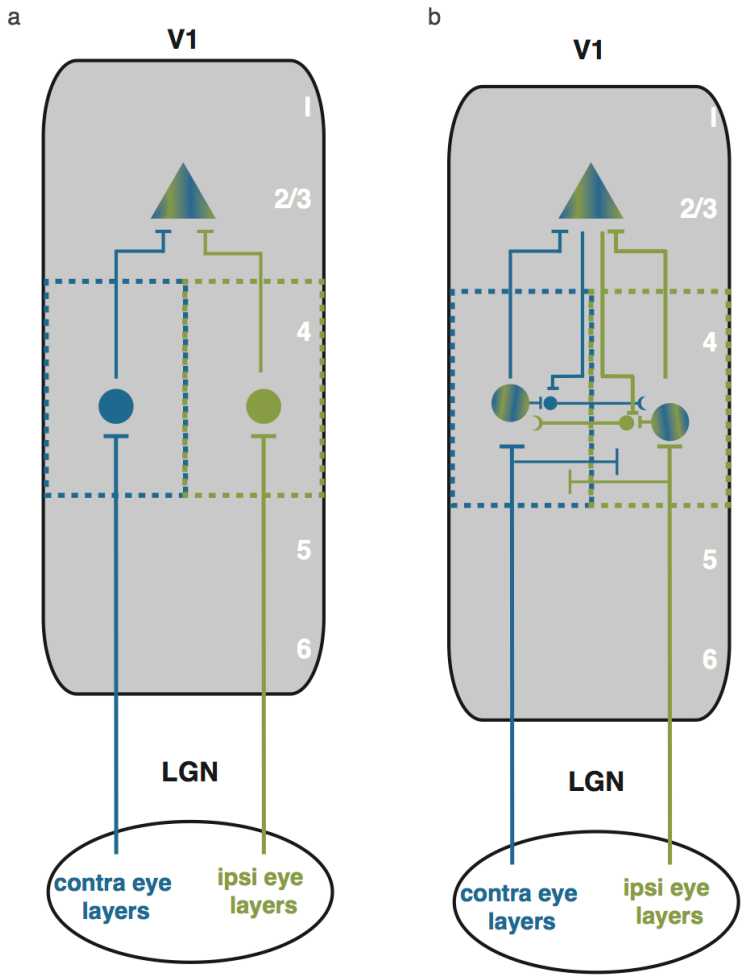

Figure 2.13 Schematic Model for the Formation of Binocular Signals in V1.
(a) Earlier models of binocular processing purported that monocular signals remain segregated in L4 of V1. Formation of a binocular signal occurs outside of L4.
(b) New, modified model that incorporates the results from this study. U-shaped connections represent inhibitory connections. Flat line connections represent excitatory connections. Excitatory connections in L4 represent axon collaterals from LGN afferents that would presumably synapse on other L4 neurons not shown. Given that most V1 monocular neurons in L4 are sensitive to both eyes, formation of a binocular signal already occurs in V1's input layer. Some of this sensitivity could arise from 1) excitatory, convergent inputs from the LGN onto L4 neurons, as well as 2) lateral connections within L4, or 3) interlaminar connections.

Relation to prior work

The findings reported here parallel similar observations in cat area 17 (Kato et al., 1981). This analogy is interesting because binocular processing in cats differs significantly from primates.

For example, eye-specific terminations of LGN neurons in L4 of visual cortex in monkeys remain more segregated in monkeys than in cats (Hubel and Wiesel, 1972, Wiesel et al., 1974). Moreover, cat LGN features anatomical connections between monocular layers that are either absent or less prominent in primates (Sanderson et al., 1971, Hayhow, 1958, Guillery and Colonnier, 1970). Accordingly, responses of the vast majority of cat LGN cells modulate under binocular stimulation, whereas only a small minority of LGN neurons in the macaque seem to be sensitive to both eyes (see (Dougherty et al., 2018) and Chapter 1 for more extensive discussion). Our results suggest that despite these species differences, monocular neurons in primary visual cortex of both cats and monkeys exhibit binocular modulation.

Given these analogous results, we decided to use the previously published cat data to compute a statistical power analysis. The result showed that for the reported effect size and estimated variance, 80% power could be achieved with 11 monocular neurons, suggesting that our sample size – though small – offered satisfactory degrees of freedom (Kato et al., 1981).

Previous work in primates inferred that most V1 neurons, including monocular neurons, are sensitive to interocular disparity (Poggio and Fischer, 1977). Our finding that virtually all V1 neurons–including monocular neurons in L4–carry binocular signals are consistent with, and corroborate, this idea. Several primate studies also quantified the fraction of binocular and monocular primate V1 cells (Kiorpes et al., 1998, Macknik and Martinez-Conde, 2004), and some considered ocularity across cortical depth (Hubel and Wiesel, 1968, Schiller et al., 1976). Several of these studies used a scale to rate the extent to which one eye or the other drives neurons (Parker, 2007, Schiller et al., 1976, Kiorpes et al., 1998). This ocular dominance scale consists of 7 distinct groups, with groups 1 and 7 corresponding to neurons driven exclusively by the contra- and ipsilateral eyes, respectively (Hubel and Wiesel, 1968). Group 4 corresponds to

neurons driven equally through both eyes. Using this technique, some authors reported distributions appearing Gaussian (Parker, 2007), matching our finding, while others reported more uniform distributions (Kiorpes et al., 1998). The subjective nature of the rating system as well as potential differences in the laminar position of sampled neurons might explain some of this variance. Importantly, though, previous studies and the data reported here agree that monocular neurons make up only a small fraction of V1 neurons (Baker, 1974).

Binocular modulation and disparity tuning

We did not systematically test our recorded neurons for interocular disparity tuning but instead presented all of our binocular stimuli at zero disparity exclusively. It is possible that stimulation of both eyes using interocular disparity might reveal that even some of the monocular neurons in our sample that did not show a significant effect of binocular modulation are nonetheless sensitive to both eyes. In other words, it is conceivable that binocular stimuli shown at disparities other than zero modulate monocular neurons that do not modulate at zero disparity. Indeed, previous studies in both cats and monkeys found disparity tuning among monocular V1 neurons (Ohzawa and Freeman, 1986, Prince et al., 2002, Read and Cumming, 2004). Our findings expand on these studies by demonstrating that a large fraction of monocular neurons V1 that are sensitive to both eyes are located in the primary input layers (L4), and that binocular modulation and ocularity are linearly related.

Possible role of the lateral geniculate nucleus

Another important consideration is that binocular convergence may initiate in the LGN. Specifically, monocular LGN neurons might modulate under binocular stimulation and imprint

this response pattern onto their projection targets in L4 of V1. Indeed, binocular modulation occurs in cat LGN (see (Dougherty et al., 2018) for review). It is unclear whether this binocular modulation results from feedback from V1 (Sanderson et al., 1971, Singer, 1970, Schmielau and Singer, 1977, Varela and Singer, 1987). However, the finding of extensive binocular modulation in cat LGN could not be replicated in primates, which suggests that the two species differ substantially in their functional organization of binocular integration (Rodieck and Dreher, 1979). Future work may determine the degree of binocular modulation in primate LGN as well as the role of corticofugal feedback in its implementation. It is also worth noting that a small fraction of primate LGN neurons can be driven through either eye (Cheong et al., 2013, Zeater et al., 2015). Whether local neural interactions or cortical feedback cause these binocular responses is unknown. However, these binocular LGN cells make up less than 3% of all LGN neurons. Taken together, these observations suggest that the vast majority of geniculate inputs to L4 do not encode binocular signals in primates. Therefore, cortical activity is likely responsibly for most of the binocular modulation of monocular neurons reported here.

Possible explanations for the binocular modulation of monocular neurons

The binocular response modulation of monocular neurons that we observed could arise through one of several mechanisms, or a combination thereof.

One possibility is that V1 monocular neurons in L4 receive subthreshold inputs from their non-dominant eye. This is an intriguing idea because several empirical and psychophysical studies suggest that monocular neurons interact at or before the point where monocular signals merge into a binocular signal (Ding and Sperling, 2006, Truchard et al., 2000), and human functional magnetic resonance imaging corroborates this prediction (Moradi and Heeger, 2009).

Indeed, some geniculate projections to V1 L4 have been shown to bifurcate and innervate neighboring ocular dominance columns (Blasdel and Lund, 1983). These axons might form—possibly less potent—connections with neurons in ocular dominance columns of the other eye, thus leading to binocular convergence at the thalamo-cortical synapse. However, this kind of connectivity could only explain binocular facilitation, and not binocular suppression, because geniculate projections to V1 are exclusively excitatory. Indeed, L4 binocularly facilitated neurons tended to modulate earlier than L4 binocularly suppressed neurons. This finding is congruent with the idea that some L4 neurons receive weak excitatory input from their non-dominant eye (**Figure 2.13b**). However, binocular facilitation occurred only among a subsection of monocular V1 neurons, which means that axonal convergence in L4 cannot explain the majority of binocular modulation that we observed.

A second possibility is that binocular modulation occurs by lateral interactions among L4 neurons, such as interneurons that cross ocular dominance columns (Buzás et al., 2001, Martin et al., 1983). This connectivity would allow for cross-talk between the signals of each eye (Ahmed et al., 1994, Katz et al., 1989). The idea that L4 interneurons are involved in L4 binocular modulation agrees with our finding that the predominant form of binocular modulation among monocular V1 neurons is suppressive. In the same vein, the fact that suppressive binocular modulation trailed the initial visually evoked sensory response by several milliseconds provides further evidence for the idea that intracortical processing is involved in the bulk of L4 binocular modulation (**Figure 2.13b**).

A third possibility is that binocular modulation occurs via excitatory and inhibitory neurons from other layers onto L4 neurons. Such interlaminar connections might feed binocular signals back to these monocular cells in L4 (Gilbert and Wiesel, 1989, Wiser and Callaway,

1997). In this case, intracellular combination of monocular inputs from either eye first occurs outside of L4. The resulting binocular signals are then fed back to L4, causing binocular modulation. This possibility can explain binocular suppression, as well as the delayed onset of binocular modulation for suppressed neurons. This idea gains even further traction given our finding that binocular modulation in L2/3 slightly preceded binocular modulation in L4. It thus seems plausible that L2/3 neurons cause some of the binocular suppression among L4 monocular neurons (**Figure 2.13b**).

2.5 Methods

Experimental model and subject details

Two adult monkeys (*Macaca radiata,* one female*)* were used in this study. Both animals were pair-housed. Both animals were on a 12-hour light-dark cycle, and all experimental procedures were carried out in the daytime. Each monkey received nutrient-rich, primate-specific food pellets twice a day, along with fresh produce and other forms of environmental enrichment at least five times a week. All procedures followed regulations by the Association for the Assessment and Accreditation of Laboratory Animal Care (AAALAC), Vanderbilt University's Institutional Animal Care and Use Committee (IACUC) and National Institutes of Health (NIH) guidelines.

Surgical procedures

Prior to data collection, each monkey was implanted with a custom-designed plastic head holder and a plastic recording chamber (Crist Instruments) in two separate surgeries under sterile conditions. The animals were administered isoflurane anesthesia (1.5-2.0%). Vital signs, including blood pressure, heart rate, SpO_2, CO_2, respiratory rate and body temperature were

continuously monitored throughout the whole procedure. During surgery, the head holder or the recording chamber was attached to the skull using transcranial ceramic screws (Thomas Recording) and self-curing dental acrylic (Lang Dental Manufacturing). A craniotomy was performed over the perifoveal visual field representation of primary visual cortex (V1) in each monkey concurrent with the positioning of the recording chamber. Each monkey was given analgesics and antibiotics, and closely observed by researchers, facility veterinarians and animal care staff for at least three days following surgery.

Data acquisition and pre-processing

During each recording session, a linear multielectrode array (U-Probe, Plexon Inc., or Vector Array, NeuroNexus) with either 24 or 32 contacts of 0.1 mm inter-contact spacing was carefully inserted into V1. Extracellular voltage fluctuations (0.5 Hz – 30 kHz) were recorded inside an electromagnetic radio frequency-shielded booth. These signals were amplified, filtered and digitized using a 128-channel Cerebus® Neural Signal Processing System (NSP; Blackrock Microsystems). Both a broadband (0.3 Hz – 7.5 kHz) signal sampled at 30 kHz and a low frequency-dominated signal (0.3 Hz – 500 Hz) sampled at 1 kHz was saved for offline analysis. The NSP also recorded the output of a photodiode signal (OSI Optoelectronics) placed on the monitor to track stimulus-related events at 30 kHz. The NSP further digitized the output of the optical eye tracking system (EyeLink II, SR Research or SensoMotoric Instruments) at 1 kHz, as well as digital event markers sent from the behavioral control system (MonkeyLogic, (Asaad et al., 2013). Both the photodiode signal and event markers were used to align the neural data with visual and behavioral events.

All neurophysiological signals, except for local field potentials (LFP), were extracted offline from the digitized broadband signal using custom written code in MATLAB (2016a; The Mathworks, Inc.). LFP was extracted from the low frequency-dominated signal described above. We extracted multiunits by applying a time-varying threshold to the envelope of the broadband signal, and saved all time points where the signal envelope exceeded a preset threshold. Specifically, we first lowpass-filtered the 30 kHz-sampled voltage signal at 5 kHz using a second order Butterworth filter. We then downsampled the signal by a factor of 3. Next, we high pass-filtered the signal at 1 kHz cut-off with a second-order Butterworth filter. Finally, we rectified the resulting data. To compute the signal envelope, we downsampled the signal by a factor of 3. To compute a threshold, we smoothed the signal by convolving the data with a 1 s boxcar function and then multiplied the result by 2.2. To recover temporal information, we extracted +/- 0.3 ms of data from the original signal for each time point where the envelope exceeded the threshold. We then adjusted these time points to correspond to the point of maximum slope within this window.

For laminar alignment (see below), we used an analog multiunit signal that was computed by high-pass filtering the broadband signal at 750 Hz with a fourth-order Butterworth filter, followed by a full-wave rectification step.

We extracted single neurons with KiloSort, an open-source unsupervised machine-learning algorithm for spike-sorting (Pachitariu et al., 2016), using the default parameters for sorting and cluster merging. We extracted +/− 1 ms of data around each KiloSort'ed spike time from the original broadband signal for each simultaneously recorded electrode contact. We then averaged across impulses to create a spatiotemporal map of the spike waveform (time x electrode contacts). The region of the spatiotemporal waveform map that exceeded +/- 30% of maximum

modulus had to span fewer than 3 electrode contacts (0.3 mm) and 0.9 ms to be included in the study. Neurons that met these criteria were localized to the electrode contact where they evoked the largest amplitude.

Spike rates were downsampled to 1 kHz. For each neuron, spike times were converted to a time-varying signal (spike density function) using 0 to represent time points without a spike and 1 for time points where a spike was detected. This time-varying signal was then convolved using a Poisson distribution resembling a postsynaptic potential (Sayer et al., 1990), with the spike rate (R) computed at time (t):

$$R(t) = \left[1 - \exp\left(-\frac{t}{\tau_g}\right)\right] * \left[\exp\left(-\frac{t}{\tau_d}\right)\right]$$

where τ_g and τ_d are the time constants for growth and decay, respectively. Values of 1 and 20 for τ_g and τ_d respectively were used based on a previous study (Thompson et al., 1996). After convolution, the signal was multiplied by the sampling frequency to convert units to spikes per second.

Current source density (CSD) analysis was performed on the LFP signal using an estimate of the second spatial derivative appropriate for electrodes with multiple contact points (Nicholson and Freeman, 1975):

$$CSD(t, c) = -\frac{\mathrm{x}(t,\ c - z) + \mathrm{x}(t,\ c + z) - 2\mathrm{x}(t, c)}{z^2}$$

where *x* is the extracellular voltage recorded in Volts at time *t* from an electrode contact at position *c*, and *z* is the electrode inter-contact distance (0.1 mm). In order to yield CSD in units of current per unit volume, the resulting CSD from the formula above was multiplied by 0.4 S/mm as an estimate of cortical conductivity (Logothetis et al., 2007).

Eye position was measured continuously using a commercially eye tracker (see details below). Using the horizontal and vertical gaze position data provided by this system, we extracted microsaccades using a previously published algorithm. (Otero-Millan et al., 2014).

Visual display

Stimuli were presented on a linearized CRT monitor with a refresh rate of either 60 Hz (resolution 1280 × 1024) or 85 Hz (resolution 1024 × 768). These visual stimuli were generated using custom-written code for MonkeyLogic (Asaad et al., 2013) in MATLAB (R2012-2014, The MathWorks) on a PC (Dell, Windows 7 or Windows 10) with a NVIDIA graphics card. Animals viewed all stimuli through a custom-built mirror stereoscope that employed infrared-light passing cold mirrors (Edmund Optics). The animal, mirrors and monitor were positioned so that the animal's right eye viewed stimuli presented on the right side of the monitor and the animal's left eye viewed stimuli on the left side of the monitor. To prevent light scatter from one side of the monitor to the opposing eye, a black, non-reflective septum was placed between the monitor and the back side of the mirrors, effectively dividing the left and right sides of the apparatus.

Infrared-light sensitive cameras, placed directly behind the cold mirrors on the stereoscope, were used to track gaze position with commercially available eye tracking software (Eye Link II, SR Research). Gaze position was converted to an analog signal and inputted to MonkeyLogic/MATLAB (NIDAQ PCI-6229) at 1 kHz. At the beginning of each recording session, the stereoscope was calibrated to facilitate binocular fusion of the left and right sides of the monitor using a behavioral task that relied on acquiring the same gaze position for corresponding locations on each side of the monitor (Maier et al., 2007, Maier et al., 2008) . To

further aid fusion, an oval aperture or set of intersecting circles in each corner was displayed at the edge of each half-screen.

Laminar alignment and RF mapping

For each penetration with the linear multielectrode array, CSD analysis was used to locate the boundary between L4 and L5. CSD analysis of visual responses to brief visual stimulation has been shown to reliably indicate the location of the primary geniculate input to V1 (in granular L4) by a distinct current sink that is thought to reflect the combined excitatory post-synaptic potentials of the initial retino-geniculate volley of activation (Mitzdorf and Singer, 1977, Schroeder et al., 1998) . Lack of multiunit responses were used to identify electrode contacts that lie outside V1, either in the subdural space or the white matter below. We excluded contacts on the extreme ends of the array that did not exhibit a visual response. After removing these contacts, the location of the initial current sink was used to align and average data across electrode penetrations, resulting in 0.1 mm +/- 0.05 mm resolution across the depth of V1 (Maier et al., 2010, Maier et al., 2011, Godlove et al., 2014, Spaak et al., 2012, Dougherty et al., 2017, van Kerkoerle et al., 2014, Hansen et al., 2012, Ninomiya et al., 2015, Cox et al., 2017).

For display, representations of CSD as a function of time and space were Gaussian-filtered ($\sigma = 0.1$). Electrode contacts were classified to be in supragranular, granular, or infragranular positions based on the CSD responses as well as neurophysiological criteria. These criteria included the power spectral density of the LFP across cortical depth, signal correlations of the LFP between all contact combinations, and stimulus-evoked analog multiunit responses. The supragranular-to-granular boundary is more challenging to define based on these criteria and was instead set to 0.5 mm above the granular to infragranular boundary.

Once the linear multielectrode array was appropriately positioned in cortex, a reverse correlation-like technique was used to map the RFs of the neurons under study. In each trial, the animals fixated while up to five circular Gabor-filtered static random noise patches appeared in sequence at pseudorandom locations within a pre-defined virtual grid of monitor locations. Each noise patch was displayed for 150 ms with an inter-stimulus interval of 150 ms. The size of each noise patch and the pre-defined grid varied between recording sessions. Typically, each session included a "coarse" mapping phase to determine the general location of the RF. We then used a subsequent "fine" mapping phase to map the precise location of the RF. We then used 3D Receptive Field Matrices (RFMs) (Cox et al., 2013) to create a map of neuronal responses to different points in visual space for each electrode contact (see **Figure 2.1a**). For every multiunit or single neuron, we averaged the spiking response to each stimulus presentation across time, resulting in a single scalar value. We then converted these scalar values to units of z-score. We filled the retinotopic portion of the RFM corresponding to the stimulus location with the z-score for every presentation. This procedure produced a 3D matrix, with two dimensions representing vertical and horizontal visual space and a third dimension representing the response magnitude for each multiunit or neuron. We then averaged this third dimension to produce a spatial map of the mean response. We computed RF centers and extents by fitting an oval to the largest, contiguous patch of the spatial map that exceeded 1 z-score.

Monocular and binocular visual stimulation

We trained each animal trained to fixate on a small (0.2 degrees of visual angle, dva) cross presented at the center of each eye's visual field. Animals held fixation for several (< 5) seconds while we presented stimuli in their perifoveal visual field. The results reported in this paper are

based on data that come from three different paradigms, all with the same or similar conditions. For all neurons, we recorded responses to high contrast (0.8 or greater) sine-wave gratings at varied orientations presented to the left eye or right eye. For 138 neurons, we also recorded responses to high contrast sine-wave gratings at varied orientations presented to both eyes simultaneously. For fewer neurons (see **Table 2.2**), we recorded responses to sine-wave gratings where the contrast in the two eyes varied at several different levels. We presented all stimuli for at least 200 ms, and limited the data to the initial 200 ms of stimulus presentation for each neuron. Where data for multiple paradigms existed for one neuron, we concatenated data across the same conditions.

In one paradigm, animals fixated on a fixation cross for at least 300 ms before a sequence of up to five circular sinusoidal gratings appeared. Each grating was presented for at least 200 ms (46 sessions) or 500 ms (23 sessions) before an inter-stimulus interval of at least 200 ms. We presented the gratings randomly to either the left eye, right eye, or both eyes over the population RF location of the recorded neurons. The grating stimuli varied in orientation but always had a Michelson contrast above 0.8 (mode: 0.9) as well as constant spatial frequency (0.5-3 cycles/deg). If the animals successfully held fixation within a 1 dva radius around the fixation cross for the entire stimulus sequence, liquid juice reward was delivered. If the animals broke fixation or blinked, the trial was aborted and a short timeout (1-5 s) was given before the start of the next trial.

In the second paradigm, we used the same parameters, including stimulus timing. However, we presented the gratings at only one of two orientations (the neurons' estimated preferred orientation or the orientation orthogonal to this preferred orientation) and varied contrast of the gratings shown to each eye across trials (see **Table 2.2**). We determined the

preferred orientation based on online analyses of the multiunit responses to sine-wave gratings of varying orientations. If preferred orientation varied across electrode contacts, we chose the preferred orientation shared by the greatest number of contacts.

In the third paradigm, the animals fixated for at least 300 ms before we presented gratings at the same orientation in both eyes (either the preferred or non-preferred orientation, as described for paradigm two) and varied contrast of the gratings shown to each eye across trials (see **Table 2.2**). Stimuli were shown for 1600 ms (12 sessions). If the animals successfully held fixation within a 1 dva radius around the fixation cross for the entire stimulus duration, liquid juice reward was delivered. If the animals broke fixation or blinked, the trial was aborted and a short timeout (1-5 s) was given before the start of the next trial.

MRI

Animals were anesthetized using the same procedure as outlined under *Animal Care and Surgical Procedures*. Anesthetized animals were placed inside a Philips Achieva 7T MRI scanner at the Vanderbilt University Institute of Imaging Science and remained anesthetized throughout the duration of the scan. Vital signs were monitored continuously. T1-weighted 3D MPRAGE scans were acquired with a 32-channel head coil equipped for SENSE imaging. Images were acquired using a 0.5 mm isotropic voxel resolution with the following parameters: repetition time (TR) 5 s, echo time (TE) 2.5 ms, flip angle 7°.

Quantification and statistical analysis

For a KiloSort'ed neuron or multiunit to be considered for analysis, it had to be located within the grey matter (see **Laminar Alignment and RF mapping**). Moreover, the neuron or

multiunit's mean initial response (40-100 ms) to the dominant eye (defined as the eye that yielded the highest mean spike rate between 40 ms and 140 ms when stimulated with a high contrast stimulus) had to exceed a maximum of 10 spikes per second. This response also had to be significantly larger than the fixation baseline (baseline window: -50-0 ms, paired t-test, $p < 0.05$). Lastly, there had to be at least 12 successfully completed presentations of each monocular contralateral and monocular ipsilateral eye stimulation using the high contrast gratings.

To compute normalized spiking, we transformed the mean responses for each neuron to z-scores. Specifically, we first subtracted their baseline firing rate. Then, we divided this value by the difference between the maximum firing rate to stimulation of the dominant eye and the baseline firing rate. Similarly, we normalized contrast response data across conditions for each neuron by subtracting the baseline firing rate from the mean response at each contrast level. Then, we divided each resulting value by the difference between high contrast dominant eye stimulation and baseline firing.

All statistical hypothesis tests, including Wilcoxon signed-rank tests (one and two-sided), ANOVAs, t-tests (paired and two-sample), Chi-square goodness of fit tests, and Pearson's correlation analysis, are fully described where used in **2.3 Results** and **2.5 Methods**. All reported confidence intervals were based on bootstrapping using 10,000 repetitions on the group statistic (mean or median) shown.

Neurons were included in the monocular category if they had a non-significant dominant eye response during the initial stimulation window (40 to 100 ms) relative to baseline (-50 to 0 ms) (one-tailed paired t-test, $p < 0.05$). We re-categorized two neurons as binocular following visual inspection of average responses.

To quantify the relative amount of excitation by stimulation of the contralateral eye versus by that of the ipsilateral eye, we calculated an ocularity index for each unit:

$$ocularity\ index = \frac{contralateral\ eye\ response - ipsilateral\ eye\ response}{contralateral\ eye\ response + ipsilateral\ eye\ response},$$

where response was defined as the half-wave rectified, baseline-subtracted mean spike rate during the initial response period (40-140 ms). We calculated a binocular modulation index to assess the strength and direction of binocular modulation using the following formula:

$$-1 \times \frac{dominant\ eye\ response - binocular\ response}{dominant\ eye\ response + binocular\ reponse}.$$

We calculated response onset for each neuron using a custom algorithm. Briefly, we used the z-scored response to stimulation in the dominant eye to determine the first time point that exceeded a threshold while trending in positive direction. Specifically, we parceled the data into overlapping windows, whose length was defined as 3% of the maximum response time. We then defined a threshold as the mean response plus two standard deviations for the time between 15 ms before to 15 ms after stimulus onset. If the resulting threshold was lower than 0.05, it was set to 0.05. Criterion was met if 90% of data points within a window exceeded this threshold while 70% of data points trended positively. If no data point fit those criteria, we used the first time point that crossed threshold instead. We used the same algorithm to calculate the binocular effect onset, except that we ran the algorithm on the rectified difference between the median response across trials to the dominant eye and the median response to binocular stimulation.

In addition to group statistics, we used receiver-operating characteristics (ROC) analysis (Green and Swets, 1966) to determine whether there was a significant difference between stimulation conditions at the single-neuron level. Specifically, for each neuron, we ran an ROC analysis with twelve thresholds using 10 ms bins of data, and a sliding window of 1 ms during

the response period (20-190 ms). Statistical significance was determined by comparing the area under the curve to a bootstrapped distribution of area under the curve values computed on 10,000 repetitions of shuffled data. We counted the number of neurons in each defined group (monocular neurons, binocular neurons, etc.) with a 10, 15, or 20 consecutive significant windows (see **Table 2.1**). Unless otherwise stated, a unit had to have 15 consecutive windows with $p < 0.05$ in order to be called significant wherever ROC analysis is reported.

3. Ongoing V1 alpha activity regulates visually driven spiking responses

3.1 Summary

The findings presented in Chapter One and Chapter Two focused on binocular integration, a primarily *feedforward process*. In the last chapter, I detailed the feedforward aspects of the microcircuitry of V1, where geniculate inputs target predominantly layer 4C. Neurons in layer 4C then target layer 2/3 neurons and those neurons target neurons in layer 5/6 (Felleman and Van Essen, 1991). While these connections describe the general progression of feedforward visual processing within V1, there are both further interlaminar connections as well as *feedback* projections from other visual structures that impact visual processing in V1. Specifically, in addition to the interlaminar feedforward connections named above, there are strong excitatory projections from layer 5 neurons to layer 2/3 neurons (Binzegger et al., 2004). Another prominent, inhibitory, interlaminar connection bridges from layer 6 to layer 4 (Binzegger et al., 2004). Given this interconnectedness of V1 laminae, ongoing neuronal activity among any population of V1 neurons is likely to profoundly impact the processing of feedforward inputs among other groups of neurons.

As described above, the interlaminar connections in the primate primary visual cortex (V1) are well described. Similarly, ongoing alpha-range (7-14 Hz) fluctuations are well-known to occur in this area (Berger, 1929, Jensen and Mazaheri, 2010). Less well understood is how these interlaminar connections and ongoing fluctuations contribute to the regulation of visual spiking responses. Here, we investigate the relationship between alpha fluctuations and spiking responses to visual stimuli across cortical layers. Using laminar probes in macaque V1, we show that neural firing couples to the phase of alpha fluctuations, and that magnitude of this coupling

is particularly pronounced during visual stimulation. The strongest modulation of spiking activity was observed in layers 2/3. Alpha-spike coupling and current source density (CSD) analysis pointed to an infragranular origin of the alpha fluctuations. Together, these results indicate that ongoing infragranular alpha-range fluctuations in V1 play a role in regulating columnar visual activity.

3.2 Introduction

Anatomical studies describe an intricate pattern of anatomical connectivity between the layers that collectively make up the cortical columnar microcircuitry of primary visual cortex (V1) (Douglas, 1989, Callaway, 1998, Bannister, 2005, Douglas and Martin, 2004). However, the functional interactions that arise from the dense connections between neurons in different laminar compartments are still largely unknown. Optogenetics has provided a novel means to disentangle the impact of neural activity in one layer on activity in layers above and below. In particular, photo-activation of neurons in deep cortical layers (layers 5&6), but not in superficial layers (1-3) modulates the magnitude of columnar spiking activity in rodent visual cortex (Olsen et al., 2012, Beltramo et al., 2013, Bortone et al., 2014). Together, these studies suggest that neurons in the deep layers of cortex are in a privileged position to regulate spiking output in other cortical layers. Infragranular control over neural excitability across the cortical column is a particularly intriguing hypothesis given that these layers are a major target of cortical feedback projections (Maunsell and Van Essen, 1983, Douglas and Martin, 2004, Nascimento-Silva et al., 2014). Through their modulation of infragranular neurons, such feedback projections could exercise gain control over spiking responses in other layers, including cortically projecting neurons in superficial layers. One possibility is that this modulation occurs through projections

from layer 5 to layer 2/3, which constitutes one of the most extensive interlaminar projections within the cortical microcircuit (Binzegger et al., 2004).

Layer 5 neurons have also been implicated in the generation of alpha-range activity (~7-15 Hz, with the exact frequency range depending on the study). The study of alpha-range activity in investigations of vision and cognition has a long history, driven by the prominence (power) of alpha measured over occipital cortex in humans (Berger, 1929). While it is currently unknown how alpha recorded from the human scalp relates to neural activity recorded intracranially, several hypotheses have been proposed. In particular, a subpopulation of layer 5 pyramidal cells that fire rhythmically in the alpha frequency range (Silva et al., 1991, Sun and Dan, 2009) has been suggested to serve as a neuronal pacemaker for the columnar microcircuit (da Silva, 1991, Connors and Amitai, 1997, Jensen and Mazaheri, 2010, Jones et al., 2000, Jones et al., 2009). One theory about the functional role of cortical alpha activity, referred to as the "pulsed inhibition" hypothesis, purports that alpha cycles reflect periodic inhibition of local neurons (Jensen and Mazaheri, 2010). A predicted outcome of this hypothesis is that the magnitude of spiking varies with the phase of concomitant alpha fluctuations. Indeed, this kind of relationship between spiking and alpha phase has been demonstrated in motor regions and somatosensory cortex (Bollimunta et al., 2008, Bollimunta et al., 2011, Haegens et al., 2011, van Kerkoerle et al., 2014) under a variety of conditions. In visual cortex, others have identified a relationship between alpha and multiunit spiking activity (Bollimunta et al., 2008, Bollimunta et al., 2011, van Kerkoerle et al., 2014). However, the role of alpha-spike coupling and its laminar specificity during sustained sensory processing remain to be elucidated.

Here, we tested for layer-specific interactions between the alpha cycle and fluctuations in spiking activity within a cortical column and the dependence of this relationship on sensory

stimulation. More specifically, we used laminar probes to record locally referenced alpha LFP and population spiking in macaque V1 during periods of sustained sensory stimulation and periods without explicit visual stimulation. We found that spiking activity throughout the column, especially in the supragranular layers, was phase locked to ongoing alpha-range fluctuations. Current source density analysis paired with coupling analysis suggested that the origin of these alpha-range fluctuations was in layer 5. Alpha-spike coupling was present across sensory conditions and was particularly pronounced during periods of visual stimulation. Together, these results are congruent with the notion that V1 activity, particularly in cortico-cortically projecting supragranular layers, is regulated by alpha fluctuations.

3.3 Results

The primary goal of this study was to determine whether coupling of spiking activity with the alpha phase cycle in V1 is of specific relevance to visual stimulation. Towards this aim, we recorded both spiking and LFP across all layers of macaque V1 simultaneously while the animals performed a visual task that was interspersed with periods without stimulation. We examined the co-variation of spiking with the endogenous alpha LFP cycle when the animal was presented with visual stimuli, comparing the phase coupling to the preceding period that was devoid of visual stimulation in each trial. The results are described in the sections below.

Phase-locking of spiking responses to alpha fluctuations

We asked whether spiking activity in V1 shows significant coupling to the alpha LFP phase during periods of prolonged (> 500 ms) visual stimulation. During each session, grating stimuli were presented inside the aggregate receptive field of the cortical column from which we

recorded (**Figure 3.1a**, **Table 3.1** & **3.2**). The visual response following the onset of the gratings initiated in the middle layers (**Figure 3.1b**, **3.1c**). The right portion of **Figure 3.1b** plots data from a single trial, showing typical oscillatory cycles. We restricted analysis to the period in which there was a sustained visual response that was long enough to evaluate the slow-varying alpha signal, which corresponded to the time between 200 to 800 ms following stimulus onset (**Figure 3.1d**). Importantly, owing to this time window, the initial transient response was not included in the analysis. On average, low frequency (< 20 Hz) LFP decreased following visual stimulation in both monkeys (**Figure 3.2b**). However, the spectral pattern differed among layers, with lower layers showing a trend of higher alpha power during visual stimulation (**Figure 3.2a**).

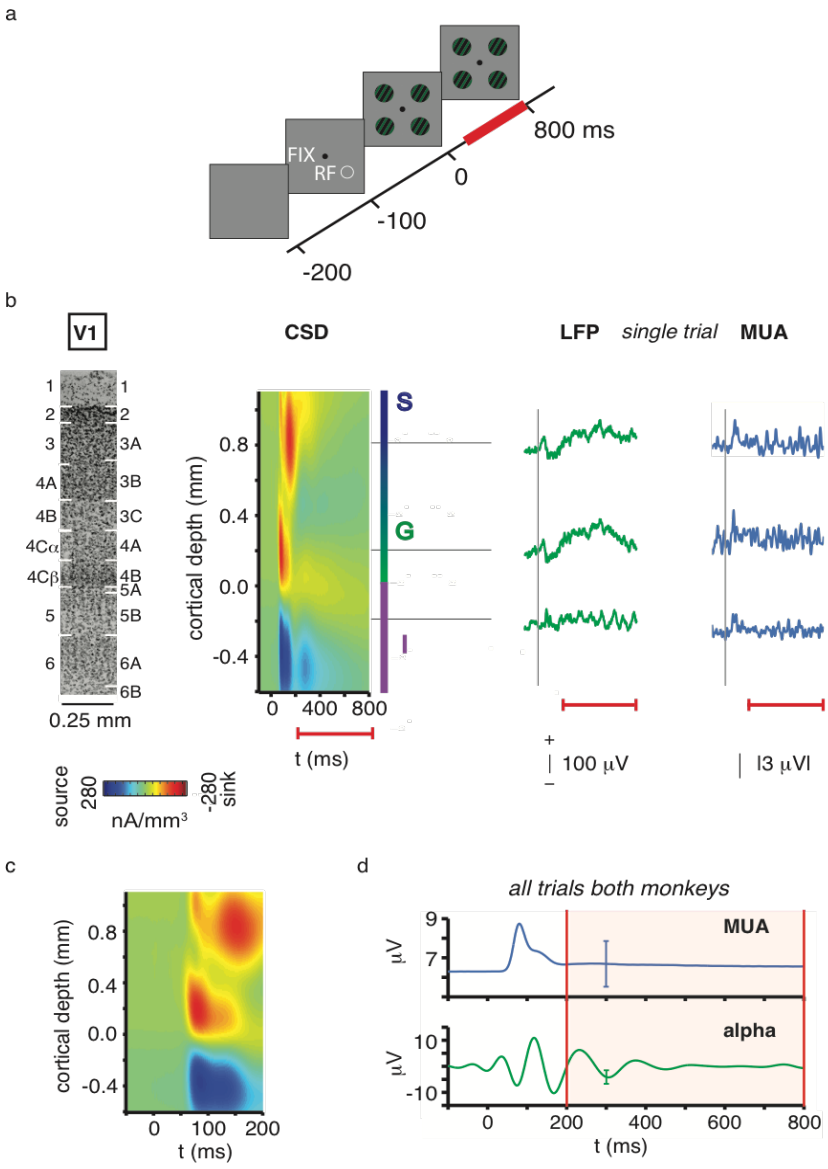

Figure 3.14 Experimental paradigm.

(a) Animals maintained steady fixation on a central fixation spot (FIX) while four equieccentric gratings appeared on the screen (t = 0 ms). One of these gratings covered the previously mapped V1 receptive field (RF).
(b) A laminar probe with 16 or 24 electrode contacts spaced 100 µm apart was used to measure LFP and MUA simultaneously across all laminae of V1. Visually evoked CSD, shown here aligned and averaged across 56 sessions in two monkeys, was used to determine the laminar position of each electrode contact. Per convention, the bottom boundary of the initial current sink served as the zero point, with positive values indicating more superficial cortical locations. S, G, and I mark the CSD-derived locations of supragranular, granular, and infragranular compartments, respectively. The Nissl-stained section shown for scale on the left is from V1 of monkey E. The image is aligned to the electrophysiological data and labeled following

Brodmann's (left) and Hässler's (right) schemes. LFP and MUA traces on the right show the visually evoked response from a single experimental trial (monkey E). Note the distinct low frequency oscillation in the infragranular LFP. Dashed vertical lines indicate the onset of the visual grating stimulus. Red lines below indicate the extent of the analysis window.
(c) CSD shows the initial CSD response with higher temporal resolution.
(d) Stimulus-evoked responses following the onset of the grating stimuli are shown for V1 spiking activity (MUA) and alpha LFP (7-14 Hz) averaged across all contacts, both animals and all sessions (N = 56). Error bars indicate standard deviation (STD). All subsequent analyses were focused on the period 200 ms through 800 ms following stimulus onset (shaded region between red vertical lines).

Table 3.1 V1 Stimulus Size

	Diameter (*dva*)					**N**
	Mean	*STD*	*Min*	*Max*	*N < 2*	
monkey B	2.1	0.2	1.8	3	1	32
monkey E	2.1	0.2	2	2.5	0	23

Table 3.2 V1 Receptive Field Eccentricity and Size

	Eccentricity (*dva*)		**Horizontal Diameter (*dva*)**		**Vertical Diameter (*dva*)**		**Area (dva^2)**		**N**
	Mean	*STD*	*Mean*	*STD*	*Mean*	*STD*	*Mean*	*STD*	
monkey B	4.0	0.7	1.6	0.9	1.8	0.9	3.4	3.2	32
monkey E	3.4	0.7	1.6	0.7	1.3	0.4	2.3	2.0	23

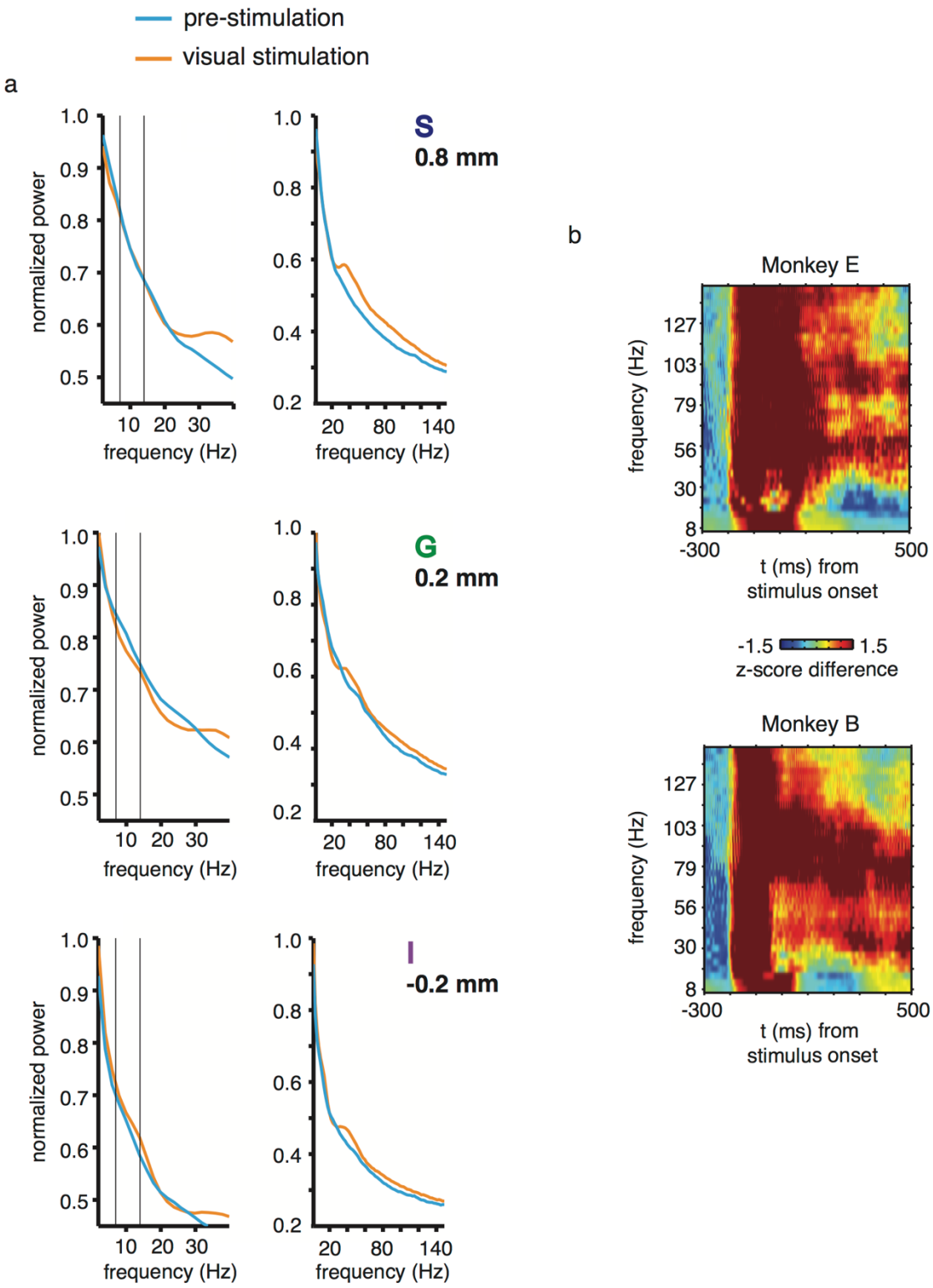
a
pre-stimulation
visual stimulation
S
0.8 mm
G
0.2 mm
I
-0.2 mm
normalized power
frequency (Hz)
b
Monkey E
Monkey B
frequency (Hz)
t (ms) from stimulus onset
-1.5
1.5
z-score difference

Figure 3.2 Power spectral density (PSD) and time-frequency representations.

(a) PSD of the bipolar LFP under two sensory conditions. PSD within each laminar compartment (0.8 mm, 0.2 mm, -0.2 mm) with and without visual stimulation for both monkeys (N = 56 sessions).
(b) Time-frequency representation of LFP from a granular site (0.2 mm), showing the temporal evolution of LFP power spectra around the time of stimulus onset for both monkey E (N = 23 sessions) and monkey B (N = 33 sessions). A multitaper approach was used with a 150 ms window moved in 1 ms steps. The spectrogram was z-score transformed and the resulting matrix was baseline corrected by subtracting the mean during the pre-stimulation period (-300 to -160 ms) from all data points.

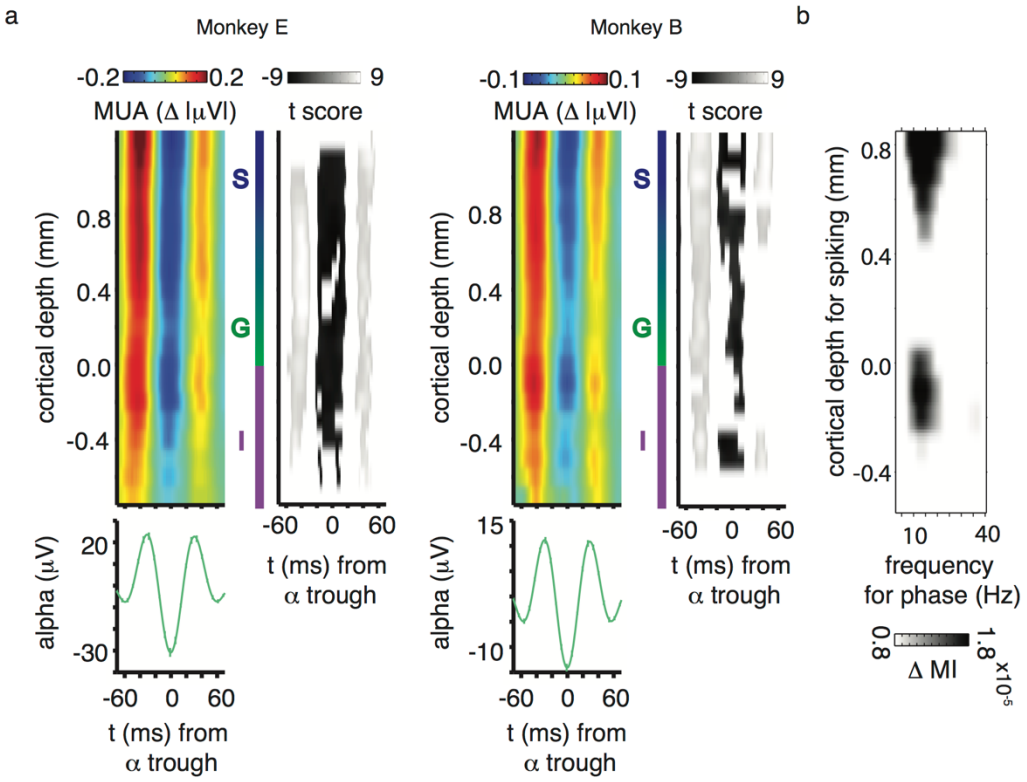

Figure 3.3 Coupling of alpha and columnar V1 spiking responses.
(a) Colored plots represent the laminar profile of population spiking (MUA) aligned to infragranular alpha troughs. Grayscale plots to the right indicate the corresponding t-score values for statistical comparison. The t-score maps are thresholded to indicate significance at the 0.05 alpha level (Bonferroni corrected). Left column: monkey E (N = 23 sessions). Right column: monkey B (N = 33 sessions). Alpha-band LFP was chosen from the electrode contact positioned 0.2 mm below the layer 4C current sink. The average alpha waveform (green) for the same set of sessions is shown below the alpha-aligned MUA (error bars are standard error of the mean, SEM).

(b) Laminar profile of phase-coupled spiking as a function of LFP frequency. Each data point represents the magnitude of coupling expressed as Tort's modulation index (MI). MI values were calculated for 3 Hz wide frequency bands incremented in steps of 1 Hz. LFP was taken from an infragranular electrode contact (-0.2 mm). In order to emphasize laminar specificity, MI values are contrasted to a similarly computed map that used LFP from the granular layer (0.2 mm). Data are averaged across both monkeys (N = 56 sessions).

We confirmed that alpha and spiking coupled as others have described (Bollimunta et al., 2008, Bollimunta et al., 2011, Buffalo et al., 2011, Haegens et al., 2011, van Kerkoerle et al., 2014) using an alpha phase reference from the deep layers. With this signal, we tested for coupling of spiking activity (MUA) along the entire cortical depth, exploiting the 100 μm sampling afforded by our laminar probes. The laminar distribution of alpha-MUA coupling is shown for both animals as mean alpha-locked MUA in **Figure 3.3a**. On average, visual spiking responses in all cortical layers varied with infragranular alpha LFP. This alpha coupling of spiking activity did not derive from the stimulus presentation itself, as it was comparable between the initial and later part of the response (Wilcoxon signed rank tests, $p > 0.05$, Bonferroni-corrected) (**Figure 3.4**). Similarly, the coupling effect remained after removal of the mean LFP response (**Figure 3.5**).

We asked whether this coupling between spikes and LFP was specific to the alpha range. We quantified phase-to-amplitude coupling between the LFP and MUA using Tort's modulation index (MI, see **3.5 Methods**; (Tort et al., 2010), and show the result as a function of cortical depth and frequency (**Figure 3.3b**). We observed that columnar spiking coupled to infragranular LFP across a broad range of low frequencies, with the strongest coupling centered on the high alpha/low beta range. This frequency-dependency of the coupling was more restricted for MUA in deep layers compared to superficial layers.

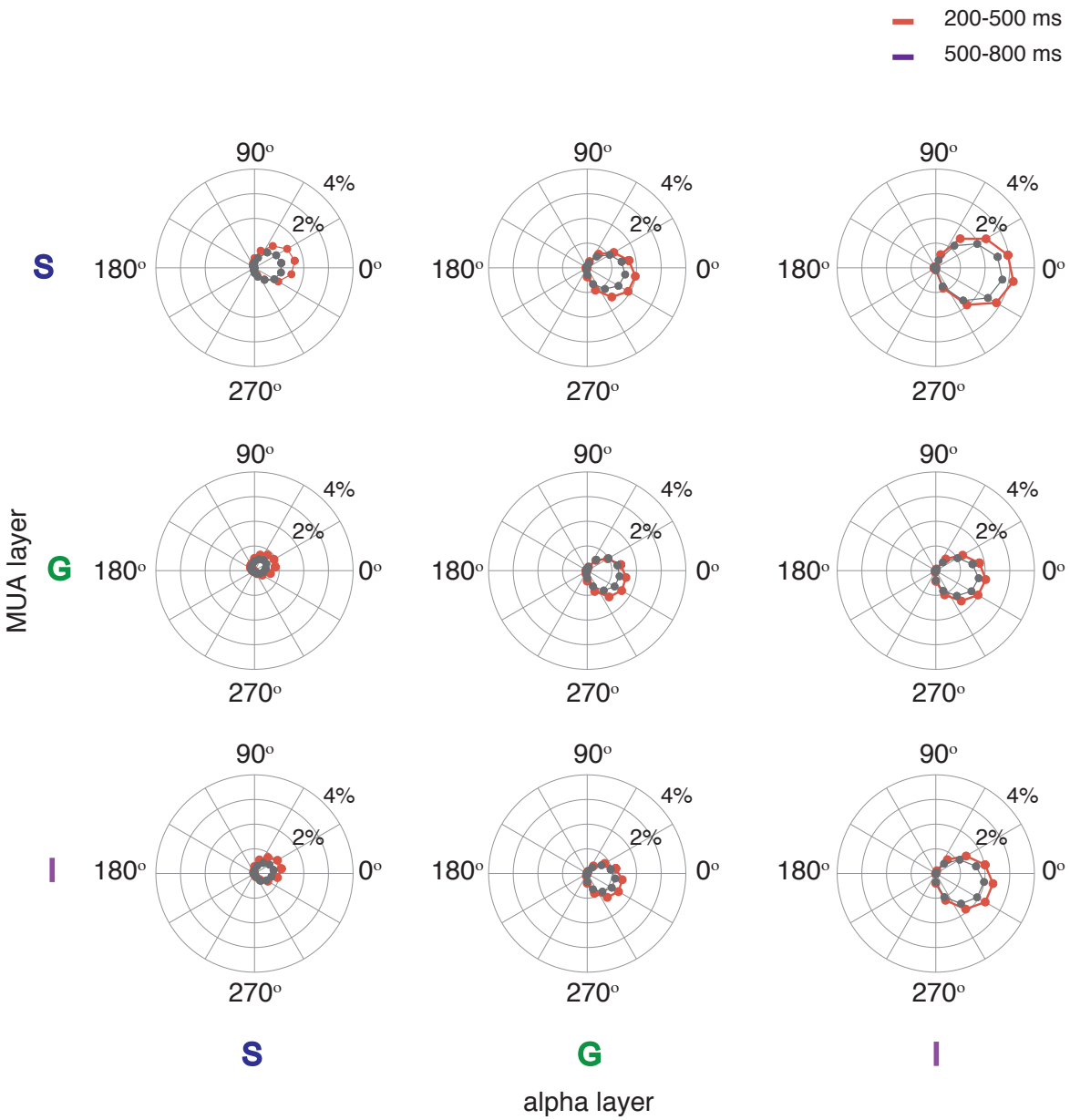

Figure 3.4 Comparison of coupling between early and late halves of the analysis window. Coupling analysis was performed for the windows 200-500 ms (orange trace) and 500-800 ms (blue trace) following stimulus onset (both monkeys, N = 56 sessions).. Polar plots show the distribution of MUA as a function of the alpha phase cycle.

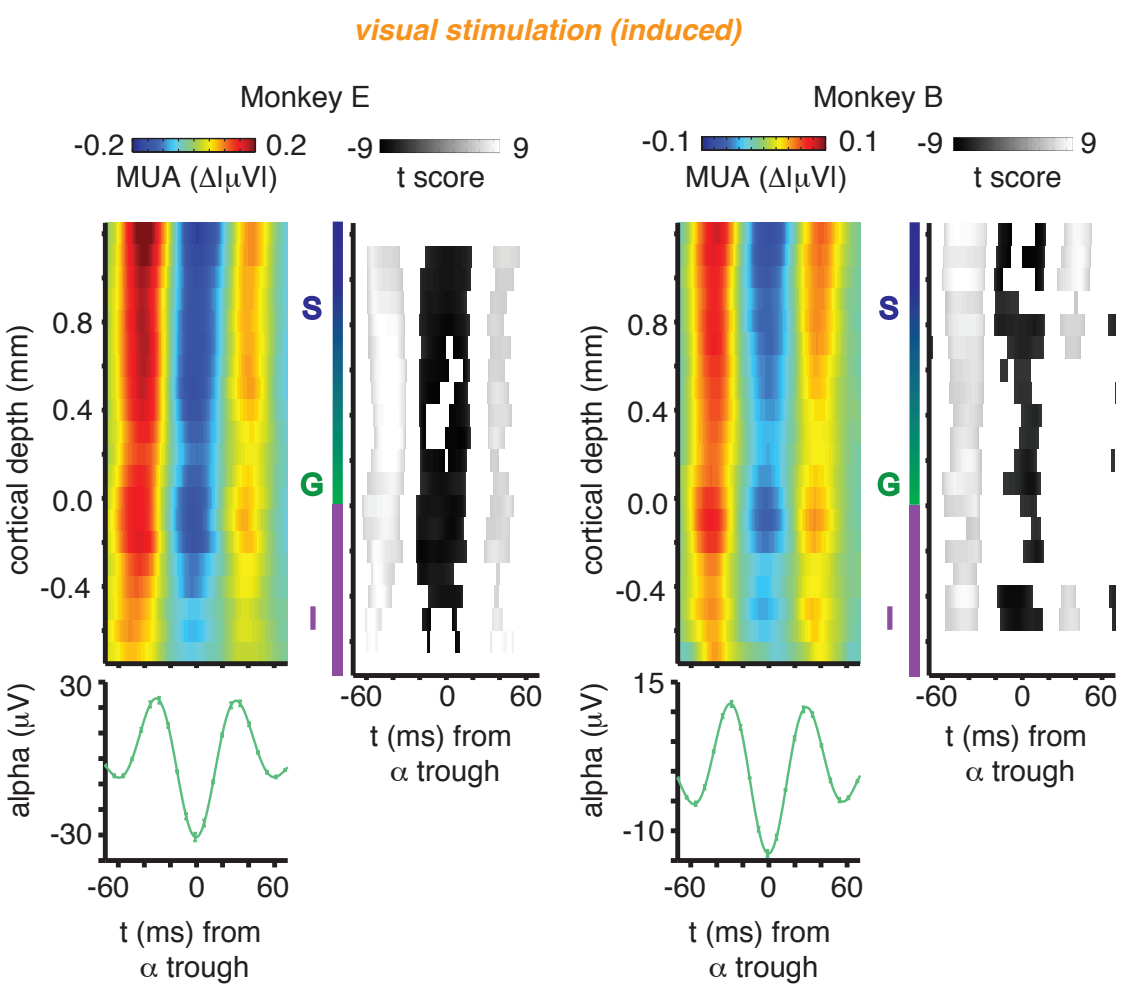

Figure 3.5 Residual (i.e., induced) coupling following removal of the evoked LFP component.
All conventions as in **Figure 3.3**.

Coupling is enhanced with stimulation and strongest for supragranular spiking

We further tested whether the observed alpha-spike coupling was dependent on visual stimulation. We compared conditions with a grating in the receptive field to the task period just prior to the onset of gratings. For the majority of sites, there was a clear and consistent phase selectivity of MUA before and after visual stimulation (**Figure 3.6**). However, the magnitude of coupling was significantly different between pre-stimulation and visual stimulation for all but two of the comparisons (paired t-tests, Bonferroni corrected, $p < 0.05$).

Spiking in the superficial layers coupled most strongly with bipolar alpha LFP in the infragranular layers (**Figure 3.6**, **Figure 3.7**). For spiking in every laminar compartment, the infragranular bipolar (re-referenced) alpha LFP provided the strongest phase reference for alpha-MUA coupling (**Figure 3.7**). For the infragranular alpha phase, coupling of spiking in supragranular layers was stronger than spiking for other compartments (3x1 ANOVA, $p<0.01$). The robust laminar specificity of alpha coupling of columnar spiking suggests a unique role for alpha activity in infragranular layers. Since additional analytic steps are needed to disambiguate the cellular origins of LFP (Kajikawa and Schroeder, 2011, Kajikawa and Schroeder, 2015), we will return to this point below. While the laminar profile of coupling was largely conserved between conditions, the magnitude of coupling was consistently enhanced with stimulation.

Laminar differences in alpha-spike coupling could be caused by higher signal-to-noise ratios (SNR) of alpha in some layers relative to others. In order to rule out this potential confound, we performed a numerical simulation. We used the mean alpha power across trials with the highest alpha power (top one-third) for high alpha simulations and mean alpha power across trials with the lowest alpha power (bottom one-third) for low alpha simulations. Unlike previous work (van Kerkoerle et al., 2014), we observed no significant difference in mean MUA across the cortical depth for low and high alpha power trials from a single depth (two sample t-test, $p = 0.662$) (**Figure 3.8a**). It is possible that the relationship between MUA and alpha power is laminar specific. The simulated results revealed no significant differences in mean MI between high and low alpha levels, suggesting that SNR differences are unlikely to account for the laminar specificity in neural coupling we observed (**Figure 3.8c**; two-sample t-tests; $p = 0.928$, $p = 0.343$, $p = 0.471$, respectively). Thus, the laminar profile of the alpha coupling of columnar

spiking must be explained by other factors, such as the intrinsic connectivity of the columnar microcircuit (see **3.4 Discussion**).

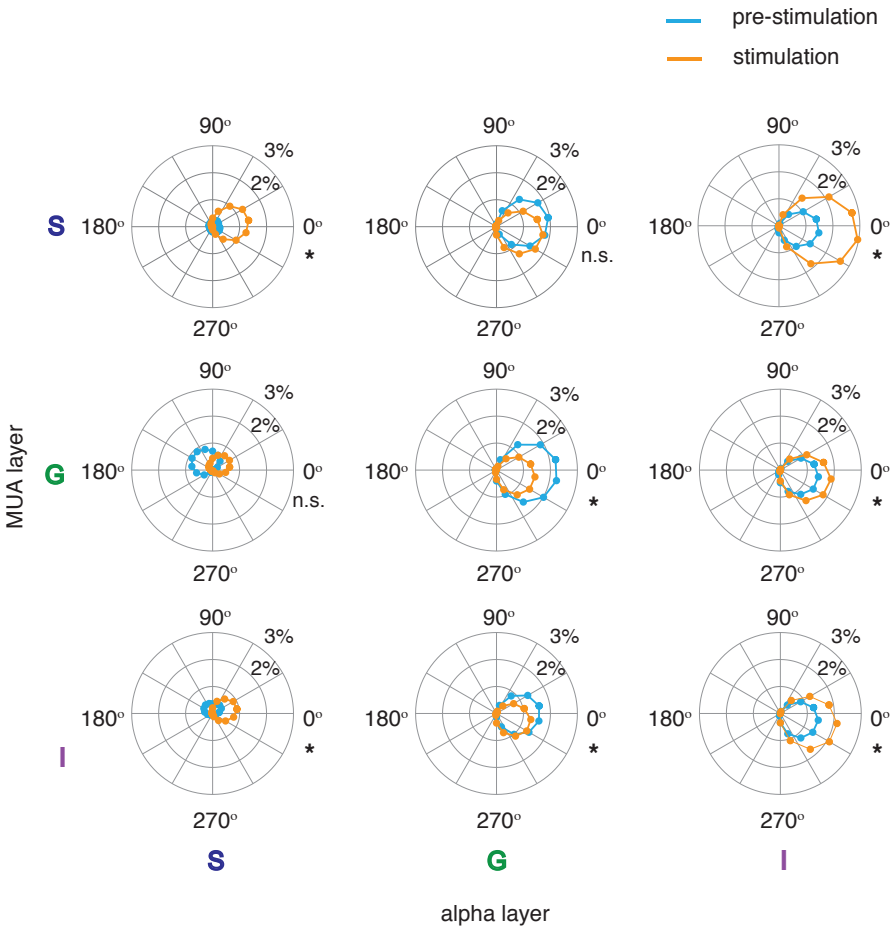

Figure 3.6 Phase coupling of V1 spiking across the infragranular alpha cycle before and after visual stimulation.
Spiking magnitude is plotted relative to alpha phase as a function of laminar position and condition. Columns correspond to alpha LFP from supragranular to infragranular layers (left to right). Rows correspond to MUA from supragranular to infragranular layers (top to bottom). Each data point depicts deviation of MUA from the mean at a given phase angle after half-wave rectifying. Data are averaged across monkeys (N = 56 sessions). Asterisks indicate statistically significant differences in peak coupling amplitude between pre-stimulation and visual stimulation (paired t-tests, $p < 0.05$, Bonferroni corrected).

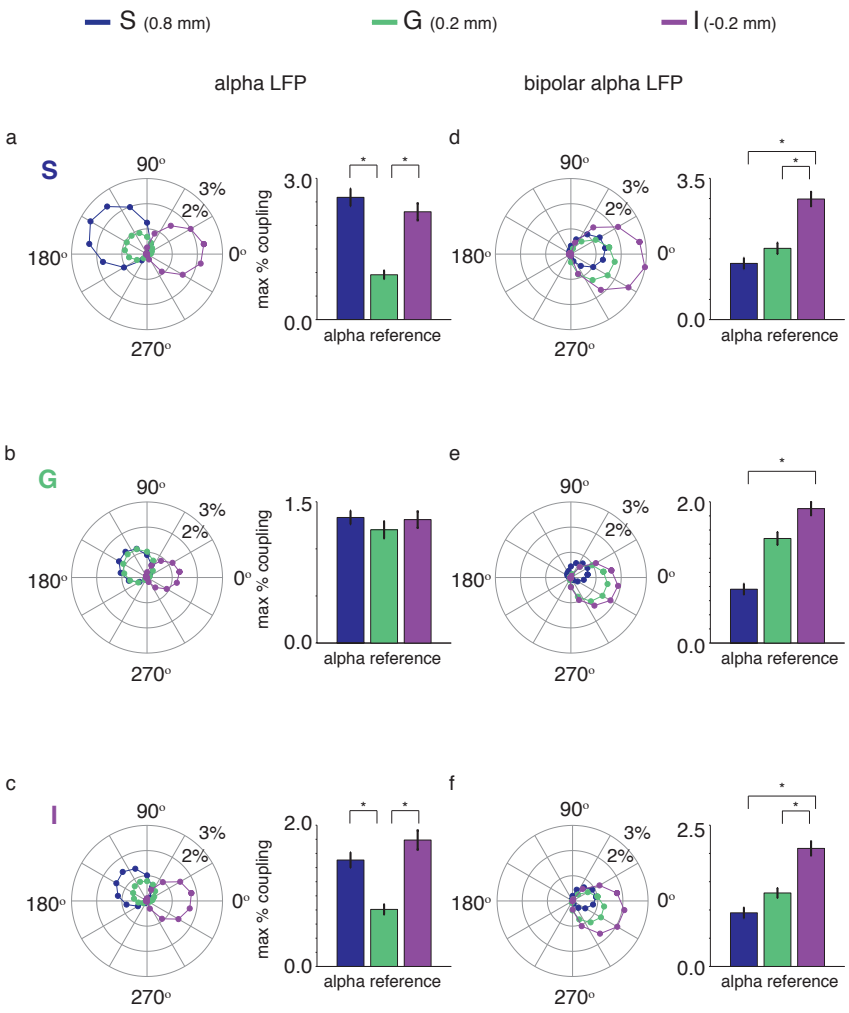

Figure 3.7 Effect of LFP re-referencing on the laminar profile of alpha-MUA coupling. Each row depicts MUA from (a) supragranular (0.8 mm), (b) granular (0.2 mm), and (c) infragranular (-0.2 mm) layers as a function of alpha from those three depths. All conventions as in **Figure 3.6**. Bar graphs depict the maximum deviation of MUA as a function of laminar compartments. Asterisks indicate statistical significance (ANOVA, $p < 0.01$) (d)-(f) Same as in (a) - (c), after re-referencing the LFP to a recording site 200 microns above each contact.

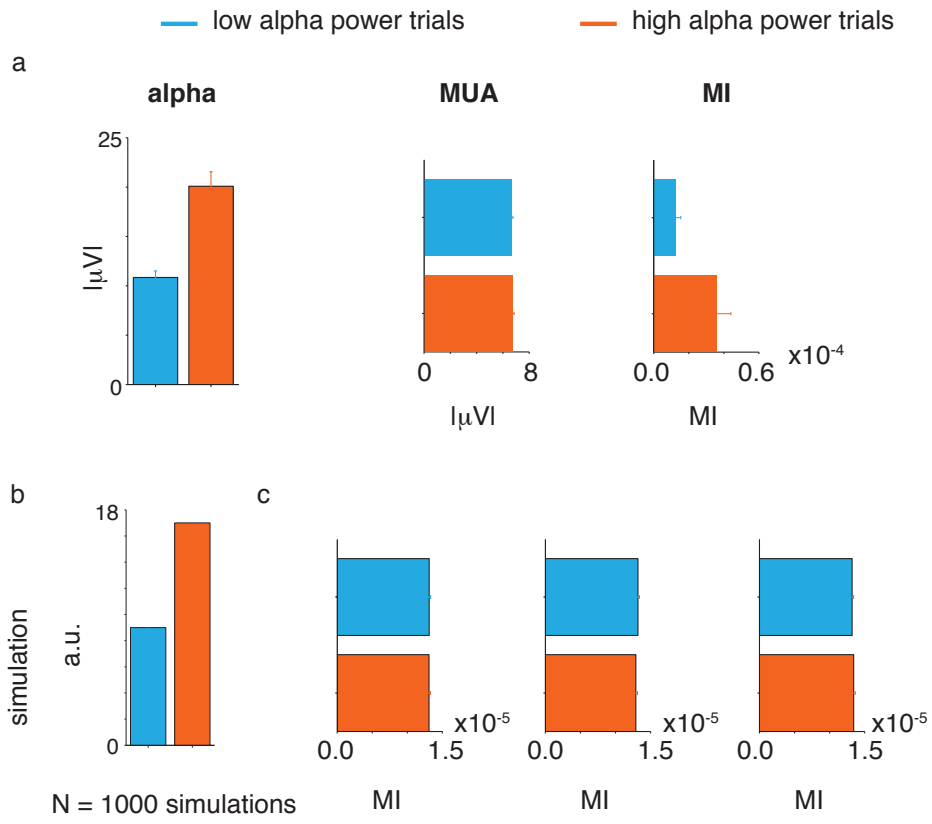

Figure 3.8 Relationship between alpha power, MUA, and coupling.
(a) All trials were divided into either a high or low alpha power category (see **3.5 Methods**). Alpha LFP for low and high alpha power trials from an infragranular site (-0.2 mm). *Left column*: Mean alpha power and SEM across cortical depth for low and high alpha power trials. *Center column*: Mean MUA and SEM across cortical depth for low and high alpha power trials. There was no significant difference in spiking activity (MUA) between low and high alpha trials when averaged across cortical depths (two sample t-test, $p = 0.662$). *Right column*: Mean MI and SEM across cortical depth for low and high alpha power trials. There was a significant difference in the average MI across cortical depths between conditions (two-sample t-test, $p = 0.006$). All data averaged across both monkeys (N = 56 sessions).
(b) Simulation of coupling between the amplitude (here: absolute value of the time-varying signal) of a high frequency (1 kHz) sinusoid and the phase of a low frequency (10 Hz) sinusoid. The magnitude of the 10 Hz signal was adjusted to simulate low and high alpha power trials, accordingly. Bar graphs show the two 10 Hz magnitudes chosen for these two conditions.
(c) Mean MI across 1000 randomized simulations of phase-amplitude coupling between these two conditions for three different levels of added noise approximating the average root mean square of the LFP for supragranular, granular, and infragranular sites. There were no significant differences between MI at low and high amplitude simulation at any noise levels (two-sample t-tests, $p > 0.05$, Bonferroni corrected for multiple comparisons).

Laminar origin of alpha fluctuations

Finally, we investigated sites of putative synaptic activity giving rise to the alpha fluctuations during visual stimulation. We used CSD analysis, which is a well-established analytic technique for estimating microscopic current sinks and sources in the extracellular low from laminar recording data (Nicholson and Freeman, 1975, Mitzdorf and Singer, 1979, Mitzdorf, 1985, Tenke et al., 1993). We were interested in the location and temporal evolution of current sinks and sources associated with the alpha cycle that underlies intracolumnar coupling. Following an approach similar to previous studies, we analyzed the distribution of laminar current sinks and sources in primary visual cortex around the alpha phase cycle (van Kerkoerle et al., 2014, Spaak et al., 2012, Bollimunta et al., 2011). Specifically, we computed the CSD on epochs of LFP aligned to peaks and troughs from alpha LFP from infragranular layers (**Figure 3.9**). This analysis revealed a columnar pattern of multiple time-varying current sinks and sources that was highly reliable in both animals. A prominent feature of this alpha-locked CSD profile was that spiking activity was lowest when prominent current sinks emerged below the layer 4C/5 boundary. These current sinks are believed to be indicative of excitatory synaptic activity (Mitzdorf, 1985); however, they could represent any voltage changes in the extracellular medium—including those from spikes and intrinsic membrane oscillations (Buzsáki et al., 2012). This pattern of sinks and sources around the alpha cycle during visual stimulation aligns with the spatial location and timing of sinks and sources from previous work during the resting state (Bollimunta et al., 2011, Spaak et al., 2012, Ninomiya et al., 2015), suggesting common generators of alpha activity across conditions. Thus the CSD analysis points to layer 5 as the most likely origin of the observed alpha fluctuations, consistent with previous experimental and

theoretical work (Silva et al., 1991, Sun and Dan, 2009, da Silva, 1991, Connors and Amitai, 1997, Jensen and Mazaheri, 2010, Jones et al., 2000, Jones et al., 2009).

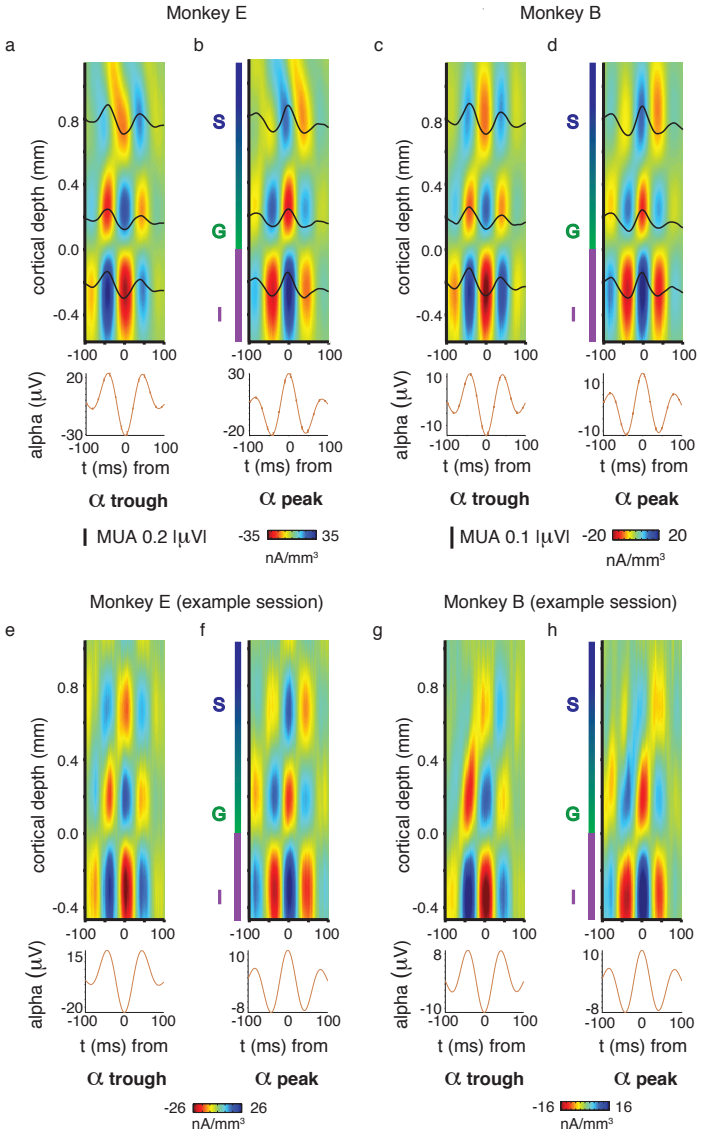

Figure 3.9 Laminar distribution of alpha-locked extracellular current sinks and sources during visual stimulation.
(a) Mean CSD around infragranular (-0.2 mm) alpha troughs for monkey E (N = 23). At three laminar locations, mean MUA for the same time period is superimposed (black lines).
(b) Mean CSD around infragranular alpha peaks for monkey B.
(c) and (d) same as (a), but for monkey B (N = 33 sessions).
(e) – (h) Same as (a) – (d) but for example sessions in each monkey.

No consistent relationship between microsaccades and alpha phase

Microsaccades can cause transient activation that might manifest as spurious coupling. We tested for this possibility by determining the instantaneous alpha phase at the time of a microsaccade. We found that there was no systematic relationship between alpha phase angle and microsaccade frequency. The distribution of alpha phase at the time of microsaccades was not significantly different from uniform for both animals (Rayleigh z-test for non-uniformity, $p > 0.05$) (**Figure 3.10**).

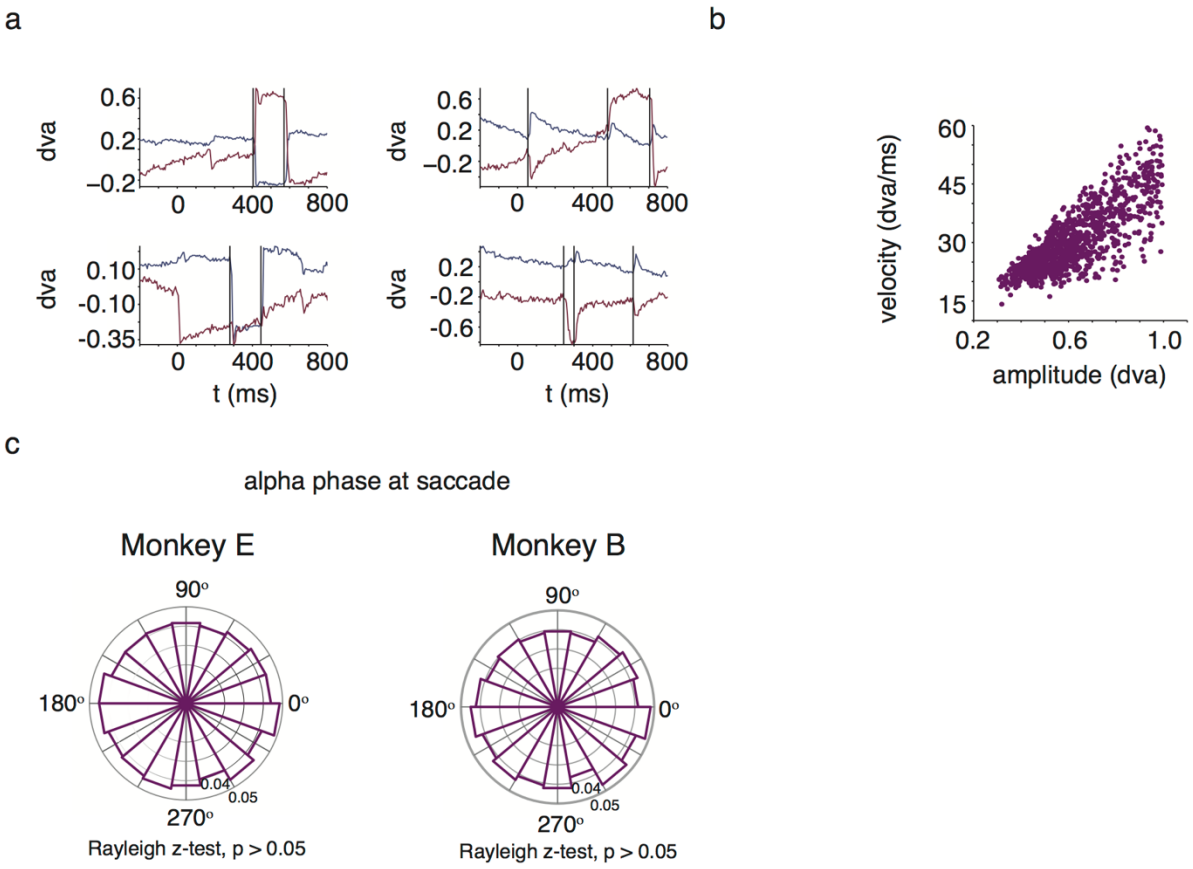

Figure 3.10 Eye movement analysis.
(a) Two example trials for monkey E (left) and monkey B (right). Traces depict the horizontal (blue) and vertical (red) gaze position as a function of time. Vertical lines indicate onset time of an algorithmically detected microsaccade. Time is relative to stimulus onset.
(b) Main sequence for an example session.

(c) Relative frequency of alpha phase at time of saccades averaged across all sessions for monkey E and monkey B. Distribution of alpha phase at time of saccades was not significantly different from uniform (Rayleigh test for non-uniformity, $p > 0.05$) for either monkey.

3.4 Discussion

The results presented in this paper show that spiking responses across all layers of primate striate cortex are coupled to alpha-range extracellular field potentials in infragranular layers. This coupling between spiking and the alpha phase cycle was strongest for spiking in upper cortical layers and strongest during periods of visual stimulation. Importantly, alpha-spike coupling persisted during the sustained visual response, after the initial transient response had tapered. This result cannot be explained by small microsaccades made during fixation. In the sections below, we discuss our findings in greater detail and provide speculative explanations that could account for our results.

Laminar specificity of alpha-spike coupling during visual stimulation

Our data show that alpha-range field potentials are strongly coupled with spiking throughout the column but especially in supragranular layers during visual stimulation. We assessed current sinks and sources related to alpha activity in primary visual cortex using an analytic approach similar to previous work (Bollimunta et al., 2008, Bollimunta et al., 2011, van Kerkoerle et al., 2014). In agreement with previous alpha CSD analyses, we found the strongest alpha-locked sink in deep layers below the layer 4C-layer 5 border at the time of alpha troughs. At counter-phase (coincident with deep layer alpha peaks), the sign of the sinks and sources reversed so that a sink was present in the granular layer. These alpha-locked CSD patterns suggest endogenous activation of granular and infragranular compartments that alternates at a low frequency (~7-14 Hz). We observed an alternation in spiking across the entire cortical column that coincided with

this rhythmic modulation. Even after attenuating the effects of volume conduction inherent in LFP signals by using bipolar LFP (Kajikawa and Schroeder, 2011, Kajikawa and Schroeder, 2015), this effect was strongest for spiking in supragranular layers around the infragranular alpha cycle.

Interlaminar control over the cortical column

Together, our findings support the hypothesis that synaptic modulation of neurons at specific locations within V1's laminar microcircuit modulates spiking throughout the entire column. The anatomical layout of the V1 microcircuit suggests that layer 5 neurons in particular exert strong control over neurons within the same cortical column (Dantzker and Callaway, 2000, Binzegger et al., 2004). Layer 5 neurons also have a tendency to produce activity in the theta/alpha range (5-12 Hz) in *in vitro* slice preparations from mouse sensorimotor cortex (Silva et al., 1991) as well as rat visual cortex (Sun and Dan, 2009). These rhythmic firing patterns are believed to be carried out by a morphologically distinct class of cells in layer 5 that elicit rhythmic bursts 5 to 15 times a second, with each train consisting of 2-5 spikes occurring at 150-300Hz (Connors and Amitai, 1997). This finding also agrees with early *in vivo* recordings in dogs, which suggest that infragranular neurons operating in the alpha range may act as "pacemakers" (Lopes da Silva and Storm Van Leeuwen, 1977).

One possible mechanistic model that could describe our results is that projections from layer 5 neurons to more superficial layers exert a net inhibitory effect through interneurons (Connors, 1984, Chagnac-Amitai et al., 1990). Activation of these superficially-projecting neurons could be reflected in the infragranular sink, coincident with the alpha LFP trough, and the net inhibitory effect could be reflected in the concomitant relative decrease in spiking (**Figure 3.4a,c**). This interpretation is congruent with the general observation that alpha activity

in visual cortex is associated with periodic inhibition of neural activity (Klimesch et al., 2007, Jensen and Mazaheri, 2010, Händel et al., 2011, Jensen et al., 2012, Bareither et al., 2014, Chaumon and Busch, 2014). Whether this rhythmic modulation of spiking is best conceived as gating or pulsed inhibition, the periodic fluctuation of columnar activity might be an important synchronizing element in the integration of feedforward visual inputs with feedback from higher cortical areas.

Role of feedback and other non-local signals

As stated above, it is possible that the rhythmic fluctuation we observed does not emerge within V1, but is inherited from other regions. One proposition is that feedback from other cortical areas regulates excitability across the column. In line with this explanation, neurons in the infragranular layers of cortex are the origin (Markov et al., 2013) and target (Maunsell and Van Essen, 1983, Nascimento-Silva et al., 2014) of cortical feedback. Alpha activity within these layers thus might constitute the spectral signature of communication between cortical areas (Donner and Siegel, 2011, Self et al., 2013, van Kerkoerle et al., 2014, Bastos et al., 2015). Indeed, intra-areal LFP coherence in the low frequency range is highest between the infragranular layers of V1 and V2 (von Stein et al., 2000).

An alternative, but not mutually exclusive, explanation is that the thalamus is involved in rhythmically modulating neurons in primary visual cortex, and ultimately intracolumnar coupling. For example, the lateral geniculate nucleus (LGN) may control neurons in primary target layers 4C and 6 in V1 in a unidirectional manner, or through a thalamocortical loop (Fitzpatrick et al., 1994, Bollimunta et al., 2011). In line with the notion of geniculate involvement, LGN interneurons modulate thalamocortical relay neurons in the alpha range

(Lőrincz et al., 2009). Indeed, alpha activity in the LGN couples with infragranular activity in V1 (Bastos et al., 2014), supporting the idea that the alpha-range fluctuations in the LGN, perhaps in concert with infragranular neural activity, could control excitability across the column in V1.

A third possibility is that second order thalamic nuclei, such as the pulvinar, are involved in regulating alpha activity in primary visual cortex (Lopes da Silva et al., 1980, Palva and Palva, 2007, Saalmann et al., 2012). Pulvinar neurons engage in low-frequency oscillatory bursting (Lopes da Silva and Storm Van Leeuwen, 1977), and supragranular V1 spiking activity has been shown to critically depend on pulvinar input (Purushothaman et al., 2012). The alpha-spike coupling observed in our study could be congruent with pulvinar-based modulation of spiking activity. However, this hypothetical scenario necessitates further explanation given the relatively weak alpha-locked current sinks and sources in the supragranular layers, which constitute the primary projection target of pulvinar neurons (Jones, 2001).

Future work will need to determine the specific cell-types within V1 involved in the rhythmic control of population spiking activity during sensory processing, if this alpha coupling of spiking activity generalizes to other visual areas, and whether this rhythmic modulation of spiking is intrinsic to V1 or if other structures are involved in its regulation.

3.5 Methods

Subjects

Two healthy adult male macaques (*Macaca mulatta*), B and E, were used in fifty-six recording sessions (23 from E). All procedures were approved by the Animal Care and Use Committee of the National Institute of Mental Health and were in compliance with regulations set by AAALAC.

Surgical preparations

Two separate surgical procedures were performed on each animal. For all surgeries, general anesthesia was induced with an intramuscular injection of ketamine hydrochloride (10 mg/kg) and maintained with isoflurane anesthesia (1.5%-2.0%) throughout the procedure. Vital signs, including blood pressure, heart rate, SpO2, CO2, respiratory rate, and body temperature, were monitored continuously. During the first surgery, a custom-made fiberglass head holder was attached to the animal's skull using self-curing dental acrylic (Lang, Inc., Wheeling, IL, USA) and ceramic screws (Thomas Recording GmbH, Giessen, Germany). In a subsequent procedure, a craniotomy was performed over the caudal aspect of area V1 where the representation of perifoveal visual field is located. A plastic recording chamber was implanted around this location using the same ceramic screws and self-curing acrylic as used for the head holder. Animals received prophylactic antibiotics and analgesics (buprenorphine, acetaminophen, ketoprofen) for at least three days following all surgical procedures.

Experimental conditions

During all experimental sessions, animals were placed in a darkened recording booth and sat in a custom designed primate chair (Precision Plastic, Gibson City, IL, USA) with their heads restrained. For the visual stimulation condition, animals were given liquid reward for successfully acquiring and maintaining fixation on a small (0.01-0.1 degrees of visual angle, dva) white spot displayed on the center of the monitor. At the beginning of each session, we manually mapped receptive fields by passing a rectangular bar of cardinal orientations across the visual field while animals fixated. We used the audible multiunit response on each electrode contact to

determine the extent of visual space that reliably evoked spiking responses at the electrode location. This aggregate receptive field then was used to determine the placement of the main stimulus set. Typically, stimuli were 2 dva in diameter (**Table 3.1**), with one stimulus completely covering the mapped receptive field (**Table 3.2**). Following receptive field mapping, we initiated the main task which proceeded as follows: after 1000 ms (monkey B) or 1500 ms (monkey E) of sustained fixation on a central cue, an array of four identical, static circular gratings appeared on the screen (**Figure 3.1a**). For reasons beyond the current study, more than one grating was shown, and these gratings were presented randomly to either the right or left eye and were displayed in either a red or green hue. Within a session, these gratings were presented at the same eccentricity, equidistant to each other such that one grating was shown in each quadrant of the visual field.

Analyses were averaged over all visual gratings since stimulus-specific response modulation was beyond the scope of this study. Unless stated otherwise, analyses for the visual stimulation condition were restricted to the time window starting 200 ms after the onset of the visual gratings through 800 ms following this onset. If the monkeys' gaze left the fixation window of 1.0-1.5 dva around the central fixation cue, the trial was aborted and the next trial began after a 1-5 s delay. The average number of trials per session was 682 (median 681). In order to compare laminar neural coupling during visual stimulation to coupling in the absence of visually driven activity, we used the pre-stimulation period in each trial (100 ms to 700 ms following fixation).

Visual display

Stimuli were presented on 27-inch thin-film transistor (TFT) monitors (X2Gen MV2701, 1024 × 768 resolution) positioned at a viewing distance of 80 cm using a mirror stereoscope. A PC (Kontron, Poway, CA, USA) using NVIDIA Quadro FX 3000 graphics boards was used to run custom-written software (ESS/STIM; copyright Dr. D. Sheinberg, Brown University, Providence, RI) to produce the visual stimuli used in this study. The animals' eye movements were continually recorded at 200Hz using an infrared light sensitive camera and commercially available eye tracking software (Eye Link II, RS Research, Osgoode, Canada). Animals performed a brief perimetric calibration procedure for the eye tracking software at the beginning of each session. All eye movements and behavioral events were synced to the neurophysiological data using a separate PC running a real-time operating system (QNX Software Systems, Kanata, Ontario, Canada).

Neurophysiological recordings

Broadband (0.5Hz – 12.207 kHz) extracellular voltage fluctuations were recorded with an acute laminar probe inside an electromagnetic radio frequency-shielded booth. For each session, a custom-made chamber-mounted microdrive was used to lower the laminar probe into dorsal V1, caudal to the lunate sulcus. The laminar probe consisted of 16 or 24 microelectrode contacts, linearly spaced 0.1 mm apart with impedances ranging 0.2-0.8 MΩ at 1kHz (Plexon UProbe, Plexon, Inc., Dallas, TX, USA). Extracellular voltages were measured in reference to the shaft of the probe and were collected simultaneously from all microelectrode contacts. Voltage-fluctuating signals were amplified, filtered, and digitized using a 64-channel RZ2 recording system (Tucker Davis Technologies, Alachua, FL). During data collection, the local field

potential (LFP) was extracted by filtering between 0.5 Hz and 500 Hz and digitizing at 1.0173 kHz. MUA was extracted by high-pass filtering at 300Hz and digitizing at 24.4141 kHz (see *Multiunit Analysis*). Both signals were stored for subsequent offline analysis.

Data analysis

All offline analysis was performed using custom-written code in MATLAB (MathWorks, Natick, MA, USA).

Multiunit analysis

Although single neurons can be isolated with laminar probes in a way that is comparable to that of standard microelectrodes, isolating cells on all electrode contacts of the array simultaneously proves difficult in practice. For this reason, we opted to use multiunit activity (MUA) as a proxy for the activity of local neurons. Specifically, we full-wave rectified the recorded high pass filtered (at 300 Hz) data, and then decimated the signal by a factor of 20 to obtain the time-varying power in the spiking range. We low pass filtered the resulting signal at 50 Hz using a Butterworth filter with an order of 4.

CSD analysis

Current source density (CSD) analysis of visual responses to brief flashes of light have been shown to reliably indicate the location of the primary geniculate input in V1 (granular layer 4C) by a distinct current sink that is thought to reflect combined excitatory post-synaptic potentials of the initial retino-geniculate volley of activation (Mitzdorf, 1985). To compute the visually

evoked CSD, we applied an estimate of the second spatial derivative appropriate for multiple contact points (Nicholson and Freeman, 1975) . Specifically, we used the three-point formula:

$$CSD\ (t,c) = -\frac{x(t,c-z) + x(t,c+z) - 2x(t,c)}{z^2}$$

where x is the extracellular voltage recorded in μV at time t from an electrode contact at position c, and z is the electrode intercontact distance (0.1 mm). In order to yield CSD in units of current per unit volume, we multiplied the resulting CSD from the formula above by 0.35 S/mm, an estimate of the conductivity of cortex (Ranck, 1963). We applied this transformation to data collected during the fixation paradigm, with each trial aligned to the onset of the visual gratings described in *Experimental Conditions*. Using this approach, we were able to locate the bottom of a prominent initial current sink in all sessions. After excluding superficial and deep electrode contacts that did not record a visual response (due to their placement outside of the cortical gray matter), we aligned all subsequent intersession averages to this reference point (**Figure 3.1b**) (Maier et al., 2011, Maier et al., 2014) . Representations of CSD as a function of time and space were computed by interpolating CSD between adjacent electrode contacts and smoothing the result with a 2D-Gaussian filter ($\sigma = 0.1$) (Pettersen et al., 2006, Godlove et al., 2014, Ninomiya et al., 2015) . While the theoretical foundations of CSD analysis are based on several assumptions regarding recording parameters and cortical geometry that are difficult to control for (Tenke et al., 1993), the technique has proven remarkably robust against many of these potential reasons for concern in practice (Kajikawa and Schroeder, 2015) .

Alpha-locked spiking

In order to determine the degree of coupling between alpha phase and columnar spiking, we band-limited the LFP from a select electrode contact (-0.2 mm) into the 7 to 14 Hz band using a bidirectional Chebyshev type I filter with an order of 2. We then detected amplitude troughs in this band-limited alpha LFP by calculating the second temporal derivative. We triggered the time-varying analog MUA from all recording contacts of the laminar probe to the time of alpha troughs, t_x. More specifically, we averaged the analog MUA between t_x−100 ms to t_x+100 ms, approximating the duration of more than one full 7 Hz cycle. Alpha amplitude troughs within the first 100 ms or last 100 ms of the analysis window were excluded. This procedure resulted in multiple alpha-locked MUA epochs for each trial and electrode contact. We averaged the trough-locked analog MUA within each electrode contact and each trial. Previous work has shown that there are frequency-specific LFP power differences among the layers of V1 (Steriade et al., 1990, Kramer et al., 2008, Sun and Dan, 2009, Maier et al., 2011, Xing et al., 2012, Smith et al., 2013). To account for baseline differences in the MUA voltage between layers, we calculated the difference between the mean alpha-locked MUA and the mean MUA amplitude across the epoch for each depth in each session. We assessed the significance of this coupling by computing a t-score for each time point in the epoch at each depth. To calculate this t-score, we compared our results against a randomly shuffled control, obtained by pairing the alpha signal from one trial with the MUA from a different, randomly selected trial, and did so for all trials and sessions in the data set. All statistics were Bonferroni-corrected for multiple comparisons.

Phase-dependency of spiking

We verified results obtained by the alpha-locking of spiking activity using a second procedure. We chose three representative laminar recording sites (0.8 mm, 0.2 mm, -0.2 mm), corresponding to supragranular (layer 2/3), granular (layer 4C), and infragranular (layer 5) locations, respectively. We band-limited bipolar (re-referenced to signal recorded 200 microns superficial to the site) LFP into the alpha band using the same filter as above for each representative depth. We extracted the phase of the band-limited alpha from the output of the Hilbert transform at each cortical depth. We then computed the mean MUA as a function of the alpha cycle. Specifically, we divided the 360-degree wide phase cycle into 20-degree wide bins. Then, we assigned all MUA samples to their respective alpha phase bin, and averaged the MUA amplitude within each bin. We calculated the amount that each MUA bin deviated from the mean MUA amplitude by converting all values into percent difference by first subtracting and then dividing by the mean MUA across all phase bins, and multiplying the result by 100. In order to visualize the data in polar coordinates, we half-wave rectified the result, which revealed positive deviations from the mean (units referred to as percent coupling). Significant differences in coupling magnitude were assessed using a paired t-test at each depth and were corrected for multiple comparisons.

Evoked vs. induced response

We repeated the percent coupling procedure described above to make several other comparisons. First, we confirmed that any coupling effect we observed was not a consequence of filtering method (**Figure 3.11**). To confirm this, we filtered the LFP from an infragranular site (-0.2 mm) into 1 Hz-wide bands centered on 8 Hz, 10 Hz, 12 Hz, and 14 Hz using a finite-impulse response

filter (FIRLS) with a frequency-dependent order (2 cycles of each frequency, or an order of 1000 Hz/frequency (Hz) * 2) (Spaak et al., 2012). Then, we computed the deviation of MUA around the phase cycle for these signals as described above. Second, we repeated the percent coupling procedure to compare coupling during the early (200-500 ms) and late (500-800 ms) halves of the analysis window (**Figure 3.4**). We tested for differences in coupling between early and late halves of the analysis window using multiple Wilcoxon signed rank tests and accounted for multiple comparisons using Bonferroni correction.

Lastly, we repeated the percent coupling procedure to compare coupling using alpha filtered from the LFP and alpha filtered from LFP re-referenced to a site 200 microns superficial to each contact (bipolar alpha LFP). We compared coupling of MUA across the three alpha phase sites (0.8 mm, 0.2 mm, -0.2 mm) for all MUA depths using 3x1 ANOVAs and post-hoc multiple comparison tests (**Figure 3.7**).

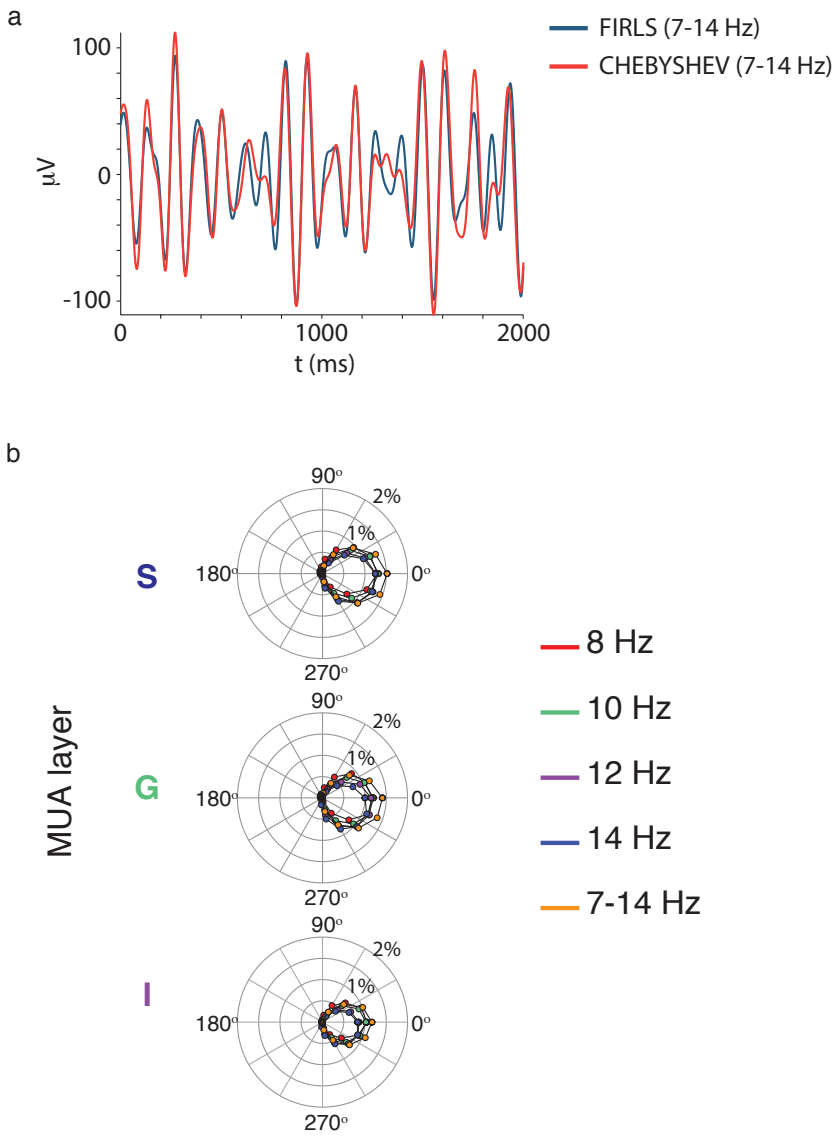

Figure 3.11 Alternative filter settings.
(a) Comparison between LFP filtered into 7 to 14 Hz range with a least squares finite impulse response filter (FIRLS, blue trace) and a Chebyshev filter (red trace).
(b) Distribution of MUA around alpha cycle from an infragranular site (-0.2 mm) for alpha filtered into the 7 to 14 Hz band and 1 Hz-wide bands at 8 Hz, 10 Hz, 12 Hz, 14 Hz, using FIRLS. Each data point represents the percent deviation of MUA amplitude for a given phase after half-wave rectifying**.** Data are from both monkeys (N = 56 sessions).

Modulation index

We used the modulation index (MI) proposed by Tort et al. (2010) to assess coupling between

MUA and the phase of LFP across a range of narrow frequency bands. Specifically, we filtered the LFP at one laminar recording location (-0.2 mm) into 2-Hz wide bands in 1 Hz increments between 3 and 40 Hz. We used a finite-impulse response filter with a frequency-dependent order (2 cycles of each frequency, or an order of 1000 Hz/frequency (Hz) * 2) (Spaak et al., 2012). Then, for each frequency, we calculated the MI between the LFP and MUA at all cortical depths. Specifically, for each of these pairs, we binned MUA amplitude as a function of alpha phase (N = 30 bins), and computed a single MI value (Tort et al., 2010). The mean MUA amplitude within each phase bin was normalized by dividing by the sum of all phase bin means, resulting in distribution *P*. Tort et al.'s (2010) MI measures the Kullback-Leibler distance between this phase-amplitude distribution and a uniform distribution using the following formula:

$$MI = \frac{\log(N) - (-\sum_{j=1}^{N} P(j) \log [P(j)])}{\log (N)}.$$

where *j* represents a single bin among *N* total bins. In order to determine which aspects of the resulting MI matrix are specific to the infragranular layers, we repeated this procedure using LFP from a granular recording location (0.2 mm) and subtracted this reference granular MI map from the infragranular MI map.

Alpha-locked CSD

In order to evaluate the laminar profile of CSD associated with alpha activity, we first extracted an infragranular alpha signal using the same approach as outlined under *Alpha-locked spiking*. We then determined the time of alpha troughs, t_x, which we used to trigger and average the LFP across all electrode contacts. We next used a Butterworth filter to high-pass filter the alpha-locked LFP at 4 Hz to account for low frequency drift, and computed an estimate of the second

spatial derivative using the procedures detailed in *CSD Analysis*. To align the alpha-locked CSD with concomitant spiking activity, we averaged MUA for each electrode contact within the same window. To investigate the temporal evolution of the laminar CSD profile throughout the alpha phase cycle, we repeated this procedure, replacing alpha troughs with alpha peaks.

Numerical simulation

In order to assess the robustness of MI to varying levels of signal, we performed a numerical simulation. We first produced a test signal by multiplying the amplitude of a high frequency periodic signal (1000 Hz) with a 10 Hz sinusoid to which we added varying levels of random (Gaussian) noise. We used three different levels of noise, each set to approximate the average root mean square (RMS) of the alpha-range LFP recorded during visual stimulation in the supragranular, granular, infragranular layers, respectively. The amplitude of the high frequency signal was set to approximate the mean magnitude of MUA. The amplitude of the low frequency signal was set to approximate the mean alpha power on low or high alpha power trials. To find these means, for each recording session, we calculated the mean band-limited alpha power for all trials. We split trials into the top 30% of the alpha power distribution and the bottom 30% of trials in the distribution, and then averaged their respective means to create a high and low alpha category of trials, respectively. Using the test signal, the MI was then computed between filtered low frequency and high frequency signals. One thousand simulations were run for each low and high alpha power level. We averaged the MI across all simulations and used two-sample t-tests to test for differences in MI between low amplitude and high amplitude low frequency simulations.

Secondary to the simulation, we used the analysis from stratifying the data into low alpha

power and high alpha power trials to confirm that differences in MI could result from equal magnitude MUA. Specifically, we averaged the MUA from low infragranular alpha power and high infragranular alpha power trials across the cortical depth. We used a two-sample t-test to compare the mean magnitude of MUA for low alpha power and high alpha power trials. Then, we computed the MI for these trials and averaged the result across the cortical depth. We performed a two-sample t-test to test for differences in MI for these two categories of trials.

Power spectral density and time-frequency representations

We computed the power spectral density (PSD) of the bipolar LFP from three representative depths (0.8 mm, 0.2 mm, -0.2 mm) for visual stimulation and pre-stimulation conditions. To calculate the PSDs, we used Welch's method with a window size of 512 and an overlap of 256. The time-frequency analysis was performed using the multitaper approach provided by the Chronux Toolbox for Matlab (http://chronux.org/; (Bokil et al., 2010). Specifically, we calculated the power in different frequency bands over time using a moving window of 150 ms, stepping every 1 ms. We converted the output into units of dB, averaged across sessions, and z-score transformed the resulting matrix. Then, at each frequency, we baseline corrected the estimation of power over time by subtracting the mean z-score for time points occurring approximately 300 ms to 160 ms before stimulus onset.

Eye movement analysis

Previous work shows that the frequency of saccades occurs at a low frequency (< 5 Hz) (Ito et al., 2013). Furthermore, saccades are accompanied by an increase in power across a range of low frequencies, including the alpha-beta band, in V1 (Bosman et al., 2009). In order to determine if

small saccades made during fixation drove the coupling effect described in this study, we related microsaccades to the alpha LFP. We used the MATLAB implementation of the microsaccade detection method published by (Otero-Millan et al., 2014) to determine the onset of microsaccades. We excluded microsaccades with amplitude of less than 0.3 degrees. Within the visual stimulation analysis window, we determined the alpha phase recorded at the time of a detected eye movement. Then, we binned the alpha phase at the time of microsaccades across 20-degree wide bins. We calculated the relative frequency of this distribution for each session by dividing the number of counts in each alpha phase bin by the total number of detected microsaccades. A Rayleigh z-test for non-uniformity was calculated on the set of phases across sessions, prior to binning, for each monkey E and monkey B. The distribution was considered statistically significantly different from uniform if $\ln(p) > \ln(-\ln(\alpha))$, with $\alpha = 0.05$ (Siapas et al., 2005, Liebe et al., 2012).

CONCLUSIONS

In this dissertation, I explored two different types of signal convergence in the primate primary visual pathway. I first considered convergence of two feedforward signals—the outputs from the two eyes. Then, I considered how feedforward visual signals converge with ongoing activity in the visual cortex.

4.1 Convergence of two feedforward signals in the primate primary visual pathway

Binocular integration has been investigated for many decades by anatomists, psychophysicists, and neurophysiologists alike. Anatomical and neurophysiological techniques are particularly suited for determining where within the primary visual pathway the outputs of the eyes meet. Based on both previous anatomical and neurophysiological studies (Fitzpatrick et al., 1985, Hubel and Wiesel, 1968, Hubel and Wiesel, 1972), one can conclude that, broadly speaking, interactions between the two eyes' signals must occur in layer 2/3 of primary visual cortex or at an earlier processing stage (closer to the eyes). In this dissertation, I determined if the outputs of the two eyes interact prior to layer 2/3 of V1 using neurophysiological techniques as evidence from earlier neuroanatomical studies hinted at the possibility of interactions in either layer 4C of V1 (Blasdel and Lund, 1983), or even the LGN (Campos-Ortega et al., 1968, Saini and Garey, 1981).

To my knowledge three previous studies tested for binocular interactions in the LGN of macaques (Rodieck and Dreher, 1979, Marrocco and McClurkin, 1979, Schroeder et al., 1990). Unlike (Rodieck and Dreher, 1979, Marrocco and McClurkin, 1979), the study reported in Chapter One was carried out in the awake macaque and not in the anesthetized preparation. This aspect is noteworthy because the activity of LGN neurons is substantially affected by varying

arousal states, including anesthesia (Alitto et al., 2011). Schroeder et al. (1990) investigated binocular interactions in the LGN of awake macaques. However, they recorded multiunit activity, which could include spikes from neurons in more than one LGN layer. While Schroeder et al. (1990) report binocular interactions in the LGN, it thus is possible that their measurements included responses from neurons in neighboring layers that receive inputs from the other eye. The study reported in Chapter One combines the single-unit measures that (Rodieck and Dreher, 1979, Marrocco and McClurkin, 1979) used with the awake preparation that Schroeder et al. (1990) employed. Chapter One showed that both certain P and certain M units showed significant binocular modulation in the awake primate. However, while we observed some binocular modulation in the LGN, it affected only a small subset of neurons. Nonetheless, this finding warrants further investigation into the origins of this binocular modulation (see below). Experiments with a larger sampling size will be needed to gain further insight to combat the fact that binocular modulation affects only a subset of LGN neurons. Furthermore, the effects shown in Chapter One were somewhat heterogenous with respect to stimulus conditions, and a larger sample size may better parse out the nature of these geniculate binocular interactions.

On a similar note, Chapter One describes a small sample of five koniocellular neurons. This number matches expectations given our overall sample size and the fact that only ~10% of LGN neurons belong to the koniocellular division (Hendry and Reid, 2000). However, given that we observed binocular modulation in two of these five neurons and recent work showing binocular responses of K neurons in marmosets (Cheong et al., 2013, Zeater et al., 2015), binocular interactions in the K pathway warrants more investigation. In Chapter One, we used cone-isolating stimuli to identify blue-ON and blue-OFF cells that are thought to be unique to the K pathway (Martin et al., 1997). However, an alternative way to identify K neurons is to exploit

their idiosyncratic biochemistry. K neurons, unlike M and P neurons, express calcium binding protein CamKIIα (Hendry and Yoshioka, 1994). A recent study used a viral marker for CamKIIα and optogenetics to target LGN K neurons (Klein et al., 2016). Future work on LGN binocular interactions may benefit from using this approach for investigating the koniocellular pathway.

What is the source of the binocular modulation of LGN neurons? As stated above, it is possible that these interactions occur through neurons that bridge eye-dominance layers (Campos-Ortega et al., 1968, Saini and Garey, 1981). Alternatively, these interactions could arise through feedback from V1. One way to distinguish between these two alternatives is to inactivate the feedback from V1 to test whether binocular modulation in the LGN occurs in the absence of cortical feedback. Future work combining cortical inactivation techniques, such as pharmacological inactivation or lesions, with LGN recordings has the potential to reveal the source of LGN binocular modulation that we and others observed.

While we observed binocular modulation in the LGN, it affected only a subset of neurons, which seems too small to fully explain the process of binocular integration. For this reason, I looked towards the next possibility of where the signals from the two eyes might first interact. Decades of research have established that most neurons in V1 respond to stimulation of either eye, particularly neurons outside of V1's primary input layer 4C. In Chapter Two, I relied on data collected from linear multicontact arrays to determine where within the V1 microcircuit we first see that neurons are sensitive to both eyes.

Linear multicontact arrays have become a popular a tool for investigating cortical microcircuits in primates. In V1 in particular, studies using these linear arrays have revealed neurophysiological patterns that can be used to identify where the array is positioned with respect to the electrode (Mitzdorf, 1985, Maier et al., 2010). Using these advances, we can record across the layers of V1 and confidently estimate the laminar location of recorded neurons.

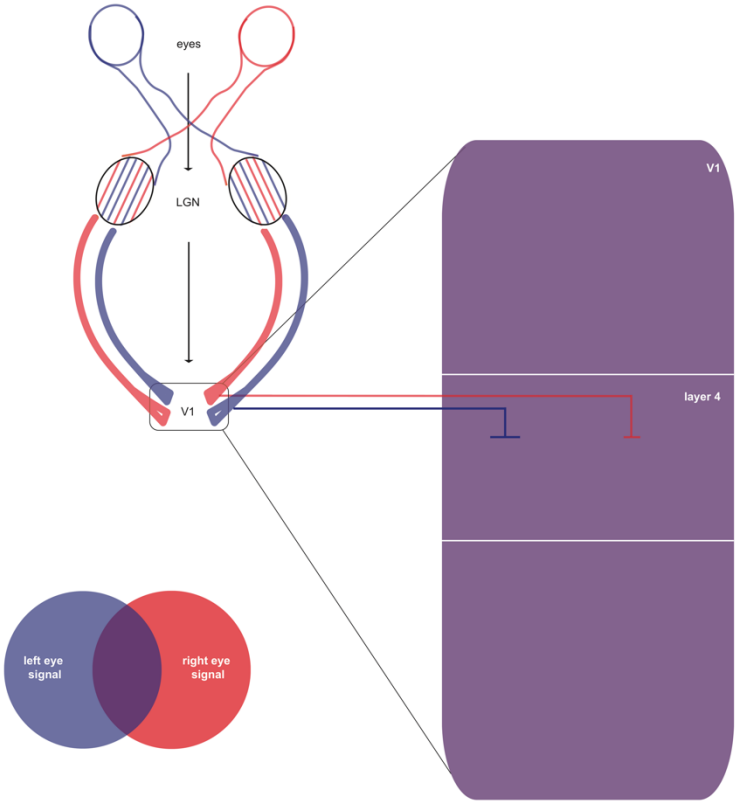

Figure 4.1 Schematic of binocular signal convergence. The signals from each eye (red and blue, respectively) are mostly segregated in the LGN. However, virtually all neurons, including those in layer 4 of V1, encode a binocular signal (purple).

Chapter Two shows that almost all neurons in V1 are sensitive to both eyes, including those in layer 4 (**Figure 4.1**). In other words, unlike the popular theoretical model proposed by Hubel and Wiesel (1972), neurons in L4 encode a binocular signal. For some neurons, a binocular signal may directly initiate at the thalamo-cortical synapse through converging excitatory inputs. However, most L4 modulation is likely the result of intra- and interlaminar connections. Future work may investigate the source of L4 binocular modulation; in particular how much of the modulation is inherited from the LGN. How much of

L4 modulation happens at the geniculo-cortical synapse versus intra- or interlaminar connections within V1? The first of these questions might be answered through the cortical inactivation with LGN recording experiment described above. Both anatomy and neurophysiology experiments may help answer the latter questions. For example, a thorough investigation of the spread of neural processes in layer 4C in primates with respect to groups of neurons of different eye dominance may elucidate whether connections within layer 4 lead to binocular modulation of these neurons. Another possibility may be to use targeted pharmacological inactivation, restricted to only the upper layers of cortex, for example, to determine if that part of the microcircuit is involved in layer 4 modulation. Chapters One and Two demonstrate that initial binocular interactions occur as early as the LGN and layer 4C of V1, which goes against the idea that each eye's signal remains segregated until it arrives in layer 2/3. The experiments described in this dissertation also provide more motivation for uncovering the role of the LGN in binocular processing.

4.2 Convergence of feedforward signals with ongoing activity in the primary visual cortex

It is tempting to think of feedforward processes, such as binocular integration, in terms of a series of concrete steps and to assume that these incoming signals meet a blank slate in the brain. Instead, incoming signals meet neurons that are already activated to a degree determined by a number of factors, including prior stimulus history and the activity of other neurons to which they are connected. The V1 microcircuit is an interesting place to study the convergence of incoming feedforward inputs with ongoing brain activity because the V1 microcircuit is relatively well-defined and its primary geniculate input layer, layer 4C, does not receive feedback inputs (Felleman and Van Essen, 1991). In other words, inputs from other brain areas

target upper and deep layers, while geniculate inputs primarily target middle layer 4C (Felleman and Van Essen, 1991). In Chapter Three, I investigated the relationship between ongoing fluctuations in the alpha range, which were most prominent in the deep layers, with spiking activity in all layers. Spiking in all layers but especially layer 2/3 modulated with alpha activity in the lower layers (layer 5&6) both during rest and active visual stimulation. In Chapter Three, I noted a set of previously described interlaminar connections that might support this functional relationship in neural activity. However, future work such as optogenetics to target specific cell populations within the microcircuit might better reveal how the microcircuit leads to this pattern of activity. Similarly, future work may reveal whether the temporal aspect of these neural correlations is critical for visual processing, or perhaps just an epiphenomenal consequence of other aspects of the circuitry that has little to no impact on perception. Broadly speaking, more work on the coordination of activity within and between cortical microcircuits may shed light on how the brain, remarkably, combines the outputs of the two eyes and forms coherent visual experience with seemingly great ease in less than 150 ms (Thorpe et al., 1996).

REFERENCES

AHMED, B., ANDERSON, J. C., DOUGLAS, R. J., MARTIN, K. A. & NELSON, J. C. 1994. Polyneuronal innervation of spiny stellate neurons in cat visual cortex. *J Comp Neurol,* 341**,** 39-49.

ALITTO, H. J., MOORE, B. D., RATHBUN, D. L. & USREY, W. M. 2011. A comparison of visual responses in the lateral geniculate nucleus of alert and anaesthetized macaque monkeys. *The Journal of Physiology,* 589**,** 87-99.

ANDREWS, T. J. & BLAKEMORE, C. 2002. Integration of motion information during binocular rivalry. *Vision Res,* 42**,** 301-9.

ASAAD, W. F., SANTHANAM, N., MCCLELLAN, S. & FREEDMAN, D. J. 2013. High-performance execution of psychophysical tasks with complex visual stimuli in MATLAB. *J Neurophysiol,* 109**,** 249-60.

BAKER, D. H., MEESE, T. S., MANSOURI, B. & HESS, R. F. 2007. Binocular Summation of Contrast Remains Intact in Strabismic Amblyopia. *Investigative Ophthalmology & Visual Science,* 48**,** 5332-5338.

BAKER, F. H., GRIGG, P., VON NOORDEN, G.K. 1974. Effects of visual deprivation and strabismus on the response of neurons in the visual cortex of the monkey, including studies on the striate and prestriate cortex in the normal animal. *Brain Res,* 66**,** 185-208.

BANNISTER, A. P. 2005. Inter- and intra-laminar connections of pyramidal cells in the neocortex. *Neuroscience Research,* 53**,** 95-103.

BAREITHER, I., CHAUMON, M., BERNASCONI, F., VILLRINGER, A. & BUSCH, N. A. 2014. Invisible visual stimuli elicit increases in alpha-band power. *Journal of Neurophysiology*.

BASTOS, A. M., BRIGGS, F., ALITTO, H. J., MANGUN, G. R. & USREY, W. M. 2014. Simultaneous recordings from the primary visual cortex and lateral geniculate nucleus reveal rhythmic interactions and a cortical source for γ-band oscillations. *Journal of Neuroscience,* 34**,** 7639-7644.

BASTOS, A. M., VEZOLI, J., BOSMAN, C. A., SCHOFFELEN, J.-M., OOSTENVELD, R., DOWDALL, J. R., DE WEERD, P., KENNEDY, H. & FRIES, P. 2015. Visual areas exert feedforward and feedback influences through distinct frequency channels. 85**,** 390-401.

BELTRAMO, R., D'URSO, G., DAL MASCHIO, M., FARISELLO, P., BOVETTI, S., CLOVIS, Y., LASSI, G., TUCCI, V., DE PIETRI TONELLI, D. & FELLIN, T. 2013. Layer-specific excitatory circuits differentially control recurrent network dynamics in the neocortex. *Nature Neuroscience,* 16**,** 227-234.

BERGER, H. 1929. Über das Elektrenkephalogramm des Menschen. *Archiv für Psychiatrie und Nervenkrankheiten,* 87**,** 527-570.

BINZEGGER, T., DOUGLAS, R. J. & MARTIN, K. A. 2004. A quantitative map of the circuit of cat primary visual cortex. *Journal of Neuroscience,* 24**,** 8441-53.

BISHOP, P. O., BURKE, W. & DAVIS, R. 1962. The interpretation of the extracellular response of single lateral geniculate cells. *Journal of Physiology,* 162**,** 451-72.

BLAKE, R. 1989. A neural theory of binocular rivalry. *Psychol Rev,* 96**,** 145-67.

BLAKE, R., COOL, S. J. & CRAWFORD, M. L. J. 1974. Visual resolution in the cat. *Vision Research,* 14**,** 1211-1217.
BLAKE, R. & FOX, R. 1973. The psychophysical inquiry into binocular summation - Springer. *Perception & Psychophysics*.
BLAKE, R., SLOANE, M. & FOX, R. 1981. Further developments in binocular summation. *Percept Psychophys,* 30**,** 266-76.
BLAKE, R. & WILSON, H. 2011. Binocular vision. *Vision Research,* 51**,** 754-770.
BLASDEL, G. G. & FITZPATRICK, D. 1984. Physiological organization of layer 4 in macaque striate cortex. *J Neurosci,* 4**,** 880-95.
BLASDEL, G. G. & LUND, J. S. 1983. Termination of afferent axons in macaque striate cortex. *Journal of Neuroscience,* 3**,** 1389-413.
BOKIL, H., ANDREWS, P., KULKARNI, J. E., MEHTA, S. & MITRA, P. P. 2010. Chronux: A platform for analyzing neural signals. 192**,** 146-151.
BOLLIMUNTA, A., CHEN, Y., SCHROEDER, C. A. E. & DING, M. 2008. Neuronal mechanisms of cortical alpha oscillations in awake-behaving macaques. *Journal of Neuroscience,* 28**,** 9976-9988.
BOLLIMUNTA, A., MO, J., SCHROEDER, C. A. E. & DING, M. 2011. Neuronal mechanisms and attentional modulation of corticothalamic α oscillations. *Journal of Neuroscience,* 31**,** 4935-4943.
BORTONE, D. S., OLSEN, S. R. & SCANZIANI, M. 2014. Translaminar inhibitory cells recruited by layer 6 corticothalamic neurons suppress visual cortex. *Neuron,* 82**,** 474-485.
BOSMAN, C. A., WOMELSDORF, T., DESIMONE, R. & FRIES, P. 2009. A microsaccadic rhythm modulates gamma-band synchronization and behavior. *Journal of Neuroscience,* 29**,** 9471-9480.
BRUNS, A. & ECKHORN, R. 2004. Task-related coupling from high- to low-frequency signals among visual cortical areas in human subdural recordings. *International Journal of Psychophysiology,* 51**,** 97-116.
BRUNSO-BECHTOLD, J. K. & CASAGRANDE, V. A. 1982. Early postnatal development of laminar characteristics in the dorsal lateral geniculate nucleus of the tree shrew. *Journal of Neuroscience,* 2**,** 589-97.
BUFFALO, E. A., FRIES, P., LANDMAN, R., BUSCHMAN, T. J. & DESIMONE, R. 2011. Laminar differences in gamma and alpha coherence in the ventral stream. *Proceedings of the National Academy of Sciences of the USA,* 108**,** 11262-11267.
BUZÁS, P., EYSEL, U. T. & ADORJÁN, P. 2001. Axonal topography of cortical basket cells in relation to orientation, direction, and ocular dominance maps. *Journal of Comparative Neurology*, 437, 259-285.
BUZSÁKI, G., ANASTASSIOU, C. A. & KOCH, C. 2012. The origin of extracellular fields and currents — EEG, ECoG, LFP and spikes. *Nature Reviews Neuroscience*, 13, 407-420.
CALLAWAY, E. M. 1998. Prenatal development of layer-specific local circuits in primary visual cortex of the macaque monkey. *The Journal of Neuroscience,* 18**,** 1505-1527.
CAMPOS-ORTEGA, J. A., GLEES, P. & NEUHOFF, V. 1968. Ultrastructural analysis of individual layers in the lateral geniculate body of the monkey. *Z Zellforsch Mikrosk Anat,* 87**,** 82-100.
CANOLTY, R. T., EDWARDS, E., DALAL, S. S., SOLTANI, M., NAGARAJAN, S. S., KIRSCH, H. E., BERGER, M. S., BARBARO, N. M. & KNIGHT, R. T. 2006. High

gamma power is phase-locked to theta oscillations in human neocortex. *Science,* 313**,** 1626-1628.
CANOLTY, R. T. & KNIGHT, R. T. 2010. The functional role of cross-frequency coupling. *Trends in Cognitive Sciences,* 14**,** 506-515.
CARLSON, T. A. & HE, S. 2000. Visible binocular beats from invisible monocular stimuli during binocular rivalry. *Current Biology,* 10**,** 1055-8.
CASAGRANDE, V. A. & BOYD, J. D. 1996. The neural architecture of binocular vision. *Eye (Lond),* 10 (Pt 2)**,** 153-60.
CASAGRANDE, V. A., YAZAR, F., JONES, K. D. & DING, Y. 2007. The morphology of the koniocellular axon pathway in the macaque monkey. *Cereb Cortex,* 17**,** 2334-45.
CHAGNAC-AMITAI, Y., LUHMANN, H. J. & PRINCE, D. A. 1990. Burst generating and regular spiking layer 5 pyramidal neurons of rat neocortex have different morphological features. *Journal of Comparative Neurology*, 296**,** 598-613.
CHAUMON, M. & BUSCH, N. 2014. Prestimulus Neural Oscillations Inhibit Visual Perception via Modulation of Response Gain. *Journal of Cognitive Neuroscience*, 26, 2514-2529.
CHEONG, S. K., TAILBY, C., SOLOMON, S. G. & MARTIN, P. R. 2013. Cortical-Like Receptive Fields in the Lateral Geniculate Nucleus of Marmoset Monkeys. *Journal of Neuroscience,* 33**,** 6864-6876.
CONLEY, M., BIRECREE, E. & CASAGRANDE, V. A. 1985. Neuronal classes and their relation to functional and laminar organization of the lateral geniculate nucleus: a Golgi study of the prosimian primate, Galago crassicaudatus. *Journal of Comparative Neurology,* 242**,** 561-83.
CONNORS, B. W. 1984. Initiation of synchronized neuronal bursting in neocortex. *Nature,* 310**,** 685-687.
CONNORS, B. W. & AMITAI, Y. 1997. Making waves in the neocortex. *Neuron,* 18**,** 347-349.
COX, M. A., DOUGHERTY, K., ADAMS, G. K., REAVIS, E. A., WESTERBERG, J. A., MOORE, B. S., LEOPOLD, D. A. & MAIER, A. 2017. Spiking Suppression Precedes Cued Attentional Enhancement of Neural Responses in Primary Visual Cortex. *Cereb Cortex***,** 1-14.
COX, M. A., SCHMID, M. C., PETERS, A. J., SAUNDERS, R. C., LEOPOLD, D. A. & MAIER, A. 2013. Receptive field focus of visual area V4 neurons determines responses to illusory surfaces. *Proc Natl Acad Sci U S A,* 110**,** 17095-100.
CUMMING, B. G. & DEANGELIS, G. C. 2001. The physiology of stereopsis. *Annu Rev Neurosci,* 24**,** 203-38.
DA COSTA, N. M. & MARTIN, K. A. C. 2011. How Thalamus Connects to Spiny Stellate Cells in the Cat's Visual Cortex. *Journal of Neuroscience,* 31**,** 2925-2937.
DA SILVA, F. L. 1991. Neural mechanisms underlying brain waves: from neural membranes to networks. *Electroencephalography and clinical neurophysiology,* 79**,** 81-93.
DACEY, D. M. 1994. Physiology, morphology and spatial densities of identified ganglion cell types in primate retina. *Ciba Found Symp,* 184**,** 12-28; discussion 28-34, 63-70.
DANTZKER, J. L. & CALLAWAY, E. M. 2000. Laminar sources of synaptic input to cortical inhibitory interneurons and pyramidal neurons. *Nature Neuroscience*.
DING, J. & SPERLING, G. 2006. A gain-control theory of binocular combination. *Proceedings of the National Academy of Sciences of the USA,* 103**,** 1141-6.
DONNER, T. H. & SIEGEL, M. 2011. A framework for local cortical oscillation patterns. *Trends in Cognitive Sciences***,** 1-9.

DOUGHERTY, K., COX, M. A., NINOMIYA, T., LEOPOLD, D. A. & MAIER, A. 2017. Ongoing Alpha Activity in V1 Regulates Visually Driven Spiking Responses. *Cereb Cortex,* 27**,** 1113-1124.
DOUGHERTY, K., SCHMID, M. C. & MAIER, A. 2018. Binocular response modulation in the lateral geniculate nucleus. *Journal of Comparative Neurology.*
DOUGLAS, R. J. & MARTIN, K. A. C. 2004. Neuronal Circuits of the Neocortex. *Annual Review of Neuroscience*, 27, 419-451.
DOUGLAS, R. J., MARTIN, K.A.C., WHITTERIDGE, D. 1989. A Canonical Microcircuit of the Neocortex. *Neural Computation,* 1**,** 480-488.
DREHER, B., FUKADA, Y. & RODIECK, R. W. 1976. Identification, classification and anatomical segregation of cells with X-like and Y-like properties in the lateral geniculate nucleus of old-world primates. *Journal of Physiology,* 258**,** 433-52.
ENDO, M., KAAS, J. H., JAIN, N. & SMITH, E. L. 2000. Binocular cross-orientation suppression in the primary visual cortex (V1) of infant rhesus monkeys. Invest. *Ophthalmol. Vis. Sci.*, 41, 4022-4031.
ENGEL, A. K., FRIES, P. & SINGER, W. 2001. Dynamic predictions: oscillations and synchrony in top-down processing. *Nature reviews. Neuroscience,* 2**,** 704-716.
ERULKAR, S. D. & FILLENZ, M. 1960. Single-unit activity in the lateral geniculate body of the cat. *Journal of Physiology,* 154**,** 206-18.
FAMIGLIETTI, E. V. 1970. Dendro-dendritic synapses in the lateral geniculate nucleus of the cat. *Brain Research,* 20**,** 181-191.
FELLEMAN, D. J. & VAN ESSEN, D. C. 1991. Distributed hierarchical processing in the primate cerebral cortex. *Cerebral Cortex (New York, N.Y. : 1991),* 1**,** 1-47.
FITZPATRICK, D., LUND, J. S. & BLASDEL, G. G. 1985. Intrinsic connections of macaque striate cortex: afferent and efferent connections of lamina 4C. *The Journal of Neuroscience,* 5**,** 3329-3349.
FITZPATRICK, D., USREY, W. M., SCHOFIELD, B. R. & EINSTEIN, G. 1994. The sublaminar organization of corticogeniculate neurons in layer 6 of macaque striate cortex. *Visual neuroscience,* 11**,** 307-315.
FREEMAN, R. D. 2017. 2015 Charles F. Prentice Medal Award Lecture: Neural Organization of Binocular Vision. *Optom Vis Sci,* 94**,** 931-938.
FREEMAN, R. D. & OHZAWA, I. 1990. On the neurophysiological organization of binocular vision. *Vision Research,* 30**,** 1661-1676.
FRÖHLICH, F. & MCCORMICK, D. A. 2010. Endogenous electric fields may guide neocortical network activity. *Neuron,* 67**,** 129-143.
GARRAGHTY, P. E., SALINGER, W. L., MACAVOY, M. G., SCHROEDER, C. E. & GUIDO, W. 1982. The shift in X/Y ratio after chronic monocular paralysis: a binocularly mediated, barbiturate-sensitive effect in the adult lateral geniculate nucleus. *Exp Brain Res,* 47**,** 301-8.
GILBERT, C. D. 1983. Microcircuitry of the Visual Cortex. *Annual Review of Neuroscience,* 6**,** 217-247.
GILBERT, C. D. & WIESEL, T. N. 1989. Columnar specificity of intrinsic horizontal and corticocortical connections in cat visual cortex. *Journal of Neuroscience,* 9**,** 2432-42.
GODLOVE, D. C., MAIER, A., WOODMAN, G. F. & SCHALL, J. D. 2014. Microcircuitry of agranular frontal cortex: testing the generality of the canonical cortical microcircuit. *Journal of Neuroscience,* 34**,** 5355-69.

GREEN, D. M. & SWETS, J. A. 1966. *Signal detection theory and psychophysics,* New York,, Wiley.
GRIEVE, K. L. 2005. Binocular visual responses in cells of the rat dLGN. *Journal of Physiology,* 566**,** 119-24.
GUIDO, W., TUMOSA, N. & SPEAR, P. D. 1989. Binocular interactions in the cat's dorsal lateral geniculate nucleus. I. Spatial-frequency analysis of responses of X, Y, and W cells to nondominant-eye stimulation. *Journal of Neurophysiology,* 62**,** 526-543.
GUILLERY, R. W. 1966. A study of Golgi preparations from the dorsal lateral geniculate nucleus of the adult cat. *Journal of Comparative Neurology,* 128**,** 21-50.
GUILLERY, R. W. 1970. The laminar distribution of retinal fibers in the dorsal lateral geniculate nucleus of the cat: A new interpretation. *Journal of Comparative Neurology,* 138**,** 339–367.
GUILLERY, R. W. & COLONNIER, M. 1970. Synaptic patterns in the dorsal lateral geniculate nucleus of the monkey. *Z Zellforsch Mikrosk Anat,* 103**,** 90-108.
HAEGENS, S., NÁCHER, V., LUNA, R., ROMO, R. & JENSEN, O. 2011. α-Oscillations in the monkey sensorimotor network influence discrimination performance by rhythmical inhibition of neuronal spiking. *Proceedings of the National Academy of Sciences of the USA,* 108**,** 19377-19382.
HAMMOND, P. & MOUAT, G. S. V. 1988. Neural correlates of motion after-effects in cat striate cortical neurones: interocular transfer. *Experimental brain research,* 72**,** 21-28.
HÄNDEL, B. F., HAARMEIER, T. & JENSEN, O. 2011. Alpha oscillations correlate with the successful inhibition of unattended stimuli. *Journal of Cognitive Neuroscience,* 23**,** 2494-2502.
HANSEN, B. J., CHELARU, M. I. & DRAGOI, V. 2012. Correlated variability in laminar cortical circuits. *Neuron,* 76**,** 590-602.
HAYHOW, W. R. 1958. The cytoarchitecture of the lateral geniculate body in the cat in relation to the distribution of crossed and uncrossed optic fibers. *Journal of Comparative Neurology,* 110**,** 1-63.
HEESY, C. P. 2004. On the relationship between orbit orientation and binocular visual field overlap in mammals. *Anat Rec A Discov Mol Cell Evol Biol,* 281**,** 1104-10.
HENDRY, S. H. & YOSHIOKA, T. 1994. A neurochemically distinct third channel in the macaque dorsal lateral geniculate nucleus. *Science,* 264**,** 575-7.
HENDRY, S. H. C. & REID, R. C. 2000. The Koniocellular Pathway in Primate Vision. *Annual Review of Neuroscience,* 23**,** 127-153.
HENRIKSEN, S., TANABE, S. & CUMMING, B. 2016. Disparity processing in primary visual cortex. *Philosophical Transactions of the Royal Society B: Biological Sciences,* 371**,** 20150255.
HICKEY, T. L. & GULLERY, R. W. 1974. An autoradiographic study of retinogeniculate pathways in the cat and the fox. *Journal of Comparative Neurology,* 156**,** 239-253.
HORTON, J. C. & HOCKING, D. R. 1996. Intrinsic variability of ocular dominance column periodicity in normal macaque monkeys. *Journal of Neuroscience,* 16**,** 7228-39.
HOWARD, I. P. 2002. *Seeing in depth, Vol. 1: Basic mechanisms,* Toronto, ON, Canada, University of Toronto Press.
HOWARTH, M., WALMSLEY, L. & BROWN, T. M. 2014. Binocular integration in the mouse lateral geniculate nuclei. *Current Biology,* 24**,** 1241-1247.

HUBEL, D. H. & FREEMAN, D. C. 1977. Projection into the visual field of ocular dominance columns in macaque monkey. *Brain Research,* 122**,** 336-343.
HUBEL, D. H. & WIESEL, T. N. 1962. Receptive fields, binocular interaction and functional architecture in the cat's visual cortex. *Journal of Physiology,* 160**,** 106-154.
HUBEL, D. H. & WIESEL, T. N. 1968. Receptive fields and functional architecture of monkey striate cortex. *Journal of Physiology,* 195**,** 215-43.
HUBEL, D. H. & WIESEL, T. N. 1969. Anatomical demonstration of columns in the monkey striate cortex. *Nature*.
HUBEL, D. H. & WIESEL, T. N. 1972. Laminar and columnar distribution of geniculo-cortical fibers in the macaque monkey. *J Comp Neurol,* 146**,** 421-50.
HUBEL, D. H. & WIESEL, T. N. 1977. Ferrier lecture. Functional architecture of macaque monkey visual cortex. *Proc R Soc Lond B Biol Sci,* 198**,** 1-59.
ITO, J., MALDONADO, P. & GRÜN, S. 2013. Cross-frequency interaction of the eye-movement related LFP signals in V1 of freely viewing monkeys. *Frontiers in systems neuroscience,* 7**,** 1.
JEFFERY, G., COWEY, A. & KUYPERS, H. G. 1981. Bifurcating retinal ganglion cell axons in the rat, demonstrated by retrograde double labelling. *Exp Brain Res,* 44**,** 34-40.
JENSEN, O., BONNEFOND, M. & VANRULLEN, R. 2012. An oscillatory mechanism for prioritizing salient unattended stimuli. *Trends in Cognitive Sciences,* 16**,** 200-206.
JENSEN, O. & COLGIN, L. L. 2007. Cross-frequency coupling between neuronal oscillations. *Trends in Cognitive Sciences,* 11**,** 267-269.
JENSEN, O. & MAZAHERI, A. 2010. Shaping Functional Architecture by Oscillatory Alpha Activity: Gating by Inhibition. *Frontiers in Human Neuroscience,* 4.
JONES, E. G. 2001. The thalamic matrix and thalamocortical synchrony. *Trends in neurosciences,* 24**,** 595-601.
JONES, S. R., PINTO, D. J., KAPER, T. J. & KOPELL, N. 2000. Alpha-frequency rhythms desynchronize over long cortical distances: a modeling study. *Journal of Computational Neuroscience,* 9**,** 271-291.
JONES, S. R., PRITCHETT, D. L., SIKORA, M. A., STUFFLEBEAM, S. M., HÄMÄLÄINEN, M. & MOORE, C. I. 2009. Quantitative analysis and biophysically realistic neural modeling of the MEG mu rhythm: rhythmogenesis and modulation of sensory-evoked responses. *Journal of Neurophysiology,* 102**,** 3554-3572.
KAAS, J. H., GUILLERY, R. W. & ALLMAN, J. M. 1972. Some principles of organization in the dorsal lateral geniculate nucleus. *Brain, Behavior and Evolution,* 6**,** 253-299.
KAJIKAWA, Y. & SCHROEDER, C. A. E. 2011. How Local Is the Local Field Potential? *Neuron,* 72**,** 847-858.
KAJIKAWA, Y. & SCHROEDER, C. A. E. 2015. Generation of field potentials and modulation of their dynamics through volume integration of cortical activity. *Journal of Neurophysiology,* 113**,** 339-351.
KATO, H., BISHOP, P. O. & ORBAN, G. A. 1981. Binocular interaction on monocularly discharged lateral geniculate and striate neurons in the cat. *Journal of Neurophysiology,* 46**,** 932-51.
KATZ, L. C., GILBERT, C. D. & WIESEL, T. N. 1989. Local circuits and ocular dominance columns in monkey striate cortex. *J Neurosci,* 9**,** 1389-99.

KINSTON, W. J., VADAS, M. A. & BISHOP, P. O. 1969. Multiple projection of the visual field to the medical portion of the dorsal lateral geniculate nucleus and the adjacent nuclei of the thalamus of the cat. *J Comp Neurol,* 136**,** 295-315.

KIORPES, L., KIPER, D. C., O'KEEFE, L. P., CAVANAUGH, J. R. & MOVSHON, J. A. 1998. Neuronal correlates of amblyopia in the visual cortex of macaque monkeys with experimental strabismus and anisometropia. *J Neurosci,* 18**,** 6411-24.

KLEIN, C., EVRARD, H. C., SHAPCOTT, K. A., HAVERKAMP, S., LOGOTHETIS, N. K. & SCHMID, M. C. 2016. Cell-Targeted Optogenetics and Electrical Microstimulation Reveal the Primate Koniocellular Projection to Supra-granular Visual Cortex. *Neuron,* 90**,** 143-51.

KLIMESCH, W., SAUSENG, P. & HANSLMAYR, S. 2007. EEG alpha oscillations: The inhibition–timing hypothesis. *Brain research reviews,* 53**,** 63-88.

KONDO, Y., TAKADA, M., HONDA, Y. & MIZUNO, N. 1993. Bilateral projections of single retinal ganglion cells to the lateral geniculate nuclei and superior colliculi in the albino rat. *Brain research,* 608**,** 204-215.

KRAMER, M. A., ROOPUN, A. K., CARRACEDO, L. M., TRAUB, R. D., WHITTINGTON, M. A. & KOPELL, N. J. 2008. Rhythm generation through period concatenation in rat somatosensory cortex. *PLoS computational biology,* 4**,** e1000169.

KUMAGAMI, T., ZHANG, B., SMITH, E. L., 3RD & CHINO, Y. M. 2000. Effect of onset age of strabismus on the binocular responses of neurons in the monkey visual cortex. *Invest Ophthalmol Vis Sci,* 41**,** 948-54.

LAKATOS, P., SHAH, A. S., KNUTH, K. H., ULBERT, I. & KARMOS, G. An oscillatory hierarchy controlling cortical excitability and stimulus processing. *researchgate.net*.

LANDAU, A. N. & FRIES, P. 2012. Attention Samples Stimuli Rhythmically. *Current Biology,* 22**,** 1000-1004.

LATIES, A. M. & SPRAGUE, J. M. 1966. The projection of optic fibers to the visual centers in the cat. *J Comp Neurol,* 127**,** 35-70.

LEGGE, G. E. & RUBIN, G. S. 1981. Binocular interactions in suprathreshold contrast perception. *Percept Psychophys,* 30**,** 49-61.

LEMON, R. & PROCHAZKA, A. 1984. *Methods for neuronal recording in conscious animals,* Chichester [West Sussex] ; New York, Wiley.

LENNIE, P. & MOVSHON, J. A. 2005. Coding of color and form in the geniculostriate visual pathway (invited review). *J Opt Soc Am A Opt Image Sci Vis,* 22**,** 2013-33.

LEOPOLD, D. A., MAIER, A., WILKE, M., & LOGOTHETIS, N. K. 2005. Binocular Rivalry and the Illusion of Monocular Vision. *MIT Press***,** 231–243.

LIEBE, S., HOERZER, G. M., LOGOTHETIS, N. K. & RAINER, G. 2012. Theta coupling between V4 and prefrontal cortex predicts visual short-term memory performance. *Nature neuroscience,* 15**,** 456-62- S1-2.

LOGOTHETIS, N. K. 1998. Single units and conscious vision. *Philos Trans R Soc Lond B Biol Sci,* 353**,** 1801-18.

LOGOTHETIS, N. K., KAYSER, C. & OELTERMANN, A. 2007. In vivo measurement of cortical impedance spectrum in monkeys: implications for signal propagation. *Neuron,* 55**,** 809-23.

LONGORDO, F., TO, M. S., IKEDA, K. & STUART, G. J. 2013. Sublinear integration underlies binocular processing in primary visual cortex. *Nat Neurosci,* 16**,** 714-23.

LOPES DA SILVA, F. H. & STORM VAN LEEUWEN, W. 1977. The cortical source of the alpha rhythm. *Neuroscience letters,* 6**,** 237-241.
LOPES DA SILVA, F. H., VOS, J. E., MOOIBROEK, J. & VAN ROTTERDAM, A. 1980. Relative contributions of intracortical and thalamo-cortical processes in the generation of alpha rhythms, revealed by partial coherence analysis. *Electroencephalography and clinical neurophysiology,* 50**,** 449-456.
LŐRINCZ, M. L., KÉKESI, K. A., JUHÁSZ, G., CRUNELLI, V. & HUGHES, S. W. 2009. Temporal Framing of Thalamic Relay-Mode Firing by Phasic Inhibition during the Alpha Rhythm. *Neuron,* 63**,** 683-696.
LÜBKE, J. & FELDMEYER, D. 2007. Excitatory signal flow and connectivity in a cortical column: focus on barrel cortex. *Brain Structure and Function,* 212**,** 3-17.
MACKNIK, S. L. & MARTINEZ-CONDE, S. 2004. Dichoptic visual masking reveals that early binocular neurons exhibit weak interocular suppression: implications for binocular vision and visual awareness. *J Cogn Neurosci,* 16**,** 1049-59.
MACKNIK, S. L. & MARTINEZ-CONDE, S. 2008. The role of feedback in visual masking and visual processing. *Adv Cogn Psychol,* 3**,** 125-52.
MAFFEI, L., BERARDI, N. & BISTI, S. 1986. Interocular transfer of adaptation after effect in neurons of area 17 and 18 of split chiasm cats. *Journal of Neurophysiology,* 55**,** 966-976.
MAIER, A., ADAMS, G. K., AURA, C. & LEOPOLD, D. A. 2010. Distinct superficial and deep laminar domains of activity in the visual cortex during rest and stimulation. *Front Syst Neurosci,* 4.
MAIER, A., AURA, C. J. & LEOPOLD, D. A. 2011. Infragranular Sources of Sustained Local Field Potential Responses in Macaque Primary Visual Cortex. *Journal of Neuroscience,* 31**,** 1971-1980.
MAIER, A., LOGOTHETIS, N. K. & LEOPOLD, D. A. 2007. Context-dependent perceptual modulation of single neurons in primate visual cortex. *Proceedings of the National Academy of Sciences of the USA,* 104**,** 5620-5.
MAIER, A., MA, C., DOUGHERTY, K., MOORE, B. & DA, L. 2014. Anisotropy of ongoing neural activity in the primate visual cortex. *Eye and Brain,* 2014**,** 113-120.
MAIER, A., WILKE, M., AURA, C., ZHU, C., YE, F. Q. & LEOPOLD, D. A. 2008. Divergence of fMRI and neural signals in V1 during perceptual suppression in the awake monkey. *Nat Neurosci,* 11**,** 1193-200.
MARKOV, N. T., VEZOLI, J., CHAMEAU, P., FALCHIER, A., QUILODRAN, R., HUISSOUD, C., LAMY, C., MISERY, P., GIROUD, P., ULLMAN, S., BARONE, P., DEHAY, C., KNOBLAUCH, K. & KENNEDY, H. 2013. The anatomy of hierarchy: Feedforward and feedback pathways in macaque visual cortex. *The Journal of Comparative Neurology***,** n/a-n/a.
MARROCCO, R. T. & LI, R. H. 1977. Monkey superior colliculus: properties of single cells and their afferent inputs. *Journal of Neurophysiology,* 40**,** 844-860.
MARROCCO, R. T. & MCCLURKIN, J. W. 1979. Binocular interaction in the lateral geniculate nucleus of the monkey. *Brain research,* 168**,** 633-637.
MARTIN, K. A. C., SOMOGYI, P. & WHITTERIDGE, D. 1983. Physiological and morphological properties of identified basket cells in the cat's visual cortex. *Experimental brain research,* 50-50.

MARTIN, P. R., WHITE, A. J., GOODCHILD, A. K., WILDER, H. D. & SEFTON, A. E. 1997. Evidence that blue-on cells are part of the third geniculocortical pathway in primates. *Eur J Neurosci,* 9**,** 1536-41.

MAUNSELL, J. H. & VAN ESSEN, D. C. 1983. The connections of the middle temporal visual area (MT) and their relationship to a cortical hierarchy in the macaque monkey. *The Journal of Neuroscience,* 3**,** 2563-2586.

MEESE, T. S., GEORGESON, M. A. & BAKER, D. H. 2006. Binocular contrast vision at and above threshold. *J Vis,* 6**,** 1224-43.

MINEAULT, P. J., ZANOS, T. P. & PACK, C. C. 2013. Local field potentials reflect multiple spatial scales in V4. *Front Comput Neurosci,* 7**,** 21.

MITZDORF, U. 1985. Current source-density method and application in cat cerebral cortex: investigation of evoked potentials and EEG phenomena. *Physiol Rev,* 65**,** 37-100.

MITZDORF, U. & SINGER, W. 1977. Laminar segregation of afferents to lateral geniculate nucleus of the cat: an analysis of current source density. *Journal of Neurophysiology,* 40**,** 1227-44.

MITZDORF, U. & SINGER, W. 1979. Excitatory synaptic ensemble properties in the visual cortex of the macaque monkey: a current source density analysis of electrically evoked potentials. *The Journal of Comparative Neurology,* 187**,** 71-83.

MOORE, R. J., SPEAR, P. D., KIM, C. B. Y. & XUE, J. T. 1992. Binocular processing in the cat's dorsal lateral geniculate nucleus III. Spatial frequency, orientation, and direction sensitivity of nondominant-eye influences - Springer. *Experimental brain research*.

MORADI, F. & HEEGER, D. J. 2009. Inter-ocular contrast normalization in human visual cortex. *J Vis,* 9**,** 13 1-22.

NAKA, K. I. & RUSHTON, W. A. 1966. S-potentials from luminosity units in the retina of fish (Cyprinidae). *Journal of Physiology,* 185**,** 587-99.

NASCIMENTO-SILVA, S., PINÕN, C., SOARES, J. G. M. & GATTASS, R. 2014. Feedforward and feedback connections and their relation to the CytOx modules of V2 in Cebus monkeys. *The Journal of Comparative Neurology,* 522**,** 3091-3105.

NICHOLSON, C. & FREEMAN, J. A. 1975. Theory of current source-density analysis and determination of conductivity tensor for anuran cerebellum. *Journal of Neurophysiology,* 38**,** 356-68.

NIELL, C. M. & STRYKER, M. P. 2008. Highly selective receptive fields in mouse visual cortex. *J Neurosci,* 28**,** 7520-36.

NINOMIYA, T., DOUGHERTY, K., GODLOVE, D. C., SCHALL, J. D. & MAIER, A. 2015. Microcircuitry of agranular frontal cortex: contrasting laminar connectivity between occipital and frontal areas. *Journal of Neurophysiology,* 113**,** 3242-55.

NORTON, T. T., CASAGRANDE, V. A., IRVIN, G. E., SESMA, M. A. & PETRY, H. M. 1988. Contrast-sensitivity functions of W-, X-, and Y-like relay cells in the lateral geniculate nucleus of bush baby, Galago crassicaudatus. *Journal of Neurophysiology,* 59**,** 1639-56.

OHZAWA, I., DEANGELIS, G. C. & FREEMAN, R. D. 1997. Encoding of binocular disparity by complex cells in the cat's visual cortex. *Journal of Neurophysiology,* 77**,** 2879-909.

OHZAWA, I. & FREEMAN, R. D. 1986. The binocular organization of simple cells in the cat's visual cortex. *Journal of Neurophysiology,* 56**,** 221-42.

OLSEN, S. R., BORTONE, D. S., ADESNIK, H. & SCANZIANI, M. 2012. Gain control by layer six in cortical circuits of vision. *Nature,* 483**,** 47-52.

OTERO-MILLAN, J., CASTRO, J. L. A., MACKNIK, S. L. & MARTINEZ-CONDE, S. 2014. Unsupervised clustering method to detect microsaccades. *Journal of Vision,* 14.
PACHITARIU, M., STEINMETZ, N., KADIR, S., CARANDINI, M. & HARRIS, K. D. 2016.
PALVA, S. & PALVA, J. M. 2007. New vistas for alpha-frequency band oscillations. *Trends in Neurosciences,* 30**,** 150-158.
PARKER, A. J. 2007. Binocular depth perception and the cerebral cortex. *Nat Rev Neurosci,* 8**,** 379-91.
PARKER, A. J. & CUMMING, B. G. 2001. Cortical mechanisms of binocular stereoscopic vision. *Prog Brain Res,* 134**,** 205-16.
PARKER, A. J., SMITH, J. E. & KRUG, K. 2016. Neural architectures for stereo vision. *Philos Trans R Soc Lond B Biol Sci,* 371.
PASTERNAK, T. & MERIGAN, W. H. 1981. The luminance dependence of spatial vision in the cat. *Vision Research,* 21**,** 1333-1339.
PETTERSEN, K. H., DEVOR, A., ULBERT, I., DALE, A. M. & EINEVOLL, G. T. 2006. Current-source density estimation based on inversion of electrostatic forward solution: Effects of finite extent of neuronal activity and conductivity discontinuities. *Journal of Neuroscience Methods,* 154**,** 116-133.
POGGIO, G. F. & FISCHER, B. 1977. Binocular interaction and depth sensitivity in striate and prestriate cortex of behaving rhesus monkey. *J Neurophysiol,* 40**,** 1392-405.
PRINCE, S. J., POINTON, A. D., CUMMING, B. G. & PARKER, A. J. 2002. Quantitative analysis of the responses of V1 neurons to horizontal disparity in dynamic random-dot stereograms. *J Neurophysiol,* 87**,** 191-208.
PURUSHOTHAMAN, G., MARION, R., LI, K. & CASAGRANDE, V. A. 2012. Gating and control of primary visual cortex by pulvinar. *Nature Neuroscience,* 15**,** 905-912.
RANCK, J. B. 1963. Analysis of specific impedance of rabbit cerebral cortex. *Experimental Neurology,* 7**,** 153-174.
READ, J. C. & CUMMING, B. G. 2004. Ocular dominance predicts neither strength nor class of disparity selectivity with random-dot stimuli in primate V1. *Journal of Neurophysiology,* 91**,** 1271-81.
READ, J. C., PARKER, A. J. & CUMMING, B. G. 2002. A simple model accounts for the response of disparity-tuned V1 neurons to anticorrelated images. *Vis Neurosci,* 19**,** 735-53.
REPERANT, J., MICELI, D., VESSELKIN, N. P. & MOLOTCHNIKOFF, S. 1989. The centrifugal visual system of vertebrates: a century-old search reviewed. *Int Rev Cytol,* 118**,** 115-71.
REZAK, M. & BENEVENTO, L. A. 1979. A comparison of the organization of the projections of the dorsal lateral geniculate nucleus, the inferior pulvinar and adjacent lateral pulvinar to primary visual cortex (area 17) in the macaque monkey. *Brain research,* 167**,** 19-40.
ROCKLAND, K. S. & PANDYA, D. N. 1979. Laminar origins and terminations of cortical connections of the occipital lobe in the rhesus monkey. *Brain research*.
RODIECK, R. W. & DREHER, B. 1979. Visual suppression from nondominant eye in the lateral geniculate nucleus: A comparison of cat and monkey. *Experimental brain research,* 35.
SAALMANN, Y. B., PINSK, M. A., WANG, L., LI, X. & KASTNER, S. 2012. The Pulvinar Regulates Information Transmission Between Cortical Areas Based on Attention Demands. *Science,* 337**,** 753-756.

SAID, C. P. & HEEGER, D. J. 2013. A model of binocular rivalry and cross-orientation suppression. *PLoS Comput Biol,* 9**,** e1002991.
SAINI, K. D. & GAREY, L. J. 1981. Morphology of neurons in the lateral geniculate nucleus of the monkey. A Golgi study. *Exp Brain Res,* 42**,** 235-48.
SANDERSON, K. J., BISHOP, P. O. & DARIAN-SMITH, I. 1971. The properties of the binocular receptive fields of lateral geniculate neurons. *Exp Brain Res,* 13**,** 178-207.
SAYER, R. J., FRIEDLANDER, M. J. & REDMAN, S. J. 1990. The time course and amplitude of EPSPs evoked at synapses between pairs of CA3/CA1 neurons in the hippocampal slice. *J Neurosci,* 10**,** 826-36.
SCHILLER, P. H., FINLAY, B. L. & VOLMAN, S. F. 1976. Quantitative studies of single-cell properties in monkey striate cortex. II. Orientation specificity and ocular dominance. *Journal of Neurophysiology,* 39**,** 1320-33.
SCHMID, M. C., SCHMIEDT, J. T., PETERS, A. J., SAUNDERS, R. C., MAIER, A. & LEOPOLD, D. A. 2013. Motion-sensitive responses in visual area V4 in the absence of primary visual cortex. *J Neurosci,* 33**,** 18740-5.
SCHMIEDT, J. T., MAIER, A., FRIES, P., SAUNDERS, R. C., LEOPOLD, D. A. & SCHMID, M. C. 2014. Beta oscillation dynamics in extrastriate cortex after removal of primary visual cortex. *J Neurosci,* 34**,** 11857-64.
SCHMIELAU, F. & SINGER, W. 1977. The role of visual cortex for binocular interactions in the cat lateral geniculate nucleus. *Brain Res,* 120**,** 354-61.
SCHOLL, B., BURGE, J. & PRIEBE, N. J. 2013. Binocular integration and disparity selectivity in mouse primary visual cortex. *Journal of Neurophysiology,* 109**,** 3013-24.
SCHROEDER, C. E., MEHTA, A. D. & GIVRE, S. J. 1998. A spatiotemporal profile of visual system activation revealed by current source density analysis in the awake macaque. *Cereb Cortex,* 8**,** 575-92.
SCHROEDER, C. E., SALINGER, W. L. & GUIDO, W. 1988. The influence of anesthesia upon binocular processes controlling the recordability of X- and Y-cells in the lateral geniculate nucleus of the cat. *Brain Research,* 454**,** 227-237.
SCHROEDER, C. E., TENKE, C. E., AREZZO, J. C. & VAUGHAN, H. G. 1990. Binocularity in the lateral geniculate nucleus of the alert macaque. *Brain Research,* 521**,** 303-310.
SELF, M. W., VAN KERKOERLE, T., SUPÈR, H. & ROELFSEMA, P. R. 2013. Distinct roles of the cortical layers of area V1 in figure-ground segregation. *Current Biology,* 23**,** 2121-2129.
SENGPIEL, F., BADDELEY, R. J., FREEMAN, T. C. B., HARRAD, R. & BLAKEMORE, C. 1998. Different mechanisms underlie three inhibitory phenomena in cat area 17. *Vision Research,* 38**,** 2067-2080.
SENGPIEL, F. & BLAKEMORE, C. 1994. Interocular control of neuronal responsiveness in cat visual cortex. *Nature,* 368**,** 847-850.
SENGPIEL, F., BLAKEMORE, C. & HARRAD, R. 1995. Interocular suppression in the primary visual cortex: a possible neural basis of binocular rivalry. *Vision Research,* 35**,** 179-195.
SIAPAS, A. G., LUBENOV, E. V. & WILSON, M. A. 2005. Prefrontal phase locking to hippocampal theta oscillations. *Neuron,* 46**,** 141-151.
SILVA, L. R., AMITAI, Y. & CONNORS, B. W. 1991. Intrinsic oscillations of neocortex generated by layer 5 pyramidal neurons. *Science,* 251**,** 432-435.

SINGER, W. 1970. Inhibitory binocular interaction in the lateral geniculate body of the cat. *Brain Res,* 18**,** 165-70.
SMITH, E. L., CHINO, Y., NI, J. & CHENG, H. 1997. Binocular Combination of Contrast Signals by Striate Cortical Neurons in the Monkey. *Journal of Neurophysiology,* 78**,** 366-382.
SMITH, M. A., JIA, X., ZANDVAKILI, A. & KOHN, A. 2013. Laminar dependence of neuronal correlations in visual cortex. *Journal of Neurophysiology,* 109**,** 940-947.
SNODDERLY, D. M. & GUR, M. 1995. Organization of striate cortex of alert, trained monkeys (Macaca fascicularis): ongoing activity, stimulus selectivity, and widths of receptive field activating regions. *J Neurophysiol,* 74**,** 2100-25.
SPAAK, E., BONNEFOND, M., MAIER, A., LEOPOLD, D. A. & JENSEN, O. 2012. Layer-Specific Entrainment of Gamma-Band Neural Activity by the Alpha Rhythm in Monkey Visual Cortex. *Current Biology,* 22**,** 2313-2318.
STEPNIEWSKA, I., QI, H. X. & KAAS, J. H. 1999. Do superior colliculus projection zones in the inferior pulvinar project to MT in primates? *The European Journal of Neuroscience,* 11**,** 469-480.
STERIADE, M., GLOOR, P., LLINÁS, R. R., LOPES DA SILVA, F. H. & MESULAM, M. M. 1990. Basic mechanisms of cerebral rhythmic activities. *Electroencephalography and clinical neurophysiology,* 76**,** 481-508.
STONE, J. & HANSEN, S. M. 1966. The projection of the cat's retina on the lateral geniculate nucleus. *J Comp Neurol,* 126**,** 601-24.
SUN, F., TONG, J., YANG, Q., TIAN, J. & HUNG, G. K. 2002. Multi-directional shifts of optokinetic responses to binocular-rivalrous motion stimuli. *Brain Res,* 944**,** 56-64.
SUN, W. & DAN, Y. 2009. Layer-specific network oscillation and spatiotemporal receptive field in the visual cortex. *Proceedings of the National Academy of Sciences of the USA,* 106**,** 17986-17991.
TAILBY, C., MAJAJ, N. J. & MOVSHON, J. A. 2010. Binocular integration of pattern motion signals by MT neurons and by human observers. *J Neurosci,* 30**,** 7344-9.
TENKE, C. E., SCHROEDER, C. E., AREZZO, J. C. & VAUGHAN, H. G. 1993. Interpretation of high-resolution current source density profiles: a simulation of sublaminar contributions to the visual evoked potential. *Experimental Brain Research,* 94**,** 183-192.
THOMPSON, K. G., HANES, D. P., BICHOT, N. P. & SCHALL, J. D. 1996. Perceptual and motor processing stages identified in the activity of macaque frontal eye field neurons during visual search. *J Neurophysiol,* 76**,** 4040-55.
THORPE, S., FIZE, D. & MARLOT, C. 1996. Speed of processing in the human visual system. *Nature,* 381**,** 520-2.
TOMBOL, T. (1969). Two types of short axon (Golgi 2nd) interneurons in the specific thalamic nuclei. *Acta Morphol Acad Sci Hun*g, 17, 285-297.
TONG, L., GUIDO, W., TUMOSA, N., SPEAR, P. D. & HEIDENREICH, S. 1992. Binocular interactions in the cat's dorsal lateral geniculate nucleus, II: Effects on dominant-eye spatial-frequency and contrast processing. *Visual Neuroscience,* 8**,** 557-566.
TORT, A. B. L., KOMOROWSKI, R., EICHENBAUM, H. & KOPELL, N. 2010. Measuring phase-amplitude coupling between neuronal oscillations of different frequencies. *Journal of Neurophysiology,* 104**,** 1195-1210.
TRUCHARD, A. M., OHZAWA, I. & FREEMAN, R. D. 2000. Contrast Gain Control in the Visual Cortex: Monocular Versus Binocular Mechanisms. *Journal of Neuroscience*, 20,

3017-3032.
VAN KERKOERLE, T., SELF, M. W., DAGNINO, B., GARIEL-MATHIS, M.-A., POORT, J., VAN DER TOGT, C. & ROELFSEMA, P. R. 2014. Alpha and gamma oscillations characterize feedback and feedforward processing in monkey visual cortex. *Proceedings of the National Academy of Sciences of the USA,* 111**,** 14332-14341.
VANRULLEN, R., CARLSON, T. & CAVANAGH, P. 2007. The blinking spotlight of attention. *Proceedings of the National Academy of Sciences of the USA,* 104**,** 19204-19209.
VANRULLEN, R. & KOCH, C. 2003. Is perception discrete or continuous? *Trends in Cognitive Sciences,* 7**,** 207-213.
VARELA, F. J. & SINGER, W. 1987. Neuronal dynamics in the visual corticothalamic pathway revealed through binocular rivalry. *Exp Brain Res,* 66**,** 10-20.
VON STEIN, A., CHIANG, C. & KÖNIG, P. 2000. Top-down processing mediated by interareal synchronization. *Proceedings of the National Academy of Sciences of the USA*, 97**,** 14748-14753.
WANG, L., SAALMANN, Y. B., PINSK, M. A., ARCARO, M. J. & KASTNER, S. 2012. Electrophysiological Low-Frequency Coherence and Cross-Frequency Coupling Contribute to BOLD Connectivity. *Neuron,* 76**,** 1010-1020.
WIESEL, T. N., HUBEL, D. H. & LAM, D. M. 1974. Autoradiographic demonstration of ocular-dominance columns in the monkey striate cortex by means of transneuronal transport. *Brain Res,* 79**,** 273-9.
WISER, A. K. & CALLAWAY, E. M. 1997. Ocular dominance columns and local projections of layer 6 pyramidal neurons in macaque primary visual cortex. *Vis Neurosci,* 14**,** 241-51.
XING, D., YEH, C.-I., BURNS, S. & SHAPLEY, R. M. 2012. Laminar analysis of visually evoked activity in the primary visual cortex. *Proceedings of the National Academy of Sciences of the USA,* 109**,** 13871-13876.
XU, X., ICHIDA, J. M., ALLISON, J. D., BOYD, J. D., BONDS, A. B. & CASAGRANDE, V. A. 2001. A comparison of koniocellular, magnocellular and parvocellular receptive field properties in the lateral geniculate nucleus of the owl monkey (Aotus trivirgatus). *Journal of Physiology,* 531**,** 203-18.
XUE, J. T., RAMOA, A. S., CARNEY, T. & FREEMAN, R. D. 1987. Binocular interaction in the dorsal lateral geniculate nucleus of the cat. *Experimental Brain Research,* 68.
ZEATER, N., CHEONG, S. K., SOLOMON, S. G., DREHER, B. & MARTIN, P. R. 2015. Binocular Visual Responses in the Primate Lateral Geniculate Nucleus. *Current Biology,* 25**,** 3190-3195.